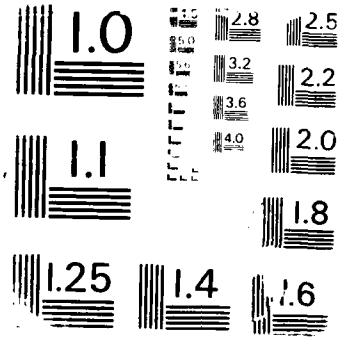
1.0
1.1
1.25
1.4
1.6
1.8
2.0
2.2
2.5
2.8
3.2
3.6
4.0

(2)

MICROWAVE LABORATORY REPORT NO. 90-P-5

THE APPLICATION OF A DETERMINISTIC SPECTRAL DOMAIN METHOD TO THE ANALYSIS OF PLANAR CIRCUIT DISCONTINUITIES ON OPEN SUBSTRATES

TECHNICAL REPORT

JAMES MCLEAN AND TATSUO ITOH

AUGUST 1990

OFFICE OF NAVAL RESEARCH GRANT NO.
N00014-89-5-1006
AND
TEXAS ADVANCED TECHNOLOGY PROGRAM

THE UNIVERSITY OF TEXAS AT AUSTIN
DEPARTMENT OF ELECTRICAL AND COMPUTER ENGINEERING
AUSTIN, TEXAS 78712

SECURITY CLASSIFICATION OF THIS PAGE (When Data Entered)

REPORT DOCUMENTATION PAGE		READ INSTRUCTIONS BEFORE COMPLETING FORM
1. REPORT NUMBER Microwave Lab. Report No. 90-P-5	2. GOVT ACCESSION NO.	3. RECIPIENT'S CATALOG NUMBER
4. TITLE (and Subtitle) The Application of a Deterministic Spectral Domain Method to the Analysis of Planar Circuit Discontinuities on Open Substraits		5. TYPE OF REPORT & PERIOD COVERED 6. PERFORMING ORG. REPORT NUMBER
7. AUTHOR(s) James McLean and Tatsuo Itoh		8. CONTRACT OR GRANT NUMBER(s) N00014-89-5-1006
9. PERFORMING ORGANIZATION NAME AND ADDRESS Department of Electrical & Computer Engineering The University of Texas Austin, Texas 78712		10. PROGRAM ELEMENT, PROJECT, TASK AREA & WORK UNIT NUMBERS
11. CONTROLLING OFFICE NAME AND ADDRESS		12. REPORT DATE August 1990 13. NUMBER OF PAGES 118
14. MONITORING AGENCY NAME & ADDRESS(if different from Controlling Office)		15. SECURITY CLASS. (of this report) 15a. DECLASSIFICATION/DOWNGRADING SCHEDULE

16. DISTRIBUTION STATEMENT (of this Report)

17. DISTRIBUTION STATEMENT (of the abstract entered in Block 20, if different from Report)

18. SUPPLEMENTARY NOTES

19. KEY WORDS (Continue on reverse side if necessary and identify by block number)

Microstrip line, slot line, discontinuities, spectral domain method.

20. ABSTRACT (Continue on reverse side if necessary and identify by block number)

A deterministic formulation of the method of moments carried out in the spectral domain is extended to include the effects of two-dimensional, two-component current flow in planar transmission line discontinuities on open substrates. The method includes the effects of space-wave and surface-wave radiation through the use of the exact spectral domain Green's function. The procedure and formulation of the method are described in detail. Also, techniques used to increase the numerical efficiency are described in detail.

DD FORM 1 JAN 73 1473 EDITION OF 1 NOV 65 IS OBSOLETE
S/N 0102-014-6601

SECURITY CLASSIFICATION OF THIS PAGE (When Data Entered)

ABSTRACT

THE APPLICATION OF A DETERMINISTIC SPECTRAL DOMAIN METHOD TO THE ANALYSIS OF PLANAR CIRCUIT DISCONTINUITIES ON OPEN SUBSTRATES

by

JAMES STUART MCLEAN, B.S., M.S.

SUPERVISING PROFESSOR: Tatsuo Itoh

A deterministic formulation of the method of moments carried out in the spectral domain is extended to include the effects of two-dimensional, two-component current flow in planar transmission line discontinuities on open substrates. The method includes the effects of space-wave and surface-wave radiation through the use of the exact spectral domain Green's function. The procedure and formulation of the method are described in detail. Also, techniques used to increase the numerical efficiency are described in detail. The

method is used to determine accurate circuit models of three types of planar circuit discontinuities on open substrates: microstrip open-end discontinuities, slotline short-circuit discontinuities, and microstrip gap discontinuities. The analysis is then applied to gap-coupled resonators. The coupling between cascaded gap discontinuities is shown to be significant when the substrate is electrically thick since surface wave excitation is strong. Possibilities for further applications of the method to more complicated discontinuities are discussed.

Table of Contents

List of Tables

List of Figures

Chapter 1

INTRODUCTION

1.1 Motivation

Planar circuits and antennas are attractive because of low cost, manufacturability, small size and light weight. Recently, integrated planar front-end systems combining both antennas and circuits have been developed. Because planar circuits are extremely difficult to modify and tune, very accurate models are required for the design process in order to avoid costly design iterations. The modelling of unshielded open planar circuits is complicated by the possibility of surface wave and space wave radiation. In the case of open planar transmission line structures, discontinuities can generate space-wave and surface-wave radiation. This may be desirable, as in the case of planar antennas. For example, in Figure 1.1 [1], a planar antenna array is shown which makes use of microstrip open-end discontinuities as radiating elements. In the case of most circuit applications, radiation is undesirable because it can cause loss and extraneous coupling. Extraneous radiation and coupling may also adversely affect the performance of antennas. In the antenna shown in Figure 1.1, radiation ideally occurs from the open-end discontinuities. However, radiation from other parts of the circuit can occur as can coupling between radiating elements through both space wave and surface wave propagation. It is, therefore, necessary to include these effects in the design of the antenna.

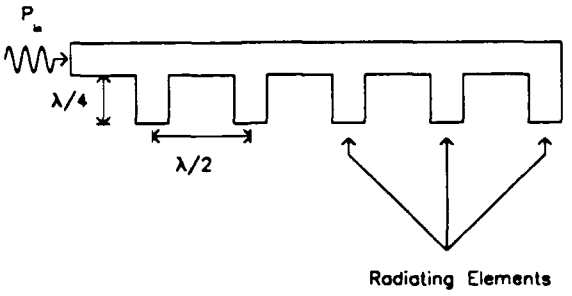

Figure 1.1: 5-Element Microstrip Combline Travelling-Wave Antenna

A grounded dielectric substrate can support both transverse magnetic (TM) and transverse electric (TE) surface wave modes of propagation. For electrically thin substrates ($d < .01\lambda$), surface waves are not strongly excited [2]. However, in the case of electrically thick substrates such as GaAs millimeter-wave integrated circuit (MMIC) substrates, the effects of surface waves are more prominent. The cutoff frequencies of the even TM and the odd TE surface wave modes of a grounded dielectric slab are given by [3]

$$f_{cn} = \frac{nc_0}{2d\sqrt{\epsilon_R - 1}}.$$

where d is the thickness of the substrate, ϵ_R is the relative dielectric constant of the substrate, c_0 is free space wave velocity and n is the order of the surface wave mode ($n = 0, 2, 4, \ldots$ for TM and $n = 1, 3, 5, \ldots$ for TE). In Table 1.1, the cutoff frequencies for the 4 lowest order surface wave modes are given for

mode	cutoff frequency	
	25 mil Alumina ($\epsilon_R = 9.9$)	25 mil GaAs ($\epsilon_R = 12.8$)
TM_0	DC	DC
TE_1	39.590 GHz	34.380 GHz
TM_2	79.180 GHz	68.770 GHz
TE_3	118.77 GHz	103.15 GHz

Table 1.1: Cutoff Frequencies for Surface-wave Modes of Conductor-backed Dielectric Slab

two widely used substrates. Because the TM_0 surface wave mode has no cutoff frequency, there is always at least one surface mode which can propagate on an open substrate. At millimeterwave frequencies, several surface wave modes may propagate. For example, in the upper K_a band (33 to 36 GHz), both TM_0 and TE_1 may propagate on a conductor backed 25 mil GaAs substrate. Surface wave excitation can result in losses and extraneous coupling in open planar circuits. The excess coupling may or may not be desirable depending on the application. However, because these effects become prominent at high frequencies, it is necessary to develop full-wave models so that they may be accounted for in the design of planar circuits and antennas.

1.2 Previous Work

Discontinuities in planar transmission lines have been the subject of numerous analytical investigations. Most of these analyses make use of quasi-static approximations [4]-[12]. These approximations limit the analysis to frequencies at which the dimensions of the circuit are small compared to a wavelength, and the effects of radiation may be neglected. This dissertation is concerned with the full-wave analysis of discontinuities in planar circuits on

open substrates. By full-wave analysis we mean that the method of analysis makes use of an exact Green's function[1] for a current source above a grounded dielectric slab. Thus the analysis includes the effects of space-wave and surface-wave radiation. It does not include the effects of conductor loss or conductor thickness.

Some work has already been done in the area of fullwave analysis of planar transmission line discontinuities. All of the work discussed below has in common the use of the exact Green's function for the grounded dielectric slab. The work may be divided into two categories, eigenvalue and deterministic approaches. The eigenvalue approach involves determining the eigenfrequencies of a resonant structure and then extracting the parameters of the discontinuity. For example, a long rectangular resonator may be analyzed in order to determine the characteristics of an open-end discontininuity [14]. First, the resonant frequencies of the resonator are determined. Then, from the resonant frequencies and the physical length of the resonator, the capacitance and conductance of the open-circuit discontinuity can be determined. The deterministic approach involves making use of a source formulation to excite a system. In the case of the open-end discontinuity, an incident wave may be used as the source formulation, and the complex reflection coefficient of the open-end may be solved for directly. Each method has specific advantages and disadvantages as described below.

[1]Several different Green's functions have been derived. See [13].

1.2.1 Eigenvalue Formulation

- The variational formulation reduces error introduced by inadequacies in basis functions.
- The determinant search is numerically expensive. In the case of a radiating structure, the eigenvalue becomes complex and the search two-dimensional.
- Network parameters are not directly determined. Instead, they must be inferred from resonant frequencies and Q values. This is inconvenient and can be numerically unstable.

1.2.2 Deterministic Formulation

- Network parameters may be directly calculated. Deterministic formulations allow for the direct calculation of scattering parameters or short-circuit parameters
- A determinant search is not required. The deterministic formulation requires only the filling and inverting of a single matrix.
- The formulation for the network parameters is not variational. Therefore, the error introduced through inadequate basis functions is not reduced.

Jackson and Pozar [15] analyzed microstrip open-end and symmetric gap discontinuities using a moment method in the spectral domain. They neglected transverse current flow on the strip and mode conversion. They made use of a travelling-wave source/load formulation. Katehi and Alexopolous [16]

also analyzed open-end and symmetric gap discontinuities using a moment method in the space domain. Their analysis was performed using a voltage-gap generator source formulation. They used approximations similar to those used by [15]. Boukamp and Jansen [17] have analyzed open-end discontinuities in a covered but laterally open environment using a moment method in the spectral domain. Their analysis included the effects of transverse current flow on the strip but not the effects of mode conversion. They made use of a travelling-wave source formulation similar to [15]. Yang and Alexopolous [18] analyzed open-end and gap discontinuities in an open microstrip with a dielectric superstrate using a spectral domain moment method and a travelling-wave source formulation. Drissi et al [19, 20] analyzed symmetric gap discontinuities in open microstrip using a space domain moment method applied to the mixed potential integral equation. Although it is not made clear in their paper, they seem to have included the effects of two-component current flow and mode conversion. They used a voltage-gap source formulation similar to [16].

Jackson [21] has analyzed open circuit discontinuities in coplanar waveguide. Yang [22] has analyzed short-circuit slotline discontinuities using a moment method in the spectral domain. He assumed a purely transverse electric field in the slot.

1.3 Organization of This Report

The remainder of this report is organized as follows. In Chapter 2, the theory underlying the method is presented. The details of the numerical computation, including the selection of basis functions and techniques to speed

up the numerical integration, are given in Chapter 3. In Chapter 4, the method is applied to the microstrip open-end discontinuity. In Chapter 5, the method is applied to the short circuit slotline discontinuity. In Chapter 6, the method is applied to the microstrip gap discontinuity and the gap-coupled resonator. Finally, in Chapter 7, some conclusions are drawn and suggestions for improvements to the method are made. Also, further applications of the method are proposed. The Green's functions used in the analysis are derived using the immitance approach [13] in Appendices 1 and 2.

Chapter 2

THEORY

In this chapter we present the theory underlying the deterministic spectral domain analysis. Only the theory common to all of the analysis will be presented here; the details of the analysis as it applies to specific discontinuities will be presented in subsequent chapters. We begin by developing the integral equation which will form the basis for all of the analysis in this study.

2.1 Integral Equation Formulation

In this section, we develop the integral equation appropriate for the analysis of microstrip line and microstrip discontinuities. Referring to the coordinate system in Figure 2.1, the electric field in the plane $y = d$ due to currents localized in the plane $y = d$ can be expressed as the convolution of a source current and a Green's function. The components of the Green's function represent the x and z directed electric field due to a z-directed and an x-directed infinitesimal horizontal current element (Hertzian dipole) over a grounded dielectric slab of infinite extent. Since the Green's function is actually a dyadic, we write two equations, one for the z-directed electric field and one for the x-directed field.

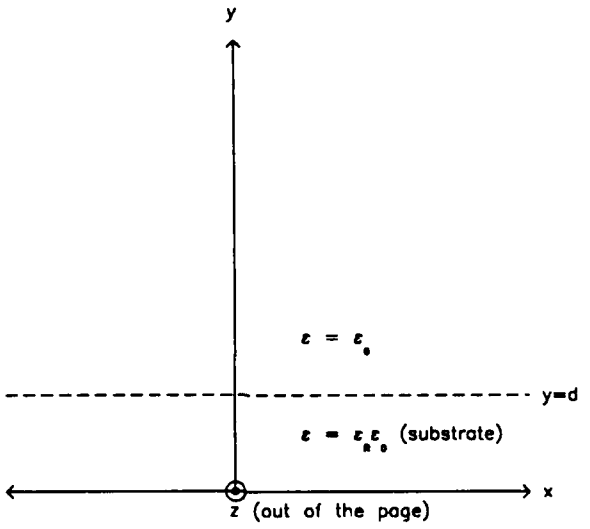

Figure 2.1: Coordinate System for Dielectric Slab

$$E_z(x,d,z) = \int_{x_0}\int_{z_0} Z_{zz}(x-x_0,z-z_0)J_z(x_0,z_0)\,dx_0\,dz_0 + \int_{x_0}\int_{z_0} Z_{zx}(x-x_0,z-z_0)J_x(x_0,z_0)\,dx_0\,dz_0 \quad (2.1)$$

$$E_x(x,d,z) = \int_{x_0}\int_{z_0} Z_{xz}(x-x_0,z-z_0)J_z(x_0,z_0)\,dx_0\,dz_0 + \int_{x_0}\int_{z_0} Z_{xx}(x-x_0,z-z_0)J_x(x_0,z_0)\,dx_0\,dz_0 \quad (2.2)$$

In order to develop the integral equation, we enforce the boundary condition requiring that the components of the tangential electric field, E_z and E_x, be zero on the conductor.

$$\int_{x_0}\int_{z_0} Z_{zz}(x-x_0,z-z_0)J_z(x_0,z_0)\,dx_0\,dz_0$$

$$+ \int_{x_0}\int_{z_0} Z_{zx}(x-x_0, z-z_0) J_x(x_0, z_0)\, dx_0\, dz_0 = 0 \text{ for } x, z \in S. \quad (2.3)$$

$$\int_{x_0}\int_{z_0} Z_{xz}(x-x_0, z-z_0) J_z(x_0, z_0)\, dx_0\, dz_0$$

$$+ \int_{x_0}\int_{z_0} Z_{xx}(x-x_0, z-z_0) J_x(x_0, z_0)\, dx_0\, dz_0 = 0 \text{ for } x, z \in S. \quad (2.4)$$

These equations constitute a set of coupled integral equations for the unknown current on the conductor. These two equations together are equivalent to the electric field integral equation (EFIE). They are Fredholm equations of the first type [24]; that is, the unknown functions, $J_z(x_0, z_0)$ and $J_x(x_0, z_0)$ appear only in the integrands. At this point we can transform the coupled integral equations into coupled algebraic equations in the spectral domain as in [26] by making use of the convolution theorem [24].

$$\tilde{Z}_{zz}(\alpha,\beta)\tilde{J}_z(\alpha,\beta) + \tilde{Z}_{zx}(\alpha,\beta)\tilde{J}_x(\alpha,\beta) = \tilde{E}_z(\alpha,\beta) \quad (2.5)$$

$$\tilde{Z}_{xz}(\alpha,\beta)\tilde{J}_z(\alpha,\beta) + \tilde{Z}_{xx}(\alpha,\beta)\tilde{J}_x(\alpha,\beta) = \tilde{E}_x(\alpha,\beta) \quad (2.6)$$

The following convention is used for the Fourier transform.

$$\tilde{F}(\alpha,\beta) = \int_{-\infty}^{+\infty}\int_{-\infty}^{+\infty} F(x,z)\exp(+j\beta z)\exp(+j\alpha x)dxdz \quad (2.7)$$

$$F(x,z) = \frac{1}{(2\pi)^2}\int_{-\infty}^{+\infty}\int_{-\infty}^{+\infty} \tilde{F}(\alpha,\beta)\exp(-j\beta z)\exp(-j\alpha x)\, d\alpha\, d\beta \quad (2.8)$$

However, although this is the usual method, it does not make any difference at which point in the analysis we transform to the spectral domain. Notice at this point the coupled algebraic equations contain the unknown functions $\tilde{J}_z(\alpha,\beta)$, $\tilde{J}_x(\alpha,\beta)$, $\tilde{E}_z(\alpha,\beta)$, and $\tilde{E}_x(\alpha,\beta)$. So it appears we have introduced two more unknown functions by transforming into the spectral domain. However, it will

be seen that the functions $\tilde{E}_z(\alpha,\beta)$, and $\tilde{E}_x(\alpha,\beta)$ will be eliminated in the solution process. Whether we choose to solve the coupled integral equations in the space domain or the coupled algebraic equations in the spectral domain, we must solve for unknown functions. To do this we make use of the method of moments to solve the coupled integral equations (in the space domain) or coupled algebraic equations (in the spectral domain). Since it is easier to visualize the problem in the space domain, we will proceed from the coupled integral equations.

2.2 The Application of the Method of Moments

As pointed out in the previous section, the coupled space-domain integral equations and the coupled spectral domain algebraic equations contain unknown functions. Therefore, the first step in solving the equations is to expand the unknown current in an appropriate set of known expansion functions.

$$J_z(x_0,z_0) = \sum_1^M a_m J_{zm}^{expa}(x_0,z_0), \text{ and}$$

$$J_x(x_0,z_0) = \sum_1^M b_m J_{xm}^{expa}(x_0,z_0),$$

where a_m and b_m are unknown constants. The required expansion functions are dependant on the particular problem. They will be discussed in detail in Chapter 3. In the deterministic formulation, in addition to the unknown current we also have a known source current the z-directed and x-directed components of which are given by

$$J_z^{source}(x_0,z_0) \text{ and}$$

$$J_x^{source}(x_0,z_0) \text{ respectively.}$$

Upon substitution into the EFIE we obtain

$$\int_{x_0}\int_{z_0} Z_{zz}(x-x_0,z-z_0)\left[\sum_1^M a_m J_{zm}^{expa}(x_0,z_0)+J_z^{source}(x_0,z_0)\right]dx_0\,dz_0$$
$$+\int_{x_0}\int_{z_0} Z_{zx}(x-x_0,z-z_0)\left[\sum_1^M b_m J_{xm}^{expa}(x_0,z_0)+J_x^{source}(x_0,z_0)\right]dx_0\,dz_0=0$$
$$x,z\in S, \text{ and} \tag{2.9}$$

$$\int_{x_0}\int_{z_0} Z_{xz}(x-x_0,z-z_0)\left[\sum_1^M a_m J_{zm}^{expa}(x_0,z_0)+J_z^{source}(x_0,z_0)\right]dx_0\,dz_0$$
$$+\int_{x_0}\int_{z_0} Z_{xx}(x-x_0,z-z_0)\left[\sum_1^M b_m J_{xm}^{expa}(x_0,z_0)+J_x^{source}(x_0,z_0)\right]dx_0\,dz_0=0$$
$$x,z\in S. \tag{2.10}$$

So we have a set of two coupled integral equations with 2M unknown constants. In order to generate a linear system of equations, we test the set of equations using an appropriate set of testing functions.

$$J_{z1}^{test}(x,z)\ldots J_{zN}^{test}(x,z).$$
$$J_{x1}^{test}(x,z)\ldots J_{xN}^{test}(x,z).$$

As with the expansion functions, the appropriate testing functions depend on the particular problem. These will be discussed in detail in Chapter 3. The testing functions are used to generate $2N$ equations as follows.

$$
\begin{aligned}
&\int_x \int_z J_{z1}^{test}(x,z) \int_{x_0} \int_{z_0} \\
&\quad \cdot \left[Z_{zz}(x-x_0, z-z_0) \left(\sum_1^M a_m J_{zm}^{expa}(x_0,z_0) + J_z^{source}(x_0,z_0) \right) \right. \\
&\quad + \left. Z_{zx}(x-x_0, z-z_0) \left(\sum_1^M b_m J_{xm}^{expa}(x_0,z_0) + J_x^{source}(x_0,z_0) \right) \right] \\
&\qquad dx_0\, dz_0\, dx\, dz = 0 \\
&\quad \vdots \\
&\int_x \int_z J_{zN}^{test}(x,z) \int_{x_0} \int_{z_0} \\
&\quad \cdot \left[Z_{zz}(x-x_0, z-z_0) \left(\sum_1^M a_m J_{zm}^{expa}(x_0,z_0) + J_z^{source}(x_0,z_0) \right) \right. \\
&\quad + \left. Z_{zx}(x-x_0, z-z_0) \left(\sum_1^M b_m J_{xm}^{expa}(x_0,z_0) + J_x^{source}(x_0,z_0) \right) \right] \\
&\qquad dx_0\, dz_0\, dx\, dz = 0 \\
&\int_x \int_z J_{x1}^{test}(x,z) \int_{x_0} \int_{z_0} \\
&\quad \cdot \left[Z_{xz}(x-x_0, z-z_0) \left(\sum_1^M a_m J_{zm}^{expa}(x_0,z_0) + J_z^{source}(x_0,z_0) \right) \right. \\
&\quad + \left. Z_{xx}(x-x_0, z-z_0) \left(\sum_1^M b_m J_{xm}^{expa}(x_0,z_0) + J_x^{source}(x_0,z_0) \right) \right] \\
&\qquad dx_0\, dz_0\, dx\, dz = 0 \\
&\quad \vdots \\
&\int_x \int_z J_{xN}^{test}(x,z) \int_{x_0} \int_{z_0} \\
&\quad \cdot \left[Z_{xz}(x-x_0, z-z_0) \left(\sum_1^M a_m J_{zm}^{expa}(x_0,z_0) + J_z^{source}(x_0,z_0) \right) \right. \\
&\quad + \left. Z_{xx}(x-x_0, z-z_0) \left(\sum_1^M b_m J_{xm}^{expa}(x_0,z_0) + J_x^{source}(x_0,z_0) \right) \right] \\
&\qquad dx_0\, dz_0\, dx\, dz = 0
\end{aligned}
\tag{2.11}
$$

In the space domain, the right-hand side of the integral equation is zero because the electric field is zero on the conductor. However, the corresponding spectral domain algebraic equation is not zero because the Fourier transform covers the entire $y = d$ plane. In the eigenvalue approach [26], Parseval's theorem is used to show that the right-hand side of the tested equations is zero. The same situation exists for the excitation case. Note here that the right-hand side of the tested space-domain equations is zero. If we had tested the equations in the spectral domain, the right-hand side would still be zero by Parseval's theorem. The source term is embedded in the left-hand side of the equation. In some situations it will be desirable to use a different number of testing functions than expansion functions to generate an overdetermined system of equations. In the case of an excitation problem, in general, it is not possible to make use of Galerkin's method[1].

The tested equations result in a linear system

$$\begin{bmatrix} [K_{zz}] & [K_{zx}] \\ [K_{xz}] & [K_{xx}] \end{bmatrix} \begin{bmatrix} [a] \\ [b] \end{bmatrix} = \begin{bmatrix} [S_z] \\ [S_x] \end{bmatrix},$$

where $[a]$ and $[b]$ are vectors of length M containing the unknown constants $a_1 \ldots a_M$ and $b_1 \ldots b_M$ in the expansions for J_x and J_z, $[K_{zz}] \ldots [K_{xx}]$ are $M \times N$ matrices given in the space domain by

[1] Actually, while it is not possible to apply Galerkin's method to a deterministic problem using a travelling wave source formulation, it is possible to do so when a localized source is used. For example a planar dipole driven by a current source at the center could be analyzed using Galerkin's method because the current exists only over a finite area.

$$K_{ij}^{zz} = \int_{-\infty}^{+\infty}\int_{-\infty}^{+\infty}\int_{-\infty}^{+\infty}\int_{-\infty}^{+\infty} J_{zi}^{test}(x,z) Z_{zz}(x-x_0, z-z_0) \cdot J_{zj}^{expa}(x_0,z_0)\, dx\, dz\, dx_0\, dz_0, \tag{2.12}$$

$$K_{ij}^{zx} = \int_{-\infty}^{+\infty}\int_{-\infty}^{+\infty}\int_{-\infty}^{+\infty}\int_{-\infty}^{+\infty} J_{zi}^{test}(x,z) Z_{zx}(x-x_0, z-z_0) \cdot J_{xj}^{expa}(x_0,z_0)\, dx\, dz\, dx_0\, dz_0, \tag{2.13}$$

$$K_{ij}^{xz} = \int_{-\infty}^{+\infty}\int_{-\infty}^{+\infty}\int_{-\infty}^{+\infty}\int_{-\infty}^{+\infty} J_{xi}^{test}(x,z) Z_{xz}(x-x_0, z-z_0) \cdot J_{zj}^{expa}(x_0,z_0)\, dx\, dz\, dx_0\, dz_0, \text{ and} \tag{2.14}$$

$$K_{ij}^{xx} = \int_{-\infty}^{+\infty}\int_{-\infty}^{+\infty}\int_{-\infty}^{+\infty}\int_{-\infty}^{+\infty} J_{xi}^{test}(x,z) Z_{xx}(x-x_0, z-z_0) \cdot J_{xj}^{expa}(x_0,z_0)\, dx\, dz\, dx_0\, dz_0 \tag{2.15}$$

and $[S_z]$ and $[S_x]$ are vectors of length M given by

$$S_i^z = -\int_{-\infty}^{+\infty}\int_{-\infty}^{+\infty}\int_{-\infty}^{+\infty}\int_{-\infty}^{+\infty} J_{zi}^{test}(x,z) Z_{zz}(x-x_0, z-z_0) \cdot J_z^{source}(x_0,z_0)\, dx\, dz\, dx_0\, dz_0 - \int_{-\infty}^{+\infty}\int_{-\infty}^{+\infty}\int_{-\infty}^{+\infty}\int_{-\infty}^{+\infty} J_{zi}^{test}(x,z) Z_{zx}(x-x_0, z-z_0) \cdot J_x^{source}(x_0,z_0)\, dx\, dz\, dx_0\, dz_0, \text{ and} \tag{2.16}$$

$$S_i^x = -\int_{-\infty}^{+\infty}\int_{-\infty}^{+\infty}\int_{-\infty}^{+\infty}\int_{-\infty}^{+\infty} J_{xi}^{test}(x,z) Z_{xz}(x-x_0, z-z_0) \cdot J_z^{source}(x_0,z_0)\, dx\, dz\, dx_0\, dz_0 - \int_{-\infty}^{+\infty}\int_{-\infty}^{+\infty}\int_{-\infty}^{+\infty}\int_{-\infty}^{+\infty} J_{xi}^{test}(x,z) Z_{xx}(x-x_0, z-z_0) \cdot J_x^{source}(x_0,z_0)\, dx\, dz\, dx_0\, dz_0. \tag{2.17}$$

However, since the Green's function is only available in closed form in the spectral domain, these integrals are six-dimensional and therefore extremely

expensive to evaluate. Some work has been performed to reduce this complexity [16]. In order to transform the integrals into the spectral domain, we express the space domain Green's function as the inverse Fourier transform of its spectral domain counterpart. For example

$$Z_{zz}(x-x_0, z-z_0) = \int_{-\infty}^{+\infty}\int_{-\infty}^{+\infty} \tilde{Z}_{zz}(\alpha,\beta)\exp(-j\beta(x-x_0)) \cdot \exp(-j\alpha(z-z_0))d\alpha d\beta \quad (2.18)$$

We then substitute this expression into the integral to obtain

$$K_{ij}^{zz} = \int_{-\infty}^{+\infty}\int_{-\infty}^{+\infty}\int_{-\infty}^{+\infty}\int_{-\infty}^{+\infty} J_{zi}^{test}(x,z) \cdot \int_{-\infty}^{+\infty}\int_{-\infty}^{+\infty} \tilde{Z}_{zz}(\alpha,\beta)\exp(-j\beta(x-x_0))\exp(-j\alpha(z-z_0))d\alpha d\beta \cdot J_{zj}^{expa}(x_0,z_0)\,dx\,dz\,dx_0\,dz_0. \quad (2.19)$$

Rearranging the order of integration, we obtain

$$K_{ij}^{zz} = \int_{-\infty}^{+\infty}\int_{-\infty}^{+\infty}\left[\int_{-\infty}^{+\infty}\int_{-\infty}^{+\infty} J_{zi}^{test}(x,z)\exp(-j\beta x)\exp(-j\alpha z)dx\,dz \cdot \tilde{Z}_{zz}(\alpha,\beta) \int_{-\infty}^{+\infty}\int_{-\infty}^{+\infty} J_{zj}^{expa}(x_0,z_0)\exp(j\beta x_0)\exp(j\alpha z_0)dx_0\,dz_0\right] d\alpha d\beta. \quad (2.20)$$

We recognize that

$$\tilde{J}_{zi}^{test*}(\alpha,\beta) = \int_{-\infty}^{+\infty}\int_{-\infty}^{+\infty} J_{zi}^{test}(x,z)\exp(-j\beta x)\exp(-j\alpha z)dx\,dz, \text{ and} \quad (2.21)$$

$$\tilde{J}_{zj}^{expa}(\alpha,\beta) = \int_{-\infty}^{+\infty}\int_{-\infty}^{+\infty} J_{zj}^{expa}(x_0,z_0)\exp(j\beta x_0)\exp(j\alpha z_0)dx_0\,dz_0. \quad (2.22)$$

Therefore, in the spectral domain, $[K_{zz}] \ldots [K_{xx}]$ are given by[2]

$$K_{zz(i,j)} = \int_{-\infty}^{+\infty}\int_{-\infty}^{+\infty} \tilde{J}_{zi}^{test*}(\alpha,\beta)\tilde{Z}_{zz}(\alpha,\beta)\tilde{J}_{zj}^{expa}(\alpha,\beta)\, d\alpha\, d\beta, \tag{2.23}$$

$$K_{zx(i,j)} = \int_{-\infty}^{+\infty}\int_{-\infty}^{+\infty} \tilde{J}_{zi}^{test*}(\alpha,\beta)\tilde{Z}_{zx}(\alpha,\beta)\tilde{J}_{xj}^{expa}(\alpha,\beta)\, d\alpha\, d\beta, \tag{2.24}$$

$$K_{xz(i,j)} = \int_{-\infty}^{+\infty}\int_{-\infty}^{+\infty} \tilde{J}_{xi}^{test*}(\alpha,\beta)\tilde{Z}_{xz}(\alpha,\beta)\tilde{J}_{zj}^{expa}(\alpha,\beta)\, d\alpha\, d\beta, \text{ and} \tag{2.25}$$

$$K_{xx(i,j)} = \int_{-\infty}^{+\infty}\int_{-\infty}^{+\infty} \tilde{J}_{xi}^{test*}(\alpha,\beta)\tilde{Z}_{xx}(\alpha,\beta)\tilde{J}_{xj}^{expa}(\alpha,\beta) d\alpha\, d\beta. \tag{2.26}$$

and $[S_z]$ and $[S_x]$ are vectors of length M given by

$$\begin{aligned} S_i^z = & \int_{-\infty}^{+\infty}\int_{-\infty}^{+\infty} \tilde{J}_{zi}^{test*}(\alpha,\beta)\tilde{Z}_{zz}(\alpha,\beta)\tilde{J}_{z}^{source}(\alpha,\beta)\, d\alpha\, d\beta \\ & + \int_{-\infty}^{+\infty}\int_{-\infty}^{+\infty} \tilde{J}_{zi}^{test*}(\alpha,\beta)\tilde{Z}_{zx}(\alpha,\beta)\tilde{J}_{x}^{source}(\alpha,\beta)\, d\alpha\, d\beta, \text{ and} \end{aligned} \tag{2.27}$$

$$\begin{aligned} S_i^x = & \int_{-\infty}^{+\infty}\int_{-\infty}^{+\infty} \tilde{J}_{xi}^{test*}(\alpha,\beta)\tilde{Z}_{xz}(\alpha,\beta)\tilde{J}_{z}^{source}(\alpha,\beta)\, d\alpha\, d\beta \\ & + \int_{-\infty}^{+\infty}\int_{-\infty}^{+\infty} \tilde{J}_{xi}^{test*}(\alpha,\beta)\tilde{Z}_{xx}(\alpha,\beta)\tilde{J}_{x}^{source}(\alpha,\beta)\, d\alpha\, d\beta. \end{aligned} \tag{2.28}$$

The linear system is now solved for $a_1 \ldots a_M$ and $b_1 \ldots b_M$ using Gaussian elimination if the system is square. If the system is overdetermined we generate

$$\begin{bmatrix} [K_{zz}][K_{zx}] \\ [K_{xz}][K_{xx}] \end{bmatrix}^T \begin{bmatrix} [K_{zz}][K_{zx}] \\ [K_{xz}][K_{xx}] \end{bmatrix} \begin{bmatrix} [a] \\ [b] \end{bmatrix} = \begin{bmatrix} [K_{zz}][K_{zx}] \\ [K_{xz}][K_{xx}] \end{bmatrix}^T \begin{bmatrix} [S_z] \\ [S_x] \end{bmatrix},$$

[2]Notice that in the formulation given here, the convention for the Fourier transform is the opposite of that used in [15]. Therefore, the conjugation in the inner products is performed on the testing functions as opposed to the expansion functions.

where the superscript "T" denotes the transpose of a matrix. We can then solve the resultant $2M \times 2M$ linear system of equations. This is equivalent to a least squares formulation.

2.3 The Green's Function

The characteristics of the Green's function are important because much information may be derived from them. The spectral domain Green's functions used in the following analysis are derived using the immittance approach [26] in Appendices 1 and 2.

The spectral domain Green's function for the grounded dielectric slab is given by

$$\tilde{Z}_{zz} = -N_z^2 \tilde{Z}^e - N_x^2 \tilde{Z}^h, \tag{2.29}$$

$$\tilde{Z}_{zx} = -N_z N_x (\tilde{Z}^e - \tilde{Z}^h), \tag{2.30}$$

$$\tilde{Z}_{xz} = -N_z N_x (\tilde{Z}^e - \tilde{Z}^h) \text{ and,} \tag{2.31}$$

$$\tilde{Z}_{xx} = -N_x^2 \tilde{Z}^e - N_z^2 \tilde{Z}^h, \tag{2.32}$$

where

$$N_z = \frac{\beta}{\sqrt{\alpha^2 + \beta^2}}, \tag{2.33}$$

$$N_x = \frac{\alpha}{\sqrt{\alpha^2 + \beta^2}}, \tag{2.34}$$

$$\tilde{Z}^e = \frac{1}{\tilde{Y}_1^e + \tilde{Y}_2^e}, \tag{2.35}$$

$$\tilde{Z}^h = \frac{1}{\tilde{Y}_1^h + \tilde{Y}_2^h}, \tag{2.36}$$

$$\tilde{Y}_1^e = \tilde{Y}_{TM1}, \tag{2.37}$$

$$\tilde{Y}_2^e = \tilde{Y}_{TM2}\coth(\gamma_2 d), \tag{2.38}$$

$$\tilde{Y}_1^h = \tilde{Y}_{TE1}, \tag{2.39}$$

$$\tilde{Y}_2^h = \tilde{Y}_{TE2}\coth(\gamma_2 d), \tag{2.40}$$

$$\tilde{Y}_{TM1} = \frac{j\omega\epsilon_0}{\gamma_1}, \tag{2.41}$$

$$\tilde{Y}_{TM2} = \frac{j\omega\epsilon_R\epsilon_0}{\gamma_2}, \tag{2.42}$$

$$\tilde{Y}_{TE1} = \frac{\gamma_1}{j\omega\mu}, \tag{2.43}$$

$$\tilde{Y}_{TE2} = \frac{\gamma_2}{j\omega\mu}, \tag{2.44}$$

$$\gamma_1 = \sqrt{\alpha^2+\beta^2-k^2} \text{ and}, \tag{2.45}$$

$$\gamma_2 = \sqrt{\alpha^2+\beta^2-\epsilon_R k^2}. \tag{2.46}$$

It can be seen that the components of the Green's function have poles corresponding to the poles of $\tilde{Z}^e$ and $\tilde{Z}^h$. The poles of $\tilde{Z}^e$ correspond to the TM surface waves, and the poles of $\tilde{Z}^h$ correspond to the TE surface waves. The poles occur when

$$\epsilon_R\gamma_1 + \gamma_2\tanh(\gamma_2 d) = 0, \text{ and} \tag{2.47}$$

$$\gamma_1 + \gamma_2\coth(\gamma_2 d) = 0. \tag{2.48}$$

In order to facilitate the study of the surface wave poles, we perform a change of variables defined by

$$\rho = \sqrt{\alpha^2+\beta^2}, \text{ and} \tag{2.49}$$

$$\theta = \tan^{-1}\left(\frac{\alpha}{\beta}\right). \tag{2.50}$$

We note that $\tilde{Z}^e$ and $\tilde{Z}^h$ are functions of ρ only. In this polar coordinate

Region	Range	γ_1	γ_2
1	$\rho < k$	imaginary	imaginary
2	$k < \rho < \sqrt{\epsilon_R}k$	real	imaginary
3	$\sqrt{\epsilon_R}k < \rho$	real	real

Table 2.1: Regions of the Radial Wavenumber, ρ

system, the integrals take the following form.

$$K_{zz(i,j)} = \int_0^{+\infty}\int_0^{2\pi} \tilde{J}_{zi}^{test*}(\rho,\theta)\tilde{Z}_{zz}(\rho,\theta)\tilde{J}_{zj}^{expa}(\rho,\theta)\rho\, d\rho\, d\theta \qquad (2.51)$$

$$\vdots$$

Now we define three regions as in Table 2.3. All of the surface wave poles occur in region 2. This is occurs because, in order for a surface wave mode to exist, the field outside the slab must be evanescent in the y-direction while the field inside must be a standing wave in the y-direction. The values of ρ at which the surface wave poles occur are the values of the propagation constants for the surface wave modes. In order to evaluate the integrals, we must circumvent the poles. The contributions of the poles are included via the calculation of the residues at the poles. We can show that the poles are of the first order. Using the integration path given in Figure 2.2 and the Cauchy's residue theorem, we can show that when only the TM_0 mode can propagate, $K_{zz(i,j)} \ldots K_{xx(i,j)}$ are given by

$$\begin{aligned} K_{zz(i,j)} &= \int_0^{\rho_{TM0}-\delta}\int_0^{2\pi} \tilde{J}_{zi}^{test*}(\rho,\theta)\tilde{Z}_{zz}(\rho,\theta)\tilde{J}_{zj}^{expa}(\rho,\theta)\,\rho d\rho\, d\theta \\ &- i\pi Res \int_0^{2\pi} \left(\tilde{J}_{zi}^{test*}(\rho,\theta)\tilde{Z}_{zz}(\rho,\theta)\tilde{J}_{zj}^{expa}(\rho,\theta)\right)|_{\rho=\rho_{TM0}} d\theta \end{aligned}$$

$$+ \int_{\rho_{TM0}+\delta}^{+\infty} \int_{0}^{2\pi} \tilde{J}_{zi}^{test*}(\rho,\theta)\tilde{Z}_{zz}(\rho,\theta)\tilde{J}_{zj}^{expa}(\rho,\theta)\,\rho d\rho\, d\theta \tag{2.52}$$

$$\vdots$$

The singularity occurs only in the Green's function, so we write

$$\begin{aligned} K_{zz(i,j)} &= \int_{0}^{\rho_{TM0}-\delta} \int_{0}^{2\pi} \tilde{J}_{zi}^{test*}(\rho,\theta)\tilde{Z}_{zz}(\rho,\theta)\tilde{J}_{zj}^{expa}(\rho,\theta)\, d\alpha\, d\beta \\ &- i\pi \int_{0}^{2\pi} \tilde{J}_{zi}^{test*}(\rho,\theta)\tilde{Z}_{zzTM}(\rho,\theta)\tilde{J}_{zj}^{expa}(\rho,\theta)\, d\alpha\, d\beta \\ &+ \int_{\rho_{TM0}+\delta}^{\infty} \int_{0}^{2\pi} \tilde{J}_{zi}^{test*}(\rho,\theta)\tilde{Z}_{zz}(\rho,\theta)\tilde{J}_{zj}^{expa}(\rho,\theta)\, d\alpha\, d\beta, \end{aligned} \tag{2.53}$$

$$\begin{aligned} K_{zx(i,j)} &= \int_{0}^{\rho_{TM0}-\delta} \int_{0}^{2\pi} \tilde{J}_{zi}^{test*}(\rho,\theta)\tilde{Z}_{zx}(\rho,\theta)\tilde{J}_{xj}^{expa}(\rho,\theta)\, d\alpha\, d\beta \\ &- i\pi \int_{0}^{2\pi} \tilde{J}_{zi}^{test*}(\rho,\theta)\tilde{Z}_{zxTM}(\rho,\theta)\tilde{J}_{xj}^{expa}(\rho,\theta)\, d\alpha\, d\beta \\ &+ \int_{\rho_{TM0}+\delta}^{\infty} \int_{0}^{2\pi} \tilde{J}_{zi}^{test*}(\rho,\theta)\tilde{Z}_{zx}(\rho,\theta)\tilde{J}_{xj}^{expa}(\rho,\theta)\, d\alpha\, d\beta, \end{aligned} \tag{2.54}$$

$$\begin{aligned} K_{xz(i,j)} &= \int_{0}^{\rho_{TM0}-\delta} \int_{0}^{2\pi} \tilde{J}_{xi}^{test*}(\rho,\theta)\tilde{Z}_{xz}(\rho,\theta)\tilde{J}_{zj}^{expa}(\rho,\theta)\, d\alpha\, d\beta \\ &- i\pi \int_{0}^{2\pi} \tilde{J}_{xi}^{test*}(\rho,\theta)\tilde{Z}_{xzTM}(\rho,\theta)\tilde{J}_{zj}^{expa}(\rho,\theta)\, d\alpha\, d\beta \\ &+ \int_{\rho_{TM0}+\delta}^{\infty} \int_{0}^{2\pi} \tilde{J}_{xi}^{test*}(\rho,\theta)\tilde{Z}_{xz}(\rho,\theta)\tilde{J}_{zj}^{expa}(\rho,\theta)\, d\alpha\, d\beta, \text{ and} \end{aligned} \tag{2.55}$$

$$K_{xx(i,j)} = \int_{0}^{\rho_{TM0}-\delta} \int_{0}^{2\pi} \tilde{J}_{xi}^{test*}(\rho,\theta)\tilde{Z}_{xx}(\rho,\theta)\tilde{J}_{xj}^{expa}(\rho,\theta)\, d\alpha\, d\beta$$

$$- \quad i\pi \int_0^{2\pi} \tilde{J}_{xi}^{test*}(\rho,\theta)\tilde{Z}_{xxTM}(\rho,\theta)\tilde{J}_{xj}^{expa}(\rho,\theta)\, d\alpha\, d\beta$$

$$+ \int_{\rho_{TM0}+\delta}^{\infty} \int_0^{2\pi} \tilde{J}_{xi}^{test*}(\rho,\theta)\tilde{Z}_{xx}(\rho,\theta)\tilde{J}_{xj}^{expa}(\rho,\theta)\, d\alpha\, d\beta \qquad (2.56)$$

where

$$\tilde{Z}_{zzTM} = -N_z^2 \tilde{Z}_{TM}^e, \qquad (2.57)$$

$$\tilde{Z}_{zxTM} = -N_z N_x \tilde{Z}_{TM}^e, \qquad (2.58)$$

$$\tilde{Z}_{xzTM} = -N_z N_x \tilde{Z}_{TM}^e, \qquad (2.59)$$

$$\tilde{Z}_{xxTM} = -N_x^2 \tilde{Z}_{TM}^e, \qquad (2.60)$$

$$\tilde{Z}_{TM}^e = \frac{1}{\frac{\partial \tilde{Y}_1^e}{\partial \rho} + \frac{\partial \tilde{Y}_2^e}{\partial \rho}}, \qquad (2.61)$$

$$\frac{\partial \tilde{Y}_1^e}{\partial \rho} = \left(\frac{-\rho}{\gamma_1^2}\right) \tilde{Y}_1^e(\rho), \text{ and} \qquad (2.62)$$

$$\frac{\partial \tilde{Y}_2^e}{\partial \rho} = \left(\frac{-\rho}{\gamma_2^2}\right) \left(\tilde{Y}_2^e(\rho) + \tilde{Y}_{TM2} d\gamma_2 (\coth^2(\gamma_1 d) - 1)\right) \qquad (2.63)$$

For TE modes the residue is given by

$$\tilde{Z}_{zzTE} = -N_x^2 \tilde{Z}_{TE}^h, \qquad (2.64)$$

$$\tilde{Z}_{zxTE} = +N_z N_x \tilde{Z}_{TE}^h, \qquad (2.65)$$

$$\tilde{Z}_{xzTE} = +N_z N_x \tilde{Z}_{TE}^h \text{ and,} \qquad (2.66)$$

$$\tilde{Z}_{xxTE} = -N_z^2 \tilde{Z}_{TE}^h \qquad (2.67)$$

where

$$\tilde{Z}_{TE}^h = \frac{1}{\frac{\partial \tilde{Y}_1^h}{\partial \rho} + \frac{\partial \tilde{Y}_2^h}{\partial \rho}}, \qquad (2.68)$$

$$\frac{\partial \tilde{Y}_1^h}{\partial \rho} = \left(\frac{\rho}{\gamma_1^2}\right) \tilde{Y}_1^h(\rho)., \text{ and} \tag{2.69}$$

$$\frac{\partial \tilde{Y}_2^h}{\partial \rho} = \left(\frac{\rho}{\gamma_2^2}\right) \left(\tilde{Y}_2^h(\rho) + \tilde{Y}_{TE2} d\gamma_2 (\coth^2(\gamma_2 d) - 1)\right). \tag{2.70}$$

It should also be noted that the Green's function has a branch point at $\rho = k_0$. However, the Green's function is bounded at the branch point and therefore, no numerical difficulty is encountered except the correct choice of Riemann sheets. This amounts to choosing γ_1 to be positive real for $\rho > k_0$ and positive imaginary for $\rho < k_0$. There is no branch point at $\rho = \sqrt{\epsilon_R} k_0$. This is because γ_2 always appears with $\coth(\gamma_2 d)$ in the Green's function thus cancelling the sign of γ_2. Therefore, the sign of γ_2 need not be specified. The pole in the Green's function corresponding to a particular surface-wave mode occurs at the branch point at the cutoff frequency of the mode and then migrates toward $\epsilon_R k_0$ with increasing frequency. Therefore, the surface wave poles occur in the order

$$k_0 < \ldots \rho_{TE3} < \rho_{TM2} < \rho_{TE1} < \rho_{TM0} < \sqrt{\epsilon_R} k_0 \tag{2.71}$$

2.4 Eigenvalue Formulation

The eigenvalue formulation is used here to analyze a uniform line. We assume that the current on the line is of the form

$$J_z(x,z) = J_z(x) \exp(-j\beta_z z) \tag{2.72}$$

$$J_x(x,z) = J_x(x) \exp(-j\beta_z z) \tag{2.73}$$

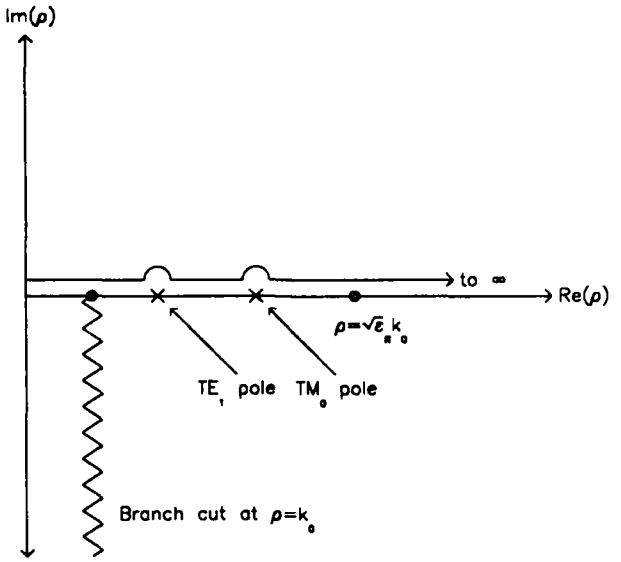

Figure 2.2: Integration Path

We make use of a Galerkin method, that is we make the testing functions identical to the expansion functions. Then we generate the determinant of the coefficient matrix. This determinant is a function of β. We determine $\beta = \beta_z$ such that the determinant is zero. This is equivalent to solving the nonlinear equation for β

$$\begin{vmatrix} [K_{zz}] & [K_{zx}] \\ [K_{xz}] & [K_{xx}] \end{vmatrix} = 0.$$

This equation is solved using an interval halving technique. Once β_z is known, we determine the transverse dependance of the current from the eigenvectors. The calculation of the characteristic impedance is not unique because the fundamental mode is not perfectly TEM. Two definitions are possible.

$$Z_0 \equiv \frac{P_z}{I_z^2} \tag{2.74}$$

$$Z_0 \equiv \frac{V^2}{P_z} \tag{2.75}$$

where P_z is the z-directed power flow, I_z is the z-directed current flow, and V is the potential between the strip and the ground plane. We use the first definition because V is not unique. The z-directed current on the strip is given by

$$J_z = \int_{-w/2}^{w/2} J_z(x)dx. \tag{2.76}$$

The z-directed power flow is given by

$$P_z = \mathrm{Re}\left[\int_0^{\infty}\int_{-\infty}^{\infty} (\mathbf{E}(x,y) \times \mathbf{H}^*(x,y)) \cdot \hat{\mathbf{z}}\, dx\, dy\right]. \tag{2.77}$$

The x-portion of the integration may be transformed into the spectral domain through the use of Parseval's theorem.

$$\begin{aligned} P_z &= \frac{1}{2\pi}\mathrm{Re}\left[\int_0^{\infty}\int_{-\infty}^{\infty} (\tilde{\mathbf{E}}(\alpha,y) \times \tilde{\mathbf{H}}^*(\alpha,y)) \cdot \hat{\mathbf{z}}\, d\alpha\, dy\right] \qquad (2.78) \\ &= \frac{1}{2\pi}\mathrm{Re}\int_d^{\infty}\int_{-\infty}^{\infty} \left[(\tilde{E}_{x1}(\alpha,y)\tilde{H}^*_{y1}(\alpha,y) - \right. \\ &\quad \left. \tilde{E}_{y1}(\alpha,y)\tilde{H}^*_{x1}(\alpha,y))\, d\alpha\, dy\right] \\ &+ \frac{1}{2\pi}\mathrm{Re}\int_0^{d}\int_{-\infty}^{\infty} \left[(\tilde{E}_{x2}(\alpha,y)\tilde{H}^*_{y2}(\alpha,y) - \right. \\ &\quad \left. \tilde{E}_{y2}(\alpha,y)\tilde{H}^*_{x2}(\alpha,y))\, d\alpha\, dy\right] \qquad (2.79) \end{aligned}$$

where

$$\begin{aligned} \tilde{E}_{x1}(\alpha,y) &= \tilde{E}^0_{x1}(\alpha)\exp(-\gamma_1 y), \\ \tilde{E}_{y1}(\alpha,y) &= \tilde{E}^0_{y1}(\alpha)\exp(-\gamma_1 y), \end{aligned}$$

$$
\begin{aligned}
\tilde{H}_{x1}(\alpha, y) &= \tilde{H}^0_{x1}(\alpha)\exp(-\gamma_1 y), \\
\tilde{H}_{y1}(\alpha, y) &= \tilde{H}^0_{y1}(\alpha)\exp(-\gamma_1 y), \\
\tilde{E}_{x2}(\alpha, y) &= \tilde{E}^0_{x2}(\alpha)\sinh(\gamma_2 y), \\
\tilde{E}_{y2}(\alpha, y) &= \tilde{E}^0_{y2}(\alpha)\cosh(\gamma_2 y), \\
\tilde{H}_{x2}(\alpha, y) &= \tilde{H}^0_{x2}(\alpha)\cosh(\gamma_2 y), \\
\tilde{H}_{y2}(\alpha, y) &= \tilde{H}^0_{y2}(\alpha)\sinh(\gamma_2 y), \\
\tilde{E}^0_{x1}(\alpha) &= -r(\frac{\gamma_1}{\tilde{y}_1})B_e + qB_h, \\
\tilde{E}^0_{y1}(\alpha) &= (\frac{j}{\tilde{y}_1})B_e \\
\tilde{H}^0_{x1}(\alpha) &= qB_e + r(\frac{\gamma_1}{\tilde{z}_1})B_h, \\
\tilde{H}^0_{y1}(\alpha) &= (\frac{j}{\tilde{z}_1})B_h, \\
\tilde{E}^0_{x2}(\alpha) &= r\frac{\gamma_2}{\tilde{2}}A_e + qA_h, \\
\tilde{E}^0_{y2}(\alpha) &= \frac{j}{\tilde{y}_2}A_e, \\
\tilde{H}^0_{x2}(\alpha) &= -qA_e + r\frac{\gamma_2}{\tilde{z}_2}A_h, \\
\tilde{H}^0_{y2}(\alpha) &= (\frac{1}{\tilde{z}_2})A_h, \\
r &= \frac{\alpha}{\rho^2}, \\
q &= \frac{\beta}{\rho^2}, \\
\tilde{y}_1 &= j\omega\epsilon_0, \\
\tilde{y}_2 &= j\omega\epsilon_0\epsilon_R, \\
\tilde{z}_1 &= j\omega\mu, \\
\tilde{z}_2 &= j\omega\mu,
\end{aligned}
$$

$$
\begin{aligned}
A_e &= \frac{1}{C_1}\frac{\gamma_1}{\tilde{y}_1}\tilde{J}_v(\alpha)\rho, \\
A_h &= \frac{1}{C_2}\frac{z_1}{\gamma 1}\tilde{J}_u(\alpha)\rho, \\
B_e &= D_1\frac{\gamma_2}{\tilde{y}_2}\tilde{J}_v(\alpha)\rho, \\
B_h &= D_2\frac{z_1}{\gamma_1}\tilde{J}_u(\alpha)\rho, \\
C_1 &= \frac{\gamma_2}{\tilde{y}_2}\sinh(\gamma_2 d) + \frac{\gamma_1}{\tilde{y}_1}\cosh(\gamma_2 d), \\
C_2 &= \sinh(\gamma_2 d) + \frac{\tilde{z}_1}{\gamma_1}\frac{\gamma_2}{\tilde{z}_2}\cosh(\gamma_2 d), \\
D_1 &= \frac{\exp(\gamma_1 d)\sinh(\gamma_2 d)}{C_1}, \\
D_2 &= \frac{\exp(\gamma_1 d)\sinh(\gamma_2 d)}{C_2}, \\
\tilde{J}_u(\alpha) &= N_x\tilde{J}_z(\alpha) - N_z\tilde{J}_x(\alpha), \text{ and} \\
\tilde{J}_v(\alpha) &= N_z\tilde{J}_z(\alpha) + N_x\tilde{J}_x(\alpha).
\end{aligned}
$$

The y-integration is simple and may be done in closed form. Therefore, we may write

$$P_z = \frac{1}{2\pi}\mathrm{Re}\left[\int_{-\infty}^{\infty}(\tilde{S}_1(\alpha) + \tilde{S}_2(\alpha))d\alpha\right] \tag{2.80}$$

where

$$\tilde{S}_1 = \left(\frac{1}{2\gamma_1}\right)\left(\tilde{E}^0_{x1}(\alpha)\tilde{H}^{0*}_{y1}(\alpha) - \tilde{E}^0_{y1}(\alpha)\tilde{H}^{0*}_{x1}(\alpha)\right)\exp(-2\gamma_1 d), \text{ and} \tag{2.81}$$

$$\begin{aligned}
\tilde{S}_2 &= [\frac{1}{2}][\tilde{E}^0_{x2}(\alpha)\tilde{H}^{0*}_{y2}(\alpha)\mathrm{sgn}(\gamma_2)[\frac{1}{\gamma_2}\sinh(\gamma_2 d)\cosh(\gamma_2 d) - d] \\
&- \tilde{E}^0_{y2}(\alpha)\tilde{H}^{0*}_{x2}(\alpha)[\frac{1}{\gamma_2}\sinh(\gamma_2 d)\cosh(\gamma_2 d) + d]].
\end{aligned} \tag{2.82}$$

where sgn is 1 when γ_2 is real and -1 when γ_2 is imaginary. The α integration is done numerically.

2.5 Source Formulation

The source formulation is the crucial part of this method. The source formulation affects the accuracy and efficiency of the method and the ease of determining network parameters. Several source formulations have been proposed. The one used here appears to have first been used by [17]. It was later, perhaps independently, proposed by [15]. This method involves the use of a traveling-wave formulation. First, a spectral domain eigenvalue method is used to determine the propagation constant and current distribution for a uniform line. Then this information is used to derive the source function, which consists of an incident current wave.

$$J_z^{source}(x,z) = \sum_{l=1}^{L} a_l J_{zl}(x) \exp(-j\beta z) \tag{2.83}$$

$$J_x^{source}(x,z) = \sum_{l=1}^{L} b_l J_{xl}(x) \exp(-j\beta z) \tag{2.84}$$

The functions J_{zm} and J_{xn} are the Maxwellian basis functions which will be discussed in the next chapter. They include the proper edge condition for the longitudinal and transverse current at the edges of the microstrip. The constants $a_1 \ldots a_L$, $b_1 \ldots b_L$, and β, the propagation constant, are determined in the spectral domain eigenvalue analysis.

Although in scattering formalism the source is postulated as an incoming wave from $z = -\infty$, the source function is truncated at some point in order to facilitate the numerical integration of the inner products.[3] We will now

[3]It is not necessary that the source functions be truncated in order for the innner products to exist. This will be discussed in Chapter 3.

show why the integrals may be truncated while maintaining the correctness of the formulation.

Consider the electric field generated by a traveling wave on an infinite line. For simplicity, consider only longitudinal current on the line.

$$E_z = \int_{x_0}\int_{x_0} Z_{zz}(x-x_0, z-z_0)\sum_{l=1}^{L} a_l J_{zl}(x_0)\exp(-j\beta_z z_0)dx_0 dz_0 \quad (2.85)$$

In the spectral domain this becomes

$$\tilde{E}_z(\alpha,\beta) = \tilde{Z}_{zz}(\alpha,\beta)\sum_{l=1}^{L} a_l \tilde{J}_{zm}(\alpha)\delta(\beta_z). \quad (2.86)$$

Therefore, after testing we have,

$$\int_{-\infty}^{+\infty}\int_{-\infty}^{+\infty} \tilde{J}_z^{test}(\alpha,\beta)\tilde{Z}_{zz}(\alpha,\beta)\tilde{J}_z^{expa}(\alpha,\beta)d\alpha d\beta \quad (2.87)$$

$$= \int_{-\infty}^{+\infty} \tilde{J}_z^{test}(\alpha,\beta_z)\tilde{Z}_{zz}(\alpha,\beta_z)\tilde{J}_z^{expa}(\alpha,\beta_z)d\alpha$$

by the sifting theorem. In the eigenvalue formulation we determined β such that

$$\int_{-\infty}^{+\infty} \tilde{J}_z^{test}(\alpha)\tilde{Z}_{zz}(\alpha,\beta_z)\tilde{J}_z^{expa}(\alpha)d\alpha = 0. \quad (2.88)$$

So we see that a traveling wave on an infinite line automatically satisfies the integral equation for the electric field. Likewise, a standing wave on an infinite line satisfies the same conditions. It seems reasonable to assume that a traveling wave on a finite line satisfies this condition far away from any discontinuities. Therefore, if we consider an incident wave on a semi-infinite microstrip line from $-\infty$, the electric field is given by

$$
\begin{aligned}
E_z(x,d,z) &= \int_{-w}^{+w}\int_{-\infty}^{0} Z_{zz}(x-x_0,z-z_0)J_z(x_0,z_0)\,dx_0\,dz_0 \\
&+ \int_{-w}^{+w}\int_{-\infty}^{0} Z_{zx}(x-x_0,z-z_0)J_x(x_0,z_0)\,dx_0\,dz_0 \\
&= \int_{-w}^{+w}\int_{-\infty}^{-z_L} Z_{zz}(x-x_0,z-z_0)J_z(x_0,z_0)\,dx_0\,dz_0 \\
&+ \int_{-w}^{+w}\int_{-\infty}^{-z_L} Z_{zx}(x-x_0,z-z_0)J_x(x_0,z_0)\,dx_0\,dz_0 \\
&+ \int_{-w}^{w}\int_{-z_L}^{0} Z_{zz}(x-x_0,z-z_0)J_z(x_0,z_0)\,dx_0\,dz_0 \\
&+ \int_{-w}^{w}\int_{-z_L}^{0} Z_{zx}(x-x_0,z-z_0)J_x(x_0,z_0)\,dx_0\,dz_0, \text{ and} \qquad (2.89)
\end{aligned}
$$

$$
\begin{aligned}
E_x(x,d,z) &= \int_{-w}^{+w}\int_{-\infty}^{0} Z_{zz}(x-x_0,z-z_0)J_z(x_0,z_0)\,dx_0\,dz_0 \\
&+ \int_{-w}^{+w}\int_{-\infty}^{0} Z_{xx}(x-x_0,z-z_0)J_x(x_0,z_0)\,dx_0\,dz_0 \\
&= \int_{-w}^{+w}\int_{-\infty}^{-z_L} Z_{xz}(x-x_0,z-z_0)J_z(x_0,z_0)\,dx_0\,dz_0 \\
&+ \int_{-w}^{+w}\int_{-\infty}^{-z_L} Z_{xx}(x-x_0,z-z_0)J_x(x_0,z_0)\,dx_0\,dz_0 \\
&+ \int_{-w}^{+w}\int_{-z_L}^{0} Z_{xz}(x-x_0,z-z_0)J_z(x_0,z_0)\,dx_0\,dz_0 \\
&+ \int_{-w}^{+w}\int_{-z_L}^{0} Z_{xx}(x-x_0,z-z_0)J_x(x_0,z_0)\,dx_0\,dz_0. \qquad (2.90)
\end{aligned}
$$

If $z >> -z_L$, then the integrals extending from $-\infty$ to $-z_L$ approach zero.

Therefore, it is equivalent to define the Fourier transform of the travelling wave current as

$$\tilde{J}(\alpha,\beta) = \int_{-\infty}^{+\infty}\int_{-z_L}^{0} J(x,z)\exp(j\alpha x)\exp(j\beta z)dx\,dz. \tag{2.91}$$

This analysis may be extended to the two-dimensional case simply by noting that the uniform line current is the homogeneous solution. Therefore, it may be added to the unknown current without affecting the problem.

The reflected wave and, in the case of a multiport, the transmitted wave(s) may be treated in a similar manner. The point at which the functions are truncated affects the rapidity of the convergence of the integrals. This will be discussed in the next chapter.

The equation is tested in order to enforce the boundary condition, $\vec{E}_{tan} = 0$ on the strip. The test region must extend far enough from the discontinuity that scattered field is taken into account. However, it must not extend too close to the point at which the uniform functions are truncated.

Chapter 3

DETAILS OF THE NUMERICAL COMPUTATION

This chapter deals with the details of the computation. Because full-wave methods such as the one presented here are computationally intensive, it is necessary to take advantage of all available numerical labor-saving devices. Therefore, we will discuss the following aspects of the computation.

- The choice of expansion and testing functions;
- The use of symmetry properties in the reduction of the numerical integration;
- The use of symmetry properties in filling of the impedance matrix;
- The conditioning of the integrands through the extraction of the singularities associated with the surface-wave poles;
- The truncation of the traveling wave functions for optimum convergence;
- The acceleration of convergence of the integrals through the extraction of asymptotic forms;
- The details of the computational algorithm.

3.1 Expansion and Testing Functions

The number of basis functions required may be minimized if basis functions represent the current on the conductors as closely as possible. The computational effort may thus be reduced significantly. The basis functions should exhibit the proper edge singularities, boundary conditions, and symmetry. Since the computations are to be performed in the spectral domain, it is desirable to be able to obtain the Fourier transforms in closed form. Both entire domain and subsectional basis functions are used in this study. Two-dimensional basis functions are expressed as separable products of a one dimensional function of x and a one dimensional function of z.

$$J_z^{expa}(x,z) = J_{z(x)}^{expa}(x)J_{z(z)}^{expa}(z) \tag{3.1}$$

$$J_z^{test}(x,z) = J_{z(x)}^{test}(x)J_{z(z)}^{test}(z) \tag{3.2}$$

$$J_x^{expa}(x,z) = J_{x(x)}^{expa}(x)J_{x(z)}^{expa}(z) \tag{3.3}$$

$$J_x^{test}(x,z) = J_{x(x)}^{test}(x)J_{x(z)}^{test}(z) \tag{3.4}$$

Therefore, the Fourier transforms are expressed as separable products of α and β.

$$\tilde{J}_z^{expa}(\alpha,\beta) = \tilde{J}_{z(\alpha)}^{expa}(\alpha)\tilde{J}_{z(\beta)}^{expa}(\beta) \tag{3.5}$$

$$\tilde{J}_z^{test}(\alpha,\beta) = \tilde{J}_{z(\alpha)}^{test}(\alpha)\tilde{J}_{z(\beta)}^{test}(\beta) \tag{3.6}$$

$$\tilde{J}_x^{expa}(\alpha,\beta) = \tilde{J}_{x(\alpha)}^{expa}(\alpha)\tilde{J}_{x(\beta)}^{expa}(\beta) \tag{3.7}$$

$$\tilde{J}_x^{test}(\alpha,\beta) = \tilde{J}_{x(\alpha)}^{test}(\alpha)\tilde{J}_{x(\beta)}^{test}(\beta) \tag{3.8}$$

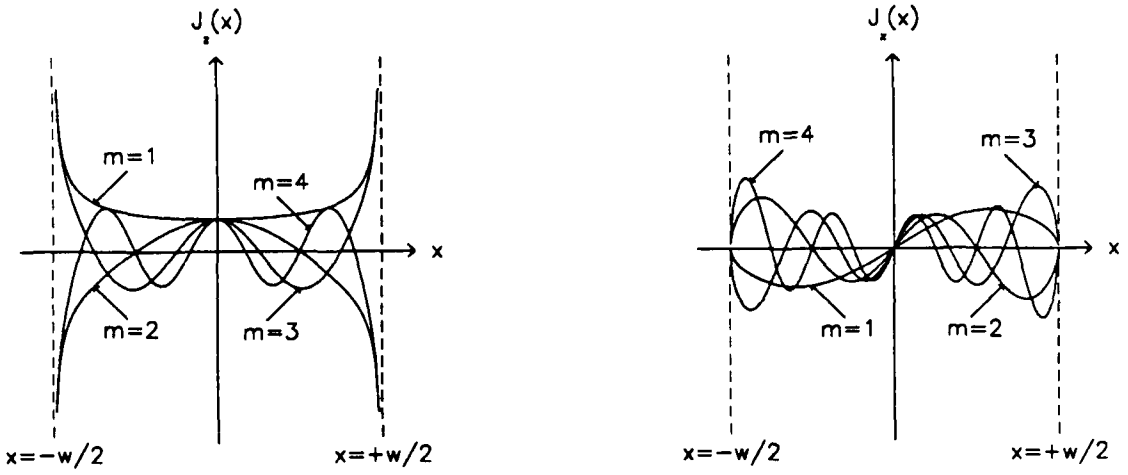

Figure 3.1: The Maxwellian Functions

3.1.1 Analysis of Uniform Microstrip Line

In the one-dimensional analysis of uniform microstrip line, entire domain basis functions and Galerkin's method were used. The Maxwellian basis functions were chosen to represent the transverse dependance of the current on the uniform portions of the conductors. These functions exhibit the proper symmetry and accurately include the effects of edge conditions.

$$J_{zm}(x) = \frac{\cos(\frac{2(m-1)\pi x}{w})}{\sqrt{1-(\frac{2x}{w})^2}} \tag{3.9}$$

$$J_{xm}(x) = \frac{\sin(\frac{2m\pi x}{w})}{\sqrt{1-(\frac{2x}{w})^2}} \tag{3.10}$$

The one-dimensional Maxwellian basis functions are shown in Figure 3.1. This choice has been shown [26] to give very accurate results with a minimal number

of functions due to the variational formulation.

3.1.2 Analysis of Discontinuities

When analyzing discontinuities, two-dimensional basis functions in which entire domain functions were used to describe the transverse dependance of the current and subsectional basis functions were used to describe the longitudinal dependance. The Maxwellian functions described above were used for the transverse dependance. Several types of subdomain functions were used for the longitudinal dependance. It was found that piecewise linear (overlapping rooftop) functions allowed approximate satisfaction of all types of edge conditions encountered. These functions are shown in Figure 3.2.

$$J_{PWLn}(z) = \left(\frac{h-|z-z_n|}{h}\right) \tag{3.11}$$

$$J_{zmn}(x,z) = \left(\frac{h-|z-z_n|}{h}\right)\frac{\cos(\frac{2(m-1)\pi x}{w})}{\sqrt{1-(\frac{2x}{w})^2}} \tag{3.12}$$

$$J_{xmn}(x,z) = \left(\frac{h-|z-z_n|}{h}\right)\frac{\sin(\frac{2m\pi x}{w})}{\sqrt{1-(\frac{2x}{w})^2}} \tag{3.13}$$

For example, the two-dimensional basis functions, $J_{z1n}(x,z)$ and $J_{x1n}(x,z)$, are shown in Figure 3.3 and Figure 3.4.

Travelling and standing waves were modelled by combining two two-dimensional basis functions in which the Maxwellian functions were used for the transverse dependance and sinusoidal functions for longitudinal dependance.

$$J_{zsin}(x,z) = \sin(\beta_z z)\frac{\cos(\frac{2(m-1)\pi x}{w})}{\sqrt{1-(\frac{2x}{w})^2}} \tag{3.14}$$

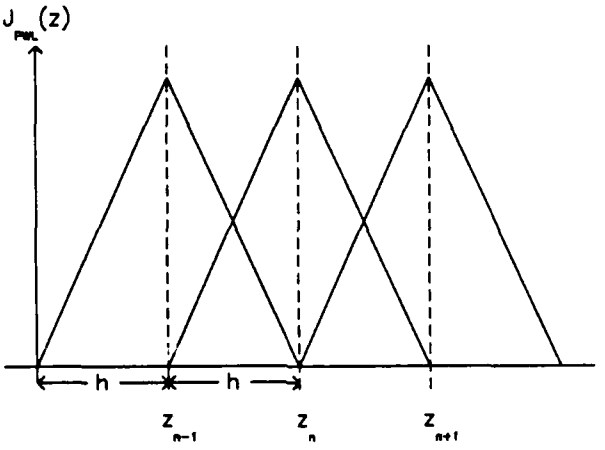

Figure 3.2: Piecewise Linear Functions

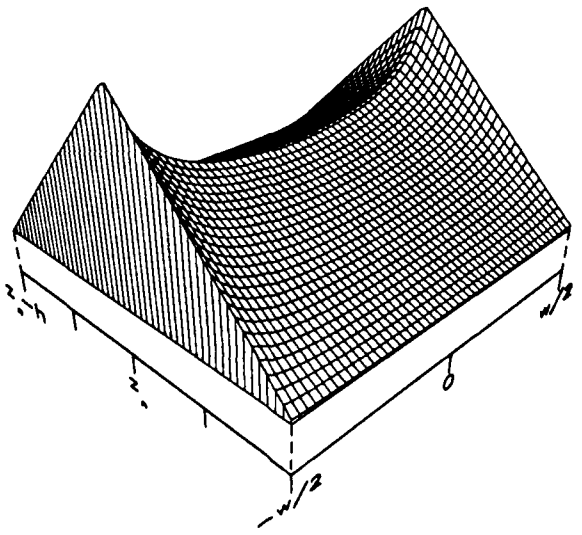

Figure 3.3: The 2-dimensional Basis Function, $J_{z1n}(x, z)$

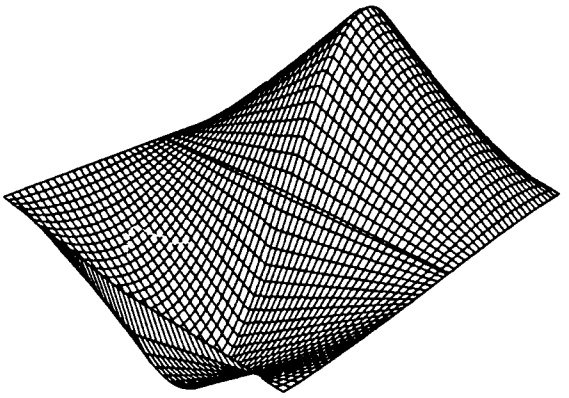

Figure 3.4: The 2-dimensional Basis Function, $J_{x1n}(x,z)$

$$J_{xsin}(x,z) = \sin(\beta_z z)\frac{\sin(\frac{2m\pi x}{w})}{\sqrt{1-(\frac{2x}{w})^2}} \tag{3.15}$$

For example, a positive travelling wave can be made up of two phase-shifted sine/Maxwellian functions.

$$\exp(j\beta_z z) = \cos(\beta_z z) - j\sin(\beta_z z) \tag{3.16}$$

$$= \sin(\beta_z z - \frac{\pi}{2}) - j\sin(\beta_z z) \tag{3.17}$$

The truncation of the sine function is detailed in section 3.5.

3.2 Symmetry Properties of the Green's Function

The spectral domain Green's function has the symmetry properties given in Table 3.2. Because all of the expansion and testing functions used are

Component	Symmetry
$\tilde{Z}_{zz}(\alpha,\beta)$	even wrt α wrt β
$\tilde{Z}_{zx}(\alpha,\beta)$	odd wrt α wrt β
$\tilde{Z}_{xz}(\alpha,\beta)$	odd wrt α wrt β
$\tilde{Z}_{xx}(\alpha,\beta)$	even wrt α wrt β

Table 3.1: Symmetry Properties of the Green's Function

purely real in the space domain, the real parts of their Fourier transforms are even functions and the imaginary parts are odd. Because of these symmetry properties, we can reduce the range of integration. The real parts of the Fourier transforms of the basis functions are always even, and the imaginary parts are always odd. Thus the integration reduces to

$$
\begin{aligned}
K_{zz(i,j)} &= \int_{-\infty}^{+\infty}\int_{-\infty}^{+\infty} \tilde{J}^{test*}_{zi}(\alpha,\beta)\tilde{Z}_{zz}(\alpha,\beta)\tilde{J}^{expa}_{zj}(\alpha,\beta)\,d\alpha\,d\beta \\
&= \int_{0}^{+\infty}\int_{0}^{+\infty} \tilde{Z}_{zz}(\alpha,\beta) \\
&\quad \Big(\mathrm{Re}\left[\tilde{J}^{test}_{z(\alpha)i}(\alpha)\right]\mathrm{Re}\left[\tilde{J}^{expa}_{z(\alpha)j}(\alpha)\right] \\
&\quad + \mathrm{Im}\left[\tilde{J}^{test}_{z(\alpha)i}(\alpha)\right]\mathrm{Im}\left[\tilde{J}^{expa}_{z(\alpha)j}(\alpha)\right]\Big) \\
&\quad \Big(\mathrm{Re}\left[\tilde{J}^{test}_{z(\beta)i}(\beta)\right]\mathrm{Re}\left[\tilde{J}^{expa}_{z(\beta)j}(\beta)\right] \\
&\quad + \mathrm{Im}\left[\tilde{J}^{test}_{z(\beta)i}(\beta)\right]\mathrm{Im}\left[\tilde{J}^{expa}_{z(\beta)j}(\beta)\right]\Big)\,d\alpha\,d\beta, \qquad (3.18) \\
K_{zx(i,j)} &= \int_{-\infty}^{+\infty}\int_{-\infty}^{+\infty} \tilde{J}^{test}_{zi}(\alpha,\beta)\tilde{Z}_{zz}(\alpha,\beta)\tilde{J}^{expa}_{xj}(\alpha,\beta)\,d\alpha\,d\beta \\
&= \int_{0}^{+\infty}\int_{0}^{+\infty} \tilde{Z}_{zx}(\alpha,\beta) \\
&\quad \Big(\mathrm{Re}\left[\tilde{J}^{test}_{z(\alpha)i}(\alpha)\right]\mathrm{Im}\left[\tilde{J}^{expa}_{x(\alpha)j}(\alpha)\right] \\
&\quad - \mathrm{Im}\left[\tilde{J}^{test}_{z(\alpha)i}(\alpha)\right]\mathrm{Re}\left[\tilde{J}^{expa}_{x(\alpha)j}(\alpha)\right]\Big)
\end{aligned}
$$

$$\left(\mathrm{Re}\left[\tilde{J}^{test}_{z(\beta)_i}(\beta)\right]\mathrm{Im}\left[\tilde{J}^{expa}_{x(\beta)_j}(\beta)\right]\right.$$
$$\left.-\,\mathrm{Im}\left[\tilde{J}^{test}_{z(\beta)_i}(\beta)\right]\mathrm{Re}\left[\tilde{J}^{expa}_{x(\beta)_j}(\beta)\right]\right)\,d\alpha\,d\beta, \tag{3.19}$$

$$K_{xz(i,j)} = \int_{-\infty}^{+\infty}\int_{-\infty}^{+\infty}\tilde{J}^{test}_{xi}(\alpha,\beta)\tilde{Z}_{xz}(\alpha,\beta)\tilde{J}^{expa}_{zj}(\alpha,\beta)\,d\alpha\,d\beta$$
$$= \int_{0}^{+\infty}\int_{0}^{+\infty}\tilde{Z}_{xz}(\alpha,\beta)$$
$$\left(\mathrm{Re}\left[\tilde{J}^{test}_{x(\alpha)_i}(\alpha)\right]\mathrm{Im}\left[\tilde{J}^{expa}_{z(\alpha)_j}(\alpha)\right]\right.$$
$$\left.-\,\mathrm{Im}\left[\tilde{J}^{test}_{x(\alpha)_i}(\alpha)\right]\mathrm{Re}\left[\tilde{J}^{expa}_{z(\alpha)_j}(\alpha)\right]\right)$$
$$\left(\mathrm{Re}\left[\tilde{J}^{test}_{x(\beta)_i}(\beta)\right]\mathrm{Im}\left[\tilde{J}^{expa}_{z(\beta)_j}(\beta)\right]\right.$$
$$\left.-\,\mathrm{Im}\left[\tilde{J}^{test}_{x(\beta)_i}(\beta)\right]\mathrm{Re}\left[\tilde{J}^{expa}_{z(\beta)_j}(\beta)\right]\right)\,d\alpha\,d\beta, \text{ and} \tag{3.20}$$

$$K_{xx(i,j)} = \int_{-\infty}^{+\infty}\int_{-\infty}^{+\infty}\tilde{J}^{test}_{xi}(\alpha,\beta)\tilde{Z}_{xx}(\alpha,\beta)\tilde{J}^{expa}_{xj}(\alpha,\beta)\,d\alpha\,d\beta$$
$$= \int_{0}^{+\infty}\int_{0}^{+\infty}\tilde{Z}_{xx}(\alpha,\beta)$$
$$\left(\mathrm{Re}\left[\tilde{J}^{test}_{x(\alpha)_i}(\alpha)\right]\mathrm{Re}\left[\tilde{J}^{expa}_{x(\alpha)_j}(\alpha)\right]\right.$$
$$\left.+\,\mathrm{Im}\left[\tilde{J}^{test}_{x(\alpha)_i}(\alpha)\right]\mathrm{Im}\left[\tilde{J}^{expa}_{x(\alpha)_j}(\alpha)\right]\right)$$
$$\left(\mathrm{Re}\left[\tilde{J}^{test}_{x(\beta)_i}(\beta)\right]\mathrm{Re}\left[\tilde{J}^{expa}_{x(\beta)_j}(\beta)\right]\right.$$
$$\left.+\,\mathrm{Im}\left[\tilde{J}^{test}_{x(\beta)_i}(\beta)\right]\mathrm{Im}\left[\tilde{J}^{expa}_{x(\beta)_j}(\beta)\right]\right)\,d\alpha\,d\beta, \tag{3.21}$$

3.3 Symmetry Properties of the Matrix

A large savings of computational effort can be obtained by taking advantage of the symmetry properties of the matrix. In general, the portion of the matrix generated with Galerkin's method applied to the identical shifted subdomain expansion functions is Toeplitz or anti-Toeplitz. That is the matrix

is of the form

$$\begin{pmatrix} T_1 & T_2 & T_3 & T_4 \\ T_{-2} & T_1 & T_2 & T_3 \\ T_{-3} & T_{-4} & T_1 & T_2 \\ T_{-4} & T_{-3} & T_{-2} & T_1 \end{pmatrix}$$

This symmetry exists because the elements depend only on the difference of centers of the testing and expansion functions. For example

$$K_{zz(i,j)} = \int_0^{+\infty}\int_0^{+\infty} \tilde{Z}_{zz}(\alpha,\beta) (\tilde{J}^{test}_{z(\alpha)i}(\alpha)\tilde{J}^{expa}_{z(\alpha)j}(\alpha) \tilde{J}^2_{z(\beta)0}(\beta) cos\,(\beta|z_{test} - z_{expa}|)\; d\alpha\, d\beta \tag{3.22}$$

$$K_{zx(i,j)} = \int_0^{+\infty}\int_0^{+\infty} \tilde{Z}_{zx}(\alpha,\beta) (\tilde{J}^{test}_{z(\alpha)i}(\alpha)\tilde{J}^{expa}_{x(\alpha)j}(\alpha) \tilde{J}^2_{z(\beta)0}(\beta) sin\,(\beta(z_{test} - z_{expa}))\; d\alpha\, d\beta \tag{3.23}$$

$$K_{xz(i,j)} = \int_0^{+\infty}\int_0^{+\infty} \tilde{Z}_{xz}(\alpha,\beta) (\tilde{J}^{test}_{x(\alpha)i}(\alpha)\tilde{J}^{expa}_{z(\alpha)j}(\alpha) \tilde{J}^2_{z(\beta)0}(\beta) sin\,(\beta(z_{test} - z_{expa}))\; d\alpha\, d\beta \tag{3.24}$$

$$K_{xx(i,j)} = \int_0^{+\infty}\int_0^{+\infty} \tilde{Z}_{xx}(\alpha,\beta) (\tilde{J}^{test}_{x(\alpha)i}(\alpha)\tilde{J}^{expa}_{x(\alpha)j}(\alpha) \tilde{J}^2_{z(\beta)0}(\beta) cos\,(\beta|z_{test} - z_{expa}|)\; d\alpha\, d\beta \tag{3.25}$$

Therefore, for K_{zz} and K_{xx}, $T_{-n} = T_n$ (Toeplitz). For K_{zx} and K_{xz}, $T_{-n} = -T_n$ (Anti-Toeplitz). In general, portions of the matrix which are not Toeplitz are still symmetric about the principle diagonal due to reciprocity. Furthermore, the zx and xz matrices are identical due to reciprocity.

3.4 Surface Wave Poles

As was pointed out in Chapter 2, the spectral domain Green's function has poles corresponding to TM and TE surface waves. These poles are the solution to the nonlinear equations

$$\epsilon_R \gamma_1 + \gamma_2 \tanh(\gamma_2 d) = 0, \text{ and} \tag{3.26}$$

$$\gamma_1 + \gamma_2 \coth(\gamma_2 d) = 0. \tag{3.27}$$

These equations are solved using an interval-halving routine. The location of the surface-wave poles must be known accurately. It has been found that the location of the poles must be known to 7 significant digits [16]. This accuracy is easily obtained, however, using the interval-halving method.

3.4.1 Extraction of Surface Wave Poles

As pointed out in Chapter 2, surface wave pole(s) can occur in the integrands. It is possible to evaluate the integrals as given in Chapter 2. In this case, δ should be on the order of $.01k_0$. However, evaluating the integral in the neighborhood of these poles is very difficult. Therefore, it is desirable to develop a technique by which these poles may be extracted leaving a well-behaved integrand. This may be done by taking the -1 term of a Laurent series for the integrand about the surface wave pole. Also, as pointed out in Chapter 2, all of the surface wave poles occur in the range $k < \rho < \epsilon_R k$. Therefore we may write

$$\int_0^{\infty}\int_0^{2\pi} \frac{N(\theta,\rho)}{D(\rho)}\, d\rho\, d\theta = \int_0^{k}\int_0^{2\pi} \frac{N(\theta,\rho)}{D(\rho)}\, d\rho\, d\theta$$

$$+ \int_{k}^{\sqrt{\epsilon_R}k} \int_{0}^{2\pi} \left(\frac{N(\theta,\rho)}{D(\rho)} - \frac{R_{TM0}(\rho_{TM0})}{\rho - \rho_{TM0}} \right) d\rho\, d\theta$$

$$+ \int_{\epsilon_R k}^{\infty} \int_{0}^{2\pi} \frac{N(\theta,\rho)}{D(\rho)}\, d\rho\, d\theta \qquad (3.28)$$

$$\begin{aligned}
K_{zz(i,j)} &= \int_{0}^{k_0} \int_{0}^{2\pi} \tilde{J}_{zi}^{test*}(\rho,\theta)\tilde{Z}_{zz}(\rho,\theta)\tilde{J}_{zj}^{expa}(\rho,\theta)\, d\alpha\, d\beta \\
&+ \int_{k_0}^{\rho_{TM0}-\delta} \int_{0}^{2\pi} \left(\tilde{J}_{zi}^{test*}(\rho,\theta)\tilde{Z}_{zz}(\rho,\theta)\tilde{J}_{zj}^{expa}(\rho,\theta) - \frac{R_{TMzz}}{\rho - \rho_{TM0}} \right) d\alpha\, d\beta \\
&+ \int_{\rho_{TM0}+\delta}^{\sqrt{\epsilon_R}k_0} \int_{0}^{2\pi} \left(\tilde{J}_{zi}^{test*}(\rho,\theta)\tilde{Z}_{zz}(\rho,\theta)\tilde{J}_{zj}^{expa}(\rho,\theta) - \frac{R_{TMzz}}{\rho - \rho_{TM0}} \right) d\alpha\, d\beta \\
&+ \int_{\sqrt{\epsilon_R}k_0}^{\infty} \int_{0}^{2\pi} \tilde{J}_{zi}^{test*}(\rho,\theta)\tilde{Z}_{zz}(\rho,\theta)\tilde{J}_{zj}^{expa}(\rho,\theta)\, d\alpha\, d\beta \\
&+ \left(\ln\left(\frac{\sqrt{\epsilon_R}k_0 - \rho_{TM0}}{k_0 - \rho_{TM0}} \right) - i\pi \right) R_{TMzz} \qquad (3.29)
\end{aligned}$$

$$\begin{aligned}
K_{zx(i,j)} &= \int_{0}^{k_0} \int_{0}^{2\pi} \tilde{J}_{zi}^{test*}(\rho,\theta)\tilde{Z}_{zx}(\rho,\theta)\tilde{J}_{xj}^{expa}(\rho,\theta)\, d\alpha\, d\beta \\
&+ \int_{k_0}^{\rho_{TM0}-\delta} \int_{0}^{2\pi} \left(\tilde{J}_{zi}^{test*}(\rho,\theta)\tilde{Z}_{zx}(\rho,\theta)\tilde{J}_{xj}^{expa}(\rho,\theta) - \frac{R_{TMzx}}{\rho - \rho_{TM0}} \right) d\alpha\, d\beta \\
&+ \int_{\rho_{TM0}+\delta}^{\sqrt{\epsilon_R}k_0} \int_{0}^{2\pi} \left(\tilde{J}_{zi}^{test*}(\rho,\theta)\tilde{Z}_{zx}(\rho,\theta)\tilde{J}_{xj}^{expa}(\rho,\theta) - \frac{R_{TMzx}}{\rho - \rho_{TM0}} \right) d\alpha\, d\beta \\
&+ \int_{\sqrt{\epsilon_R}k_0}^{\infty} \int_{0}^{2\pi} \tilde{J}_{zi}^{test*}(\rho,\theta)\tilde{Z}_{zx}(\rho,\theta)\tilde{J}_{xj}^{expa}(\rho,\theta)\, d\alpha\, d\beta \\
&+ \left(\ln\left(\frac{\sqrt{\epsilon_R}k_0 - \rho_{TM0}}{k_0 - \rho_{TM0}} \right) - i\pi \right) R_{TMzx} \qquad (3.30)
\end{aligned}$$

$$
\begin{aligned}
K_{xz(i,j)} &= \int_0^{k_0}\int_0^{2\pi} \tilde{J}_{xi}^{test*}(\rho,\theta)\tilde{Z}_{xz}(\rho,\theta)\tilde{J}_{zj}^{expa}(\rho,\theta)\,d\alpha\,d\beta \\
&+ \int_{k_0}^{\rho_{TM0}-\delta}\int_0^{2\pi}\left(\tilde{J}_{xi}^{test*}(\rho,\theta)\tilde{Z}_{xz}(\rho,\theta)\tilde{J}_{zj}^{expa}(\rho,\theta) - \frac{R_{TMxz}}{\rho-\rho_{TM0}}\right)d\alpha\,d\beta \\
&+ \int_{\rho_{TM0}+\delta}^{\sqrt{\epsilon_R}k_0}\int_0^{2\pi}\left(\tilde{J}_{xi}^{test*}(\rho,\theta)\tilde{Z}_{xz}(\rho,\theta)\tilde{J}_{zj}^{expa}(\rho,\theta) - \frac{R_{TMxz}}{\rho-\rho_{TM0}}\right)d\alpha\,d\beta \\
&+ \int_{\sqrt{\epsilon_R}k_0}^{\infty}\int_0^{2\pi}\tilde{J}_{xi}^{test*}(\rho,\theta)\tilde{Z}_{xz}(\rho,\theta)\tilde{J}_{zj}^{expa}(\rho,\theta)\,d\alpha\,d\beta \\
&+ \left(\ln\left(\frac{\sqrt{\epsilon_R}k_0-\rho_{TM0}}{k_0-\rho_{TM0}}\right) - i\pi\right)R_{TMxz} \qquad (3.31)
\end{aligned}
$$

$$
\begin{aligned}
K_{xx(i,j)} &= \int_0^{k_0}\int_0^{2\pi} \tilde{J}_{xi}^{test*}(\rho,\theta)\tilde{Z}_{xx}(\rho,\theta)\tilde{J}_{xj}^{expa}(\rho,\theta)\,d\alpha\,d\beta \\
&+ \int_{k_0}^{\rho_{TM0}-\delta}\int_0^{2\pi}\left(\tilde{J}_{xi}^{test*}(\rho,\theta)\tilde{Z}_{xx}(\rho,\theta)\tilde{J}_{xj}^{expa}(\rho,\theta) - \frac{R_{TMxx}}{\rho-\rho_{TM0}}\right)d\alpha\,d\beta \\
&+ \int_{\rho_{TM0}+\delta}^{\sqrt{\epsilon_R}k_0}\int_0^{2\pi}\left(\tilde{J}_{xi}^{test*}(\rho,\theta)\tilde{Z}_{xx}(\rho,\theta)\tilde{J}_{xj}^{expa}(\rho,\theta) - \frac{R_{TMxx}}{\rho-\rho_{TM0}}\right)d\alpha\,d\beta \\
&+ \int_{\sqrt{\epsilon_R}k_0}^{\infty}\int_0^{2\pi}\tilde{J}_{xi}^{test*}(\rho,\theta)\tilde{Z}_{xx}(\rho,\theta)\tilde{J}_{xj}^{expa}(\rho,\theta)\,d\alpha\,d\beta \\
&+ \left(\ln\left(\frac{\sqrt{\epsilon_R}k_0-\rho_{TM0}}{k_0-\rho_{TM0}}\right) - i\pi\right)R_{TMxx} \qquad (3.32)
\end{aligned}
$$

where

$$
R_{TMzz} = \int_0^{2\pi}\tilde{J}_{zi}^{test*}(\rho,\theta)\tilde{Z}_{zzTM}(\rho,\theta)\tilde{J}_{zj}^{expa}(\rho,\theta)\,d\theta
$$

$$
R_{TMzx} = \int_0^{2\pi}\tilde{J}_{zi}^{test*}(\rho,\theta)\tilde{Z}_{zxTM}(\rho,\theta)\tilde{J}_{xj}^{expa}(\rho,\theta)\,d\theta
$$

$$R_{TMxz} = \int_0^{2\pi} \tilde{J}_{xi}^{test*}(\rho,\theta)\tilde{Z}_{xzTM}(\rho,\theta)\tilde{J}_{zj}^{expa}(\rho,\theta)\,d\theta$$
$$R_{TMxx} = \int_0^{2\pi} \tilde{J}_{xi}^{test*}(\rho,\theta)\tilde{Z}_{xxTM}(\rho,\theta)\tilde{J}_{xj}^{expa}(\rho,\theta)\,d\theta. \tag{3.33}$$

3.5 Extraction of asymptotic forms

The second difficulty encountered in the evaluation of the integrals is the evaluation of the asymptotic portion of the integral. The integrand decays slowly, as will be shown, and therefore the integration must be carried out to a very large value. This, too, is numerically expensive. Therefore, it is desirable to extract the asymptotic portion of the integrand and integrate it analytically. However, this has only been satisfactorily implemented for the one-dimensional case. An alternative method has been implemented for the two-dimensional case.

3.5.1 One-dimensional case

In the calculation of the propagation constant and the current distribution for the modes of a uniform line, it is possible to obtain an asymptotic form of the integrand, which may be integrated in closed form. We now examine the asymptotic form of the Green's function for large α and β. For large values of α, Equations 2.37-2.50 become

$$\gamma_1 \sim \alpha, \tag{3.34}$$
$$\gamma_2 \sim \alpha, \tag{3.35}$$

$$\tilde{Y}_{TM1} \sim \frac{j\omega\epsilon_0}{\alpha}, \tag{3.36}$$

$$\tilde{Y}_{TM2} \sim \frac{j\omega\epsilon_0\epsilon_R}{\alpha}, \tag{3.37}$$

$$\tilde{Y}_{TE1} \sim \frac{\alpha}{j\omega\mu}, \tag{3.38}$$

$$\tilde{Y}_{TE1} \sim \frac{\alpha}{j\omega\mu}, \tag{3.39}$$

$$\tilde{Y}_1^e \sim \frac{j\omega\epsilon_0}{\alpha}, \tag{3.40}$$

$$\tilde{Y}_2^e \sim \frac{j\omega\epsilon_0\epsilon_R}{\alpha}, \tag{3.41}$$

$$\tilde{Y}_1^h \sim \frac{\alpha}{j\omega\mu}, \tag{3.42}$$

$$\tilde{Y}_2^h \sim \frac{\alpha}{j\omega\mu}, \tag{3.43}$$

$$\tilde{Z}^e \sim \frac{\alpha}{j\omega\epsilon_0(1+\epsilon_R)}, \tag{3.44}$$

$$\tilde{Z}^h \sim \frac{j\omega\mu}{2\alpha}, \tag{3.45}$$

$$\tilde{N}_z \sim \frac{\beta}{\alpha}, \text{ and} \tag{3.46}$$

$$\tilde{N}_x \sim 1. \tag{3.47}$$

Therefore, for large values of α, the spectral domain Green's function components behave as follows.

$$\tilde{Z}_{zz} \sim -\frac{\beta^2}{\alpha j\omega\epsilon_0(1+\epsilon_R)} - \frac{j\omega\mu}{2\alpha} = \tilde{Z}_{zz}^{asymp}, \tag{3.48}$$

$$\tilde{Z}_{zx} \sim -\frac{\beta}{\alpha}\left(\frac{\alpha}{j\omega\epsilon_0(1+\epsilon_R)} + \frac{j\omega\mu}{2\alpha}\right) = \tilde{Z}_{zx}^{asymp}, \tag{3.49}$$

$$\tilde{Z}_{xz} \sim -\frac{\beta}{\alpha}\left(\frac{\alpha}{j\omega\epsilon_0(1+\epsilon_R)} + \frac{j\omega\mu}{2\alpha}\right) = \tilde{Z}_{xz}^{asymp}, \text{ and} \tag{3.50}$$

$$\tilde{Z}_{xx} \sim \frac{\alpha}{j\omega\epsilon_0(1+\epsilon_R)} - \frac{\beta^2 j\omega\mu}{2\alpha^3} = \tilde{Z}_{xx}^{asymp}. \tag{3.51}$$

So the Green's function behaves asymptotically as

$$\tilde{Z}_{zz} \sim O(\frac{1}{\alpha}), \tag{3.52}$$

$$\tilde{Z}_{zx} \sim O(1), \tag{3.53}$$

$$\tilde{Z}_{xz} \sim O(1), \text{ and} \tag{3.54}$$

$$\tilde{Z}_{xx} \sim O(\alpha). \tag{3.55}$$

Therefore, in order to ensure the convergance of the integrals, the basis functions used to represent $\tilde{J}_z$ must behave asymptotically as $\frac{1}{\alpha}$, and the basis function used to represent $\tilde{J}_x$ must behave asymptotically as $\frac{1}{\alpha\sqrt{\alpha}}$, if Galerkin's method is used.

The Fourier transforms of the Maxwellian basis functions are given by

$$\begin{aligned} \tilde{J}_{zm}(\alpha) &= \frac{\pi w}{4}\left[J_0(|\frac{w\alpha}{2}+(m-1)\pi|)\right. \\ &+ \left. J_0(|\frac{w\alpha}{2}-(m-1)\pi|)\right], \text{ and} \end{aligned} \tag{3.56}$$

$$\tilde{J}_{xm}(\alpha) = \frac{\pi w}{4j}\left[J_0(|\frac{w\alpha}{2}+m\pi|)-J_0(|\frac{w\alpha}{2}-m\pi|)\right]. \tag{3.57}$$

where $J_0(x)$ denotes the zeroth-order Bessel function. This function is evaluated numerically using a rational function approximation. From the asymptotic form of J_0 [24], it can be seen that the asymptotic forms for the Maxwellian functions are

$$\tilde{J}_{zm}(\alpha) \sim \frac{4}{\sqrt{\pi w\alpha}}\sin\left(\frac{w\alpha}{2}\right)(-1)^{m-1} = \tilde{J}_{zm}^{asymp}(\alpha), \text{ and} \tag{3.58}$$

$$\tilde{J}_{xm}(\alpha) \sim \frac{2}{\sqrt{\pi w\alpha}}\frac{m\pi}{w\alpha}\sin\left(\frac{w\alpha}{2}\right)(-1)^{m+1} = \tilde{J}_{xm}^{asymp}(\alpha). \tag{3.59}$$

Therefore, the Fourier transforms of the Maxwellian functions behave asymptotically as

$$\tilde{J}_{zm}(\alpha) \sim O\left(\frac{1}{\sqrt{\alpha}}\right), \text{ and} \tag{3.60}$$

$$\tilde{J}_{xn}(\alpha) \sim O\left(\frac{1}{\alpha\sqrt{\alpha}}\right). \tag{3.61}$$

The integrands then decay as $\frac{1}{\alpha^2}$. This is a fairly slow convergance. Without any acceleration technique, the integrals must be carried out to a large value of α as much as $1000k_0$. However, since the asymptotic forms of the basis functions and Green's function are relatively simple, it is possible to evaluate the asymptotic portion of the integral analytically.

$$\int_a^\infty \tilde{J}_{zm}^{asymp}(\alpha)\tilde{Z}_{zz}^{asymp}(\alpha)\tilde{J}_{zn}^{asymp}(\alpha)\,d\alpha = \left((-1)^{m+n-2}\right) \left(\frac{\beta^2}{\omega\epsilon_0(1+\epsilon_R)} - \frac{\omega\mu}{2}\right)\left(\frac{8}{\pi w}\right)\left(\frac{1}{a} + \frac{1}{a}\sin(aw) - w\mathrm{Ci}(aw)\right) \tag{3.62}$$

$$\int_a^\infty \tilde{J}_{zm}^{asymp}(\alpha)\tilde{Z}_{zx}^{asymp}(\alpha)\tilde{J}_{xn}^{asymp}(\alpha)\,d\alpha = \left((-1)^{m+n}\right) \left(\frac{\beta}{\omega\epsilon_0(1+\epsilon_R)}\right)\left(\frac{8n}{w^2}\right)\left(\frac{1}{a} + \frac{1}{a}\sin(aw) - w\mathrm{Ci}(aw)\right) \tag{3.63}$$

$$\int_a^\infty \tilde{J}_{xm}^{asymp}(\alpha)\tilde{Z}_{xz}^{asymp}(\alpha)\tilde{J}_{zn}^{asymp}(\alpha)\,d\alpha = \left((-1)^{m+n}\right) \left(\frac{\beta}{\omega\epsilon_0(1+\epsilon_R)}\right)\left(\frac{8m}{w^2}\right)\left(\frac{1}{a} + \frac{1}{a}\sin(aw) - w\mathrm{Ci}(aw)\right) \tag{3.64}$$

$$\int_a^\infty \tilde{J}_{xm}^{asymp}(\alpha)\tilde{Z}_{xx}^{asymp}(\alpha)\tilde{J}_{xn}^{asymp}(\alpha)\,d\alpha = \left((-1)^{m+n+2}\right) \left(\frac{1}{\omega\epsilon_0(1+\epsilon_R)}\right)\left(\frac{8\pi mn}{w^3}\right)\left(\frac{1}{a} + \frac{1}{a}\sin(aw) - w\mathrm{Ci}(aw)\right) \tag{3.65}$$

where

$$\mathrm{Ci}(z) = -\int_z^\infty \frac{\cos(t)}{t}\,dt. \tag{3.66}$$

The cosine integral may be efficiently and accurately approximated with a rational function [23]. So the integrals are evaluated as

$$\begin{aligned}
\int_0^\infty \tilde{J}_z(\alpha)\tilde{Z}_{zz}(\alpha)\tilde{J}_z(\alpha)\,d\alpha &= \int_0^a \tilde{J}_z(\alpha)\tilde{Z}_{zz}(\alpha)\tilde{J}_z(\alpha)\,d\alpha \\
&+ \int_a^\infty [\tilde{J}_z(\alpha)\tilde{Z}_{zz}(\alpha)\tilde{J}_z(\alpha) \\
&- \tilde{J}_z^{asymp}(\alpha)\tilde{Z}_{zz}^{asymp}(\alpha)\tilde{J}_z^{asymp}(\alpha)]\,d\alpha \\
&+ (-1)^{m+n-2}\left(\frac{\beta^2}{\omega\epsilon_0(1+\epsilon_R)} - \frac{\omega\mu}{2}\right)\left(\frac{8}{\pi w}\right) \\
&\left(\frac{1}{a} + \frac{1}{a}\sin(aw) - w\mathrm{Ci}(aw)\right),
\end{aligned} \tag{3.67}$$

$$\begin{aligned}
\int_0^\infty \tilde{J}_z(\alpha)\tilde{Z}_{zx}(\alpha)\tilde{J}_x(\alpha)\,d\alpha &= \int_0^a \tilde{J}_z(\alpha)\tilde{Z}_{zx}(\alpha)\tilde{J}_x(\alpha)\,d\alpha \\
&+ \int_a^\infty [\tilde{J}_z(\alpha)\tilde{Z}_{zx}(\alpha)\tilde{J}_x(\alpha) \\
&- \tilde{J}_z^{asymp}(\alpha)\tilde{Z}_{zx}^{asymp}(\alpha)\tilde{J}_x^{asymp}(\alpha)]\,d\alpha \\
&+ (-1)^{m+n}\left(\frac{\beta}{\omega\epsilon_0(1+\epsilon_R)}\right)\left(\frac{8n}{w^2}\right) \\
&\left(\frac{1}{a} + \frac{1}{a}\sin(aw) - w\mathrm{Ci}(aw)\right),
\end{aligned} \tag{3.68}$$

$$\begin{aligned}
\int_0^\infty \tilde{J}_x(\alpha)\tilde{Z}_{xz}(\alpha)\tilde{J}_z(\alpha)\,d\alpha &= \int_0^a \tilde{J}_x(\alpha)\tilde{Z}_{xz}(\alpha)\tilde{J}_z(\alpha)\,d\alpha \\
&+ \int_a^\infty [\tilde{J}_x(\alpha)\tilde{Z}_{xz}(\alpha)\tilde{J}_z(\alpha) \\
&- \tilde{J}_x^{asymp}(\alpha)\tilde{Z}_{xz}^{asymp}(\alpha)\tilde{J}_z^{asymp}(\alpha)]\,d\alpha \\
&+ (-1)^{m+n}\left(\frac{\beta}{\omega\epsilon_0(1+\epsilon_R)}\right)\left(\frac{8m}{w^2}\right)
\end{aligned}$$

$$\left(\frac{1}{a}+\frac{1}{a}\sin(aw)-w\mathrm{Ci}(aw)\right), \text{ and} \tag{3.69}$$

$$\begin{aligned}\int_0^\infty \tilde{J}_x(\alpha)\tilde{Z}_{xx}(\alpha)\tilde{J}_x(\alpha)\,d\alpha &= \int_0^a \tilde{J}_x(\alpha)\tilde{Z}_{xx}(\alpha)\tilde{J}_x(\alpha)\,d\alpha \\ &+ \int_a^\infty [\tilde{J}_x(\alpha)\tilde{Z}_{xx}(\alpha)\tilde{J}_x(\alpha) \\ &- \tilde{J}_x^{asymp}(\alpha)\tilde{Z}_{xx}^{asymp}(\alpha))\tilde{J}_x^{asymp}(\alpha)]\,d\alpha \\ &+ (-1)^{m+n+2}\left(\frac{1}{\omega\epsilon_0(1+\epsilon_R)}\right)\left(\frac{8\pi mn}{w^3}\right) \\ &\left(\frac{1}{a}+\frac{1}{a}\sin(aw)-w\mathrm{Ci}(aw)\right). \end{aligned} \tag{3.70}$$

3.5.2 Two-dimensional case

In Section 3.1.2, it was seen that the longitudinal dependance of the current is represented by two types of basis functions, piecewise linear and sinusoidal. The piecewise linear function is repeated here for convenience.

$$J_{PWLn}(z) = \left(\frac{h-|z-z_n|}{h}\right)$$

The Fourier transform of the piecewise linear function is

$$\tilde{J}_{PWLn}(\beta) = \frac{2}{\beta^2}\frac{1}{h}(1-\cos(\beta h))\exp(j\beta z_m).$$

As can be seen, the transforms behave asymptotically for large β as

$$\tilde{J}_{PWLn}(\beta) \sim O(\frac{1}{\beta^2}). \tag{3.71}$$

As noted, the sinusoidal basis functions are truncated. The length of the sinusoid, as pointed out by [15] should be an integer number of half-wavelengths in order to obtain the fastest convergence of the integrals. This can be seen as follows.

Let

$$J_{sin}(z) = \begin{cases} \sin(\beta_z z) & \text{if } 0 < z < z_L, \text{ and} \\ 0 & \text{otherwise.} \end{cases} \tag{3.72}$$

Then

$$\begin{aligned} \tilde{J}_{sin}(\beta) \sim & \frac{1}{2}\frac{1}{\beta+\beta_z} \\ & - \frac{1}{2}\frac{1}{\beta-\beta_z} \\ & - \frac{1}{2}\frac{1}{\beta+\beta_z}\cos((\beta+\beta_z)z_t) \\ & + \frac{1}{2}\frac{1}{\beta-\beta_z}\cos((\beta-\beta_z)z_t) \\ & - \frac{1}{2}\frac{1}{\beta+\beta_z}\sin((\beta+\beta_z)z_t) \\ & + \frac{1}{2}\frac{1}{\beta-\beta_z}\sin((\beta-\beta_z)z_t). \end{aligned} \tag{3.73}$$

For $z_t = \frac{n\lambda_{eff}}{2}$,

$$\begin{aligned} \tilde{J}_{sin}(\beta) \sim & \frac{1}{2}\frac{1}{\beta+\beta_z} \\ & - \frac{1}{2}\frac{1}{\beta-\beta_z} \\ & - \frac{1}{2}\frac{1}{\beta+\beta_z}\cos(\beta z_t) \\ & + \frac{1}{2}\frac{1}{\beta-\beta_z}\cos(\beta z_t) \\ & - \frac{1}{2}\frac{1}{\beta+\beta_z}\sin(\beta z_t) \\ & + \frac{1}{2}\frac{1}{\beta-\beta_z}\sin(\beta z_t). \end{aligned} \tag{3.74}$$

For large values of β,

$$\tilde{J}_{sin} \sim \frac{\beta_z}{\beta^2}(1+\cos(\beta z_t)+\sin(\beta z_t)). \tag{3.75}$$

Therefore,

$$\tilde{J}_{sin} \sim O(\frac{1}{\beta^2}). \tag{3.76}$$

On the other hand, if the sine function were truncated at an odd integer number of quarter-wavelengths, $\tilde{F}_{sin}(\beta)$ would decay as $\frac{1}{\beta}$ for large β. It is desirable to truncate the sine function at an integer number of half-wavelengths not only because this speeds convergence, but also because the subsectional and entire domain basis functions will then decay at the same rate. As it stands, $\tilde{J}_{sin}(\beta)$ can have a pole at $\beta = \beta_z$. However, by further constraining the truncation to an even integer number of half guide wavelengths, we can eliminate the pole. Let

$$z_L = n\lambda_{eff}. \tag{3.77}$$

Then

$$\begin{aligned} \cos(\beta z_L) &= 1, \text{ and} \\ \sin(\beta z_L) &= 0. \end{aligned} \tag{3.78}$$

Therefore,

$$\lim_{\beta \to \beta_z} \tilde{J}_{sin}(\beta) = 0 \tag{3.79}$$

As noted in Chapter 2, the traveling-wave function does not have to be truncated at all in order for its Fourier transform to exist. That is

$$J_{source}(z) = \begin{cases} e^{-j\beta_z z} & \text{if } z < 0, \text{ and} \\ 0 & \text{otherwise.} \end{cases} \tag{3.80}$$

The Fourier transform is then derived as follows.

$$\begin{aligned}
\tilde{J}_{source}(\beta) &= \int_{-\infty}^{0} e^{-j\beta_z z} e^{j\beta z}\, dz \\
&= \int_{-\infty}^{0} e^{j(\beta-\beta_z)z}\, dz \\
&= \int_{-\infty}^{0} \cos(\beta-\beta_z)z\, dz + j\int_{-\infty}^{0} \sin(\beta-\beta_z)z\, dz \\
&= \frac{1}{2}\int_{-\infty}^{+\infty} e^{(\beta-\beta_z)z}\, dz + j\int_{-\infty}^{0} \sin(\beta-\beta_z)z\, dz \\
&= \frac{1}{2}\int_{-\infty}^{+\infty} e^{(\beta-\beta_z)z}\, dz + j\lim_{\alpha\to 0}\int_{-\infty}^{0} e^{\alpha z}\sin(\beta-\beta_z)z\, dz
\end{aligned}$$

Therefore,

$$\begin{aligned}
\tilde{J}_{source}(\beta) &= \frac{1}{2}[2\pi\delta(\beta-\beta_z)] \\
&+ j\lim_{\alpha\to 0}\left[\frac{e^{\alpha z}}{\alpha^2+(\beta-\beta_z)^2}\left(\alpha\sin([\beta-\beta_z]z) - (\beta-\beta_z)\cos([\beta-\beta_z]z)\right)\right]_{-\infty}^{0}
\end{aligned}$$

$$\tilde{J}_{source}(\beta) = \pi\delta(\beta-\beta_z) + \frac{1}{j(\beta-\beta_z)}. \tag{3.81}$$

It is immediately seen that this function presents two numerical problems. First, it has a pole at $\beta = \beta_z$. Also, it behaves asymptotically as $\frac{1}{\beta}$. Therefore, it is numerically more expensive to evaluate than the source function used here. However, it should be noted that it is more rigorously correct and may be necessary when surface wave coupling is strong or complex circuit geometries generate strong coupling.

For large values of β, the spectral domain Green's function compo-

nents behave as follows.

$$\tilde{Z}_{zz} \sim \frac{\beta}{j\omega\epsilon_0(1+\epsilon_R)} - \frac{\alpha^2 j\omega\mu}{2\alpha^3}, \tag{3.82}$$

$$\tilde{Z}_{zx} \sim -\frac{\alpha}{\beta}\left(\frac{\beta}{j\omega\epsilon_0(1+\epsilon_R)} + \frac{j\omega\mu}{2\beta}\right), \tag{3.83}$$

$$\tilde{Z}_{xz} \sim -\frac{\alpha}{\beta}\left(\frac{\beta}{j\omega\epsilon_0(1+\epsilon_R)} + \frac{j\omega\mu}{2\beta}\right), \text{ and} \tag{3.84}$$

$$\tilde{Z}_{xx} \sim -\frac{\alpha^2}{\beta j\omega\epsilon_0(1+\epsilon_R)} - \frac{j\omega\mu}{2\beta}. \tag{3.85}$$

So the Green's function behaves asymptotically as

$$\tilde{Z}_{zz} \sim O(\beta), \tag{3.86}$$

$$\tilde{Z}_{zx} \sim O(1), \tag{3.87}$$

$$\tilde{Z}_{xz} \sim O(1), \text{ and} \tag{3.88}$$

$$\tilde{Z}_{xx} \sim O(\frac{1}{\beta}). \tag{3.89}$$

From the asymptotic forms of the Green's function for large β and the asymptotic forms of the basis functions, we see that the two-dimensional Z_{zz} integrals converge as $\frac{1}{\beta^3}$, the Z_{zx} and Z_{xz} integrals converge as $\frac{1}{\beta^4}$, and the Z_{xx} integrals converge as $\frac{1}{\beta^5}$ along the β axis.

In the two-dimensional case, the extraction of the asymptotic form is not straightforward. Because the transverse dependence of the two-dimensional basis functions is the same as that of the one-dimensional basis functions used in the analysis of uniform line, the convergence along the α axis is the same as that for the one dimensional analysis. Along the β axis, the convergence is better because the basis functions exhibit more rapid convergence. The integration is performed in a cylindrical coordinate system, and while an asymptotic form

is available for the Green's function for large ρ, no such forms are available for the basis functions. This is because they are separable in α and β. The asymptotic form of the Green's function for large ρ[1] is given by

$$\tilde{Z}_{zz}(\rho,\theta) = -\frac{\rho\cos^2(\theta)}{j\omega\epsilon_0(1+\epsilon_R)} - \frac{j\omega\mu\sin^2(\theta)}{2\rho} \tag{3.90}$$

$$= \frac{\beta^2}{j\omega\epsilon_0(1+\epsilon_R)\rho} + \frac{j\omega\mu\alpha^2}{2\rho^3}, \tag{3.91}$$

$$\tilde{Z}_{zx}(\rho,\theta) = -\frac{\cos(\theta)\sin(\theta)}{j\omega\epsilon_0(1+\epsilon_R)\rho} - \frac{j\omega\mu\cos(\theta)\sin(\theta)}{2\rho^3}, \tag{3.92}$$

$$\tilde{Z}_{xz}(\rho,\theta) = -\frac{\cos(\theta)\sin(\theta)}{j\omega\epsilon_0(1+\epsilon_R)\rho} - \frac{j\omega\mu\cos(\theta)\sin(\theta)}{2\rho^3}, \text{ and} \tag{3.93}$$

$$\tilde{Z}_{xx}(\rho,\theta) = -\frac{\rho\sin^2(\theta)}{j\omega\epsilon_0(1+\epsilon_R)} - \frac{j\omega\mu\cos^2(\theta)}{2\rho}. \tag{3.94}$$

For a conductor backed homogeneous medium of relative dielectric constant ϵ_e, the space domain Green's function is given in closed form by

$$Z_{zz}(x-x_0,z-z_0) = \frac{-j}{4\pi\omega\epsilon_0\epsilon_R}(\epsilon_e k_0^2 + \frac{\partial^2}{\partial z^2})[\frac{\exp(-jkR_s)}{R_s} - \frac{\exp(-jkR_i)}{R_i}], \tag{3.95}$$

$$Z_{zx}(x-x_0,z-z_0) = \frac{-j}{4\pi\omega\epsilon_0\epsilon_R}(\epsilon_e k_0^2 + \frac{\partial^2}{\partial z\partial x})[\frac{\exp(-jkR_s)}{R_s} - \frac{\exp(-jkR_i)}{R_i}], \tag{3.96}$$

$$Z_{xz}(x-x_0,z-z_0) = \frac{-j}{4\pi\omega\epsilon_0\epsilon_R}(\epsilon_e k_0^2 + \frac{\partial^2}{\partial x\partial z})[\frac{\exp(-jkR_s)}{R_s} - \frac{\exp(-jkR_i)}{R_i}], \text{ and} \tag{3.97}$$

[1]The asymptotic form for $\tilde{Z}_{zz}$ in [36] appears to be incorrect.

$$Z_{xx}(x-x_0, z-z_0) = \frac{-j}{4\pi\omega\epsilon_0\epsilon_R}(\epsilon_e k_0^2 + \frac{\partial^2}{\partial x^2})[\frac{\exp(-jkR_s)}{R_s} - \frac{\exp(-jkR_i)}{R_i}] \quad (3.98)$$

where

$$R_s = \sqrt{(z-z_0)^2 + (x-x_0)^2}, \text{ and} \quad (3.99)$$

$$R_i = \sqrt{(z-z_0)^2 + (x-x_0)^2 + (2d)^2}. \quad (3.100)$$

Using the identity given on page 179 of [25] and the differentiation theorem for Fourier transforms, the spectral domain form of this Green's function is given by

$$\tilde{Z}_{zz}(\alpha,\beta) = \frac{(\epsilon_e k_0^2 - \beta^2)}{2j\omega\epsilon_0\epsilon_e\gamma_2}(1-\exp(-2\gamma_2 d)), \quad (3.101)$$

$$\tilde{Z}_{zx}(\alpha,\beta) = \frac{(\epsilon_e k_0^2 - \beta\alpha)}{2j\omega\epsilon_0\epsilon_e\gamma_2}(1-\exp(-2\gamma_2 d)), \quad (3.102)$$

$$\tilde{Z}_{xz}(\alpha,\beta) = \frac{(\epsilon_e k_0^2 - \alpha\beta)}{2j\omega\epsilon_0\epsilon_e\gamma_2}(1-\exp(-2\gamma_2 d)), \text{ and} \quad (3.103)$$

$$\tilde{Z}_{xx}(\alpha,\beta) = \frac{(\epsilon_e k_0^2 - \alpha^2)}{2j\omega\epsilon_0\epsilon_e\gamma_2}(1-\exp(-2\gamma_2 d)). \quad (3.104)$$

This behaves asymptotically for large ρ as

$$\tilde{Z}_{zz}(\alpha,\beta) = \frac{k_0^2}{2\rho} - \frac{\beta^2}{2j\omega\epsilon_0\epsilon_e\rho}, \quad (3.105)$$

$$\tilde{Z}_{zx}(\alpha,\beta) = \frac{k_0^2}{2\rho} - \frac{\beta\alpha}{2j\omega\epsilon_0\epsilon_e\rho}, \quad (3.106)$$

$$\tilde{Z}_{xz}(\alpha,\beta) = \frac{k_0^2}{2\rho} - \frac{\alpha\beta}{2j\omega\epsilon_0\epsilon_e\rho}, \text{ and} \quad (3.107)$$

$$\tilde{Z}_{xx}(\alpha,\beta) = \frac{k_0^2}{2\rho} - \frac{\alpha^2}{2j\omega\epsilon_0\epsilon_e\rho}. \quad (3.108)$$

Therefore, if we let $\epsilon_e = \frac{\epsilon_R+1}{2}$, the asymptotic forms become

$$\tilde{Z}_{zz}(\alpha,\beta) = -\frac{\beta^2}{j\omega\epsilon_0(1+\epsilon_R)\rho} - \frac{j\omega\mu}{2\rho}, \quad (3.109)$$

$$\tilde{Z}_{xx}(\alpha,\beta) = -\frac{\beta\alpha}{j\omega\epsilon_0(1+\epsilon_R)\rho} - \frac{j\omega\mu}{2\rho}, \tag{3.110}$$

$$\tilde{Z}_{xz}(\alpha,\beta) = -\frac{\alpha\beta}{j\omega\epsilon_0(1+\epsilon_R)\rho} - \frac{j\omega\mu}{2\rho}, \text{ and} \tag{3.111}$$

$$\tilde{Z}_{xx}(\alpha,\beta) = -\frac{\alpha^2}{j\omega\epsilon_0(1+\epsilon_R)\rho} - \frac{j\omega\mu}{2\rho}. \tag{3.112}$$

It can be seen that the TM term of the asymptotic form for the homogeneous case is identical to that of the grounded dielectric slab. Therefore, this asymptotic form may be subtracted from the spectral domain Green's function to yield a more rapidly converging kernel. Although the additive term may not be evaluated analytically as in the one-dimensional case, it may be evaluated in the space domain. This requires the computation of a four-dimensional finite integral. When simple basis functions are used, this four-dimensional integral may be further reduced to two-dimensions because two of the integrations may be performed analytically. However, the use of the Maxwellian functions allows only one of the integrations to be done analytically. Because the integration is in the space domain, a singularity exists at the source point. In order to perform the integration efficiently, this singularity must be extracted and integrated analytically.

$$\int_0^{\infty}\int_0^{\frac{\pi}{2}} \tilde{J}_z^{test*}(\rho,\theta)\tilde{Z}_{zz}(\rho,\theta)\tilde{J}_z^{expa}(\rho,\theta)\rho\,d\rho\,d\theta =$$

$$\int_0^{\infty}\int_0^{\frac{\pi}{2}} \tilde{J}_z^{test*}(\rho,\theta)\left[\tilde{Z}_{zz}(\rho,\theta) - \tilde{Z}_{zz}^{h}(\rho,\theta)\right]\tilde{J}_z^{expa}(\rho,\theta)\rho\,d\rho\,d\theta +$$

$$\int_x\int_z\int_{x_0}\int_{z_0} J_z^{test}(x,z)Z_{zz}^{h}(x-x_0,z-z_0)J_z^{expa}(x,z)dx_0\,dz_0\,dx\,dz \tag{3.113}$$

Because the space domain integration is still somewhat laborious, it nas been found that this method did not reduce the computation time significantly.

3.6 Numerical Evaluation of the Integrals

Because the the range of integration is the same for all the integrals, it is advantageous to precompute and store the components of the Green's function and the expansion and testing functions. Thus the Green's function is computed only once for each integration step for the entire matrix. This has been noted by [2]. Some savings is realized in the computation of the basis functions due the eliminated redundancy. This is particularly suited to vector processors because the computation of the integrals may be vectorized.

Chapter 4

THE OPEN-CIRCUIT MICROSTRIP DISCONTINUITY

4.1 Introduction

Microstrip open-end discontinuities are an integral part of most microstrip circuits and antennas. The geometry of a microstrip open-end discontinuity is shown in Figure 4.1. Open-end discontinuities in open microstrip are imperfect open-circuits because of energy storage in non-radiating fields and energy leakage into radiating fields. Energy leakage into both space waves and surface waves occurs. The discontinuity exhibits a minimum susceptance immitance function. Therefore, an appropriate circuit model is a parallel combination of a reactance and a conductance as shown in Figure 4.2. In general, both the reactance and the conductance are frequency dependent. In this chapter, microstrip open-end discontinuities in open environments are analyzed using a combination of the the deterministic and eigenvalue formulations of the spectral domain approach presented in Chapters 2 and 3. The study includes the effects of both longitudinal and transverse currents and incorporates the proper edge conditions for each component of the current at the edges of the strip and the open end of the strip.

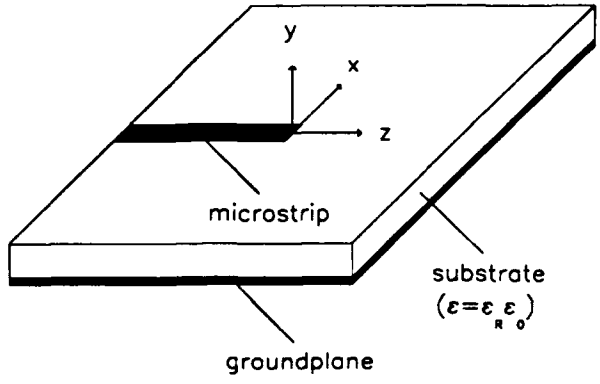

Figure 4.1: Geometry of Microstrip Open-End Discontinuity

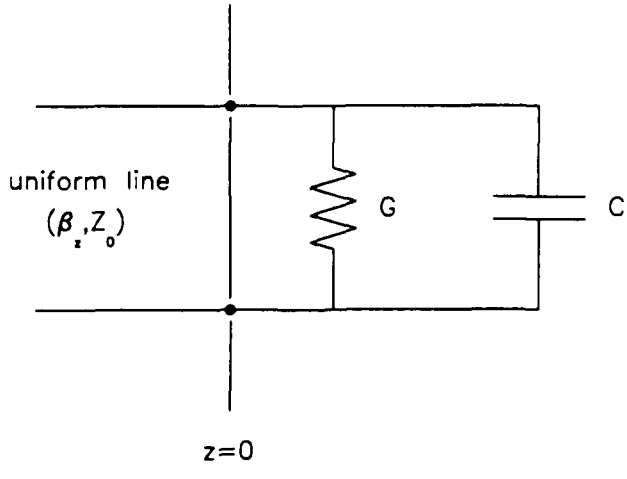

Figure 4.2: Equivalent Circuit of Microstrip Open-End Discontinuity

4.2 Method

The computational method consists of two parts. In the first part, the spectral domain eigenvalue formulation is used to compute the propagation constant, characteristic impedance, and longitudinal and transverse current distributions for the fundamental mode on an infinitely long open microstrip corresponding to the uniform region. The source current to be used in the second part of the method is then given by

$$J_z^{source}(x,z) = \sum_{l=1}^{L} a_l J_{zl}(x) \exp(-j\beta_z z), \text{ and} \tag{4.1}$$

$$J_x^{source}(x,z) = \sum_{l=1}^{L} b_l J_{xl}(x) \exp(-j\beta_z z). \tag{4.2}$$

The functions J_{zm} and J_{xn} are the Maxwellian basis functions described in Chapter 3 They include the proper edge condition for the longitudinal and transverse current at the edges of the microstrip. The constants $a_1 \ldots a_L$, $b_1 \ldots b_L$, and β, the propagation constant, are determined in the spectral domain analysis. In practice, $L = 2$ yielded good results and was therefore used throughout the analysis. The propagation constant for the fundamental mode, β_z, is always greater than the value of ρ for any surface-wave pole. Therefore, the fundamental mode is always slow compared with any surface wave mode and thus does not radiate any power into surface-waves. In the second part of the method, the microstrip is divided into two overlapping regions: a uniform region far away from the open end and a perturbed region near the open end, as in [15]. In the uniform region, the current is assumed to consist of only the fundamental mode. This will be true if the higher order modes are either leaky or evanescent. The current in the uniform region is represented by the source

function and a reflected wave with an unknown amplitude, Γ.

$$J_z^{uniform}(x,z) = \sum_{l=1}^{L} a_l J_{zl}(x)(\exp(-j\beta_z z) - \Gamma \exp(+j\beta_z z)), \text{ and} \quad (4.3)$$

$$J_x^{uniform}(x,z) = \sum_{l=1}^{L} b_l J_{xl}(x)(\exp(-j\beta_z z) + \Gamma \exp(+j\beta_z z)). \quad (4.4)$$

Note that Γ is the voltage reflection coefficient. As discussed in Chapter 3, the exponential functions are split into sine and cosine functions which are truncated to give the most rapidly converging Fourier transforms.

The longitudinal dependence of the current in the perturbed region near the open end is augmented with piecewise linear (rooftop) subsectional basis functions, which are defined in Chapter 3. The piecewise linear functions allow a reasonable approximation to the edge condition for the both the transverse and the longitudinal currents at the open end. The transverse dependance of the current in the perturbed region is represented with Maxwellian basis functions with variable coefficients. This takes into account mode conversion in the perturbed region. Therefore, the current in the perturbed region is given by

$$J_z^{perturbed}(x,z) = \sum_{m=1}^{M} J_{zm}(x) \sum_{n=1}^{N} c_{mn} F_n(z) + J_z^{uniform}(x,z), \text{ and}$$

$$J_x^{perturbed}(x,z) = \sum_{m=1}^{M} J_{xm}(x) \sum_{n=1}^{N} d_{mn} F_n(z) + J_x^{uniform}(x,z).$$

where $F_1(z) \ldots F_n(z)$ are piecewise linear subsectional basis functions. The positioning of the basis functions is shown in Figure 4.3.

If just the longitudinal current, J_z, is taken into account and mode conversion is neglected ($M = 1$), as it was in [15], there are $N + 1$ unknowns,

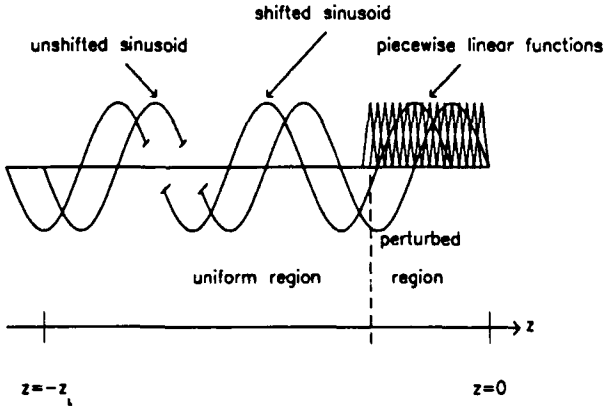

Figure 4.3: Positioning of Longitudinal Basis Functions for Analysis of Microstrip Open-end Discontinuity

the complex coefficients of the subdomain expansion functions and the complex reflection coefficient. Since it is not possible to test the equation with the source function, Galerkin's method cannot be used here. However, it is still useful to use the M subsectional basis functions as testing functions in a "nearly Galerkin" method. This generates an underdetermined linear system with one less equation than unknowns. One method of solving the problem is to simply use one more testing function to generate one more equation. The linear system is then square and may be solved using Gaussian elimination. This method was proposed by [15]. Thus, the following linear system is derived.

$$\begin{bmatrix} \begin{bmatrix} K_{1,1}^{zzpp} & K_{1,2}^{zzpp} & \dots & K_{1,N}^{zzpp} \\ K_{2,1}^{zzpp} & K_{2,2}^{zzpp} & \dots & K_{2,N}^{zzpp} \\ \vdots & \vdots & & \vdots \\ K_{N,1}^{zzpp} & K_{N,2}^{zzpp} & \dots & K_{N,N}^{zzpp} \end{bmatrix} & \begin{bmatrix} K_1^{zzp-} \\ K_2^{zzp-} \\ \vdots \\ K_N^{zzp-} \end{bmatrix} \\ \begin{bmatrix} K_{N+1,1}^{zzpp} & K_{N+1,2}^{zzpp} & \dots & K_{N+1,N}^{zzpp} \end{bmatrix} & \begin{bmatrix} K_{N+1}^{zzp-} \end{bmatrix} \end{bmatrix} \begin{bmatrix} a_1 \\ a_2 \\ \vdots \\ a_N \\ a_{N+1} \end{bmatrix} = \begin{bmatrix} -S_1^{zzp+} \\ -S_2^{zzp+} \\ \vdots \\ -S_N^{zzp+} \\ -S_{N+1}^{zzp+} \end{bmatrix}$$

The portion of the matrix generated by testing and expanding with subdomain expansion functions has Toeplitz symmetry. Therefore, only one row of elements needs to be calculated. To generate the entire linear system, $4N + 2$ integrals must be computed.

When two dimensional current is considered, the linear system becomes

$$\begin{bmatrix} [K_{zz}][K_{zx}] \\ [K_{xz}][K_{xx}] \end{bmatrix} \begin{bmatrix} [a] \\ [b] \end{bmatrix} = \begin{bmatrix} [S_z] \\ [S_x] \end{bmatrix}$$

where K_{zz} denotes the coefficient matrix given above and K_{zx} etc. are similar. By reciprocity, $K_{zx} = K_{xz}$. We note that $a_{N+1} = -\Gamma$ and $b_{N+1} = \Gamma$. Therefore, the system of equations given above is over-determined by one equation. The overdetermined system was solved using a least-squares approach. The numer-

ical cost of including the effects of two-dimensional current are substantial; we must evaluate $11N + 5$ two-dimensional integrals.

One drawback to this method is that there are several unknown quantities which must be determined empirically: the length of the uniform line basis functions, z_l, the length of the region of subdomain expansion, and the length of the subdomain expansion functions. It has been empirically determined that using $z_l = 6\lambda_{eff}$ yields satisfactory results. Also, it has been found that using subdomain expansion functions of width, $2h = \frac{\lambda_{eff}}{16}$, yields satisfactory results. However, the length of the subdomain expansion region, and hence the number of subdomain expansion functions, depends on the geometry of the discontinuity.

Some of this uncertainty may be removed by generating an overdetermined system by using more subsectional testing functions to generate more equations. The over determined system is solved via a least squares method. Γ is the complex reflection coefficient for the fundamental mode. From $a_1 \ldots a_M$ and Γ, the current over the entire strip can be determined. From Γ, the reflection coefficient, and Z_0, the characteristic impedance of the uniform line, an equivalent admittance can be calculated

$$Y_{equiv} = Y_0 \left(\frac{1 - \Gamma}{1 + \Gamma} \right) \tag{4.5}$$

where $Y_0 = \frac{1}{Z_0}$.

4.3 Numerical Results

In Figures 4.4 and 4.5, the longitudinal (z-directed) current and the transverse (x-directed) current on an open circuited microstrip line are plotted

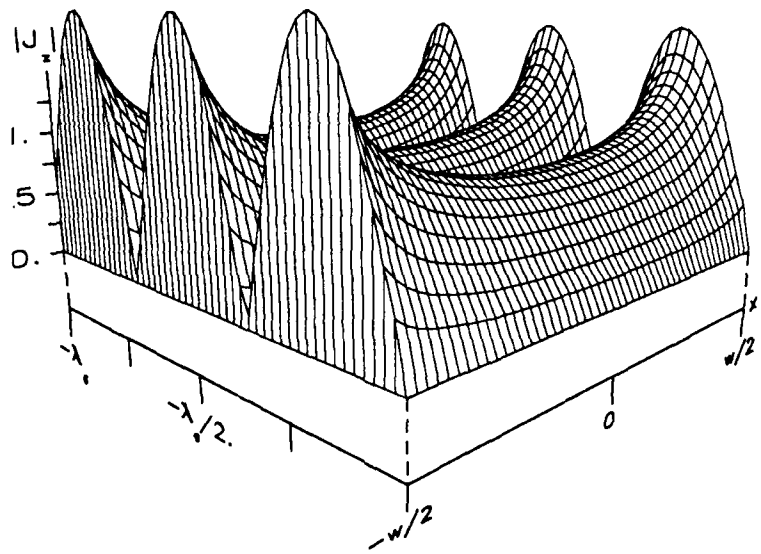

Figure 4.4: Magnitude of z-directed Current on Microstrip Open-end Discontinuity

to show the edge conditions for a typical case. The characteristics are as follows:

- Relative dielectric constant, ϵ_R : 12.8
- Substrate height, h = .300 mm
- Strip width, w = .600 mm
- Frequency = 4.00 GHz

It can be seen that the piecewise linear functions allow the edge conditions at the open end for both the transverse current and the longitudinal current to

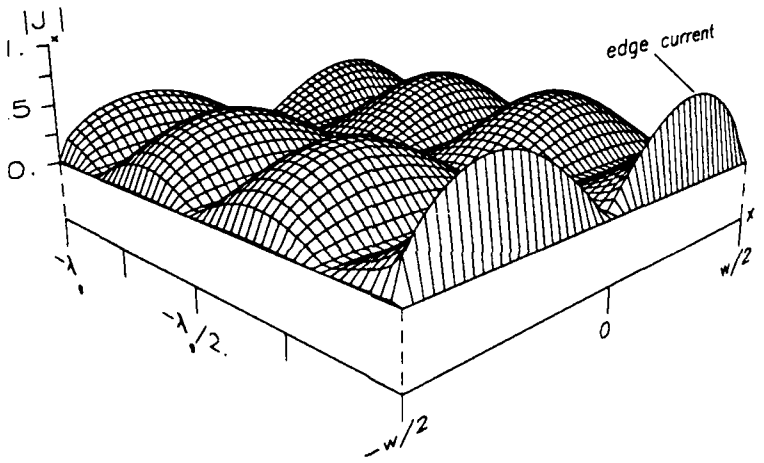

Figure 4.5: Magnitude of x-directed Current on Microstrip Open-end Discontinuity

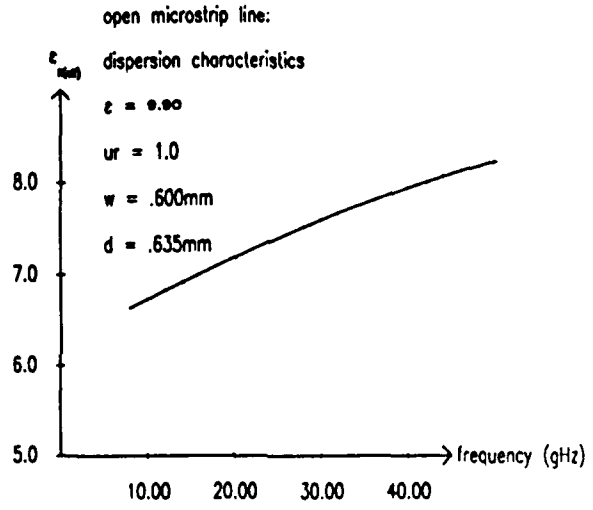

Figure 4.6: Effective Dielectric Constant of Uniform Microstrip Line

be accurately modeled.

In order to allow comparison with previously published experimental data, [49] an analysis was made of an open-end discontinuity in microstrip line with the following parameters.

- Relative dielectric constant, ϵ_R : 9.9
- Substrate height, h = .635 mm
- Strip width, w = .600 mm

The dispersion curve for ϵ_{eff} is shown in Figure 4.6. In Figure 4.7, the characteristic impedance is plotted as a function of frequency. Figures 4.8 and 4.9, show the magnitude and phase of the reflection coefficent for an open circuit

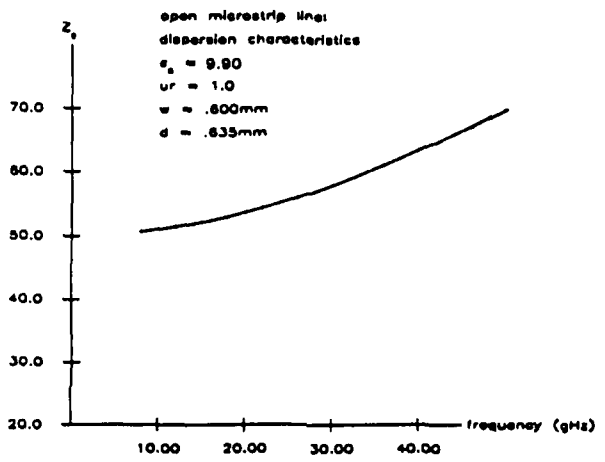

Figure 4.7: Characteristic Impedance of Uniform Microstrip Line

discontinuity. In Figures 4.10 and 4.11 G and B are plotted as functions of frequency. This line is very narrow electrically; at 20 GHz the line is still only 0.04 free-space wavelengths wide. The phase agrees reasonably well with the measured data in [49] (the magnitude was not presented in [49]) and with calculated data in [18] and [44].

In order to quantify the effect of the transverse current on the reflection coefficient of a microstrip open-end discontinuity, an analysis was made of an open-end discontinuity in microstrip line with the following parameters.

- Relative dielectric constant, ϵ_R : 9.6
- Substrate height, h = .635 mm
- Strip widths, w = .600 mm and w = 1.20 mm.

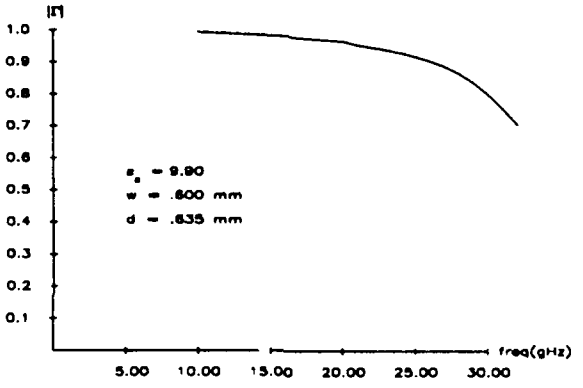

Figure 4.8: Magnitude of Reflection Coefficient of Microstrip Open-end Discontinuity

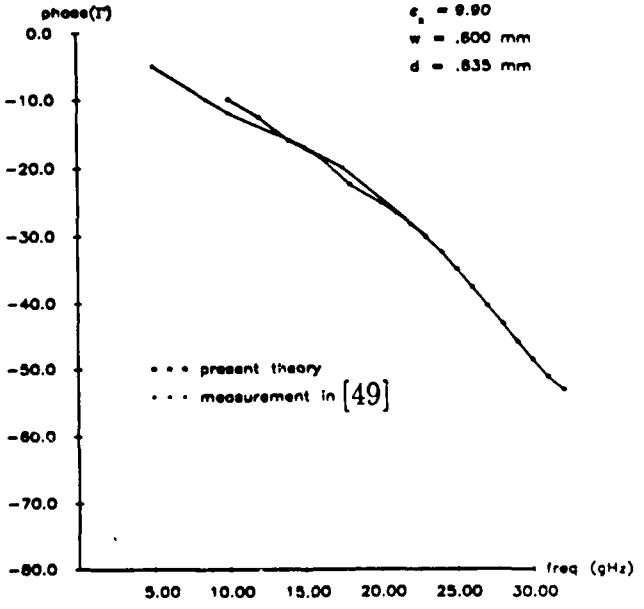

Figure 4.9: Phase of Reflection Coefficient of Microstrip Open-End Discontinuity

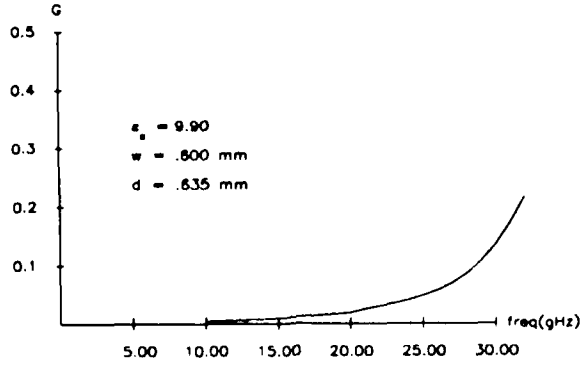

Figure 4.10: Equivalent Conductance of Microstrip Open-end Discontinuity

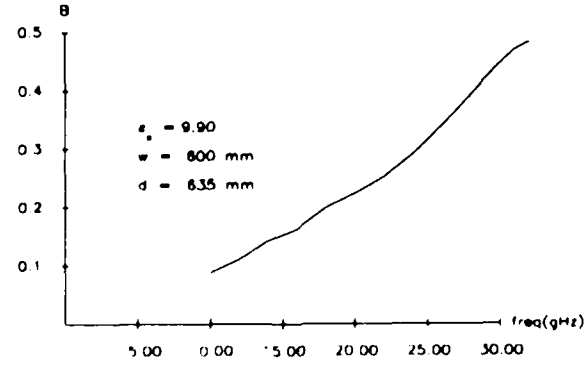

Figure 4.11: Equivalent Capacitance of Microstrip Open end Discontinuity

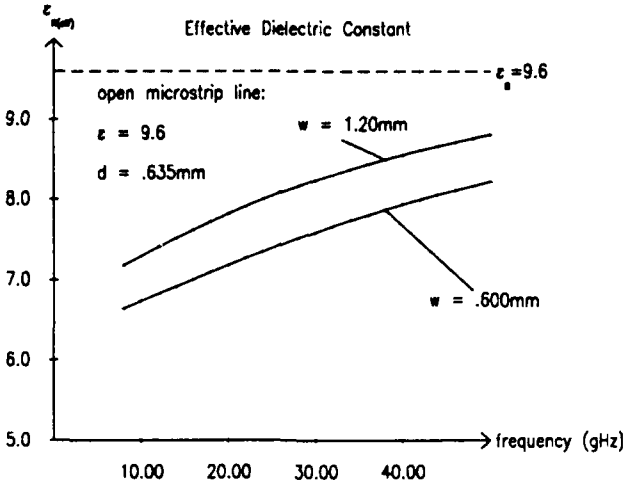

Figure 4.12: Effective Dielectric Constant of Uniform Microstrip Line

The narrow line is very similar to that in the above analysis. It was chosen because it is a very commonly used design. The dispersion curves for ϵ_{eff} are shown in Figure 4.12. In Figure 4.13, the characteristic impedances are plotted as a function of frequency. As can be seen, the narrow line exhibits a characteristic impedance which varies from approximately 50 ohms at 10 GHz to 70 ohms at 40 GHz. The characteristic impedance of the wide line varies from approximately 35 ohms to 45 ohms over the same range. In Figure 4.14, the ratio of the transverse to longitudinal current is plotted. It can be seen that the transverse current on the narrow line is not very significant in comparison to the longitudinal current. However, the transverse current on the wide line can be quite appreciable. In Figure 4.15 and Figure 4.16 the magnitude and the phase of the reflection coefficient of the open-end discontinuity are plotted.

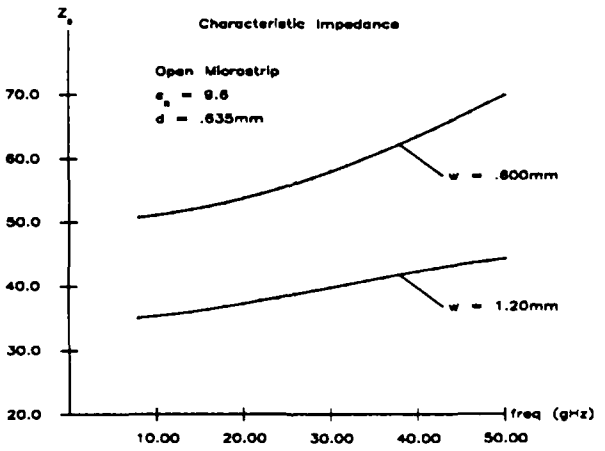

Figure 4.13: Characteristic Impedance of Uniform Microstrip Line

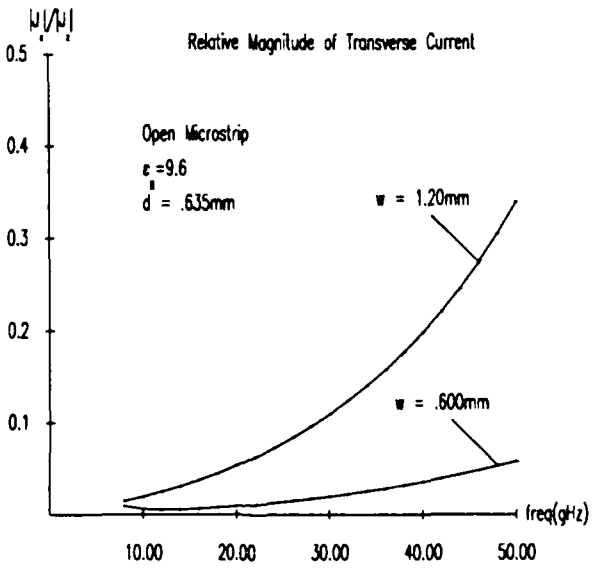

Figure 4.14: Transverse Current on Uniform Microstrip Line

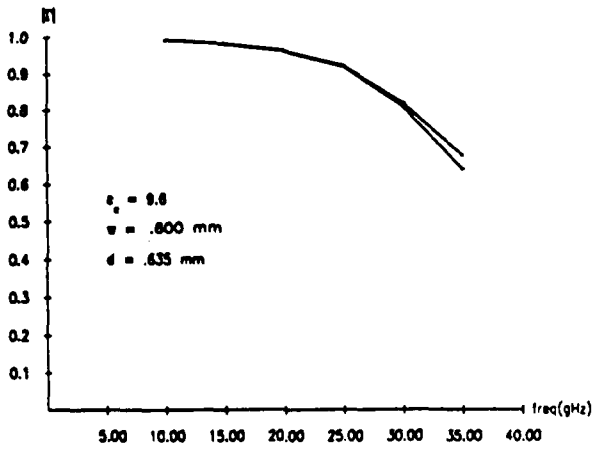

Figure 4.15: Magnitude of Reflection Coefficient of Microstrip Open-End Discontinuity $\frac{w}{d} = \approx .945$

It can be seen that the inclusion of the transverse current in the analysis mainly affects the phase of the reflection coefficient. It can also be seen that the effect of the transverse current is a decrease in the phase of the reflection coefficient. This seems resonable because the transverse current tends to store magnetic energy. The longitudinal current stores mainly electric energy. Thus the effect of the transverse current can cancel the effect of the longitudinal current to some extent.

In order to further compare this analysis with previous numerical work, and analysis was made of an open-end discontinuity in microstrip line of width $.1\lambda_0$ on a substrate with a relative dielectric constant of 12.8. The magnitude of the reflection coefficient of the open-circuited microstrip line is

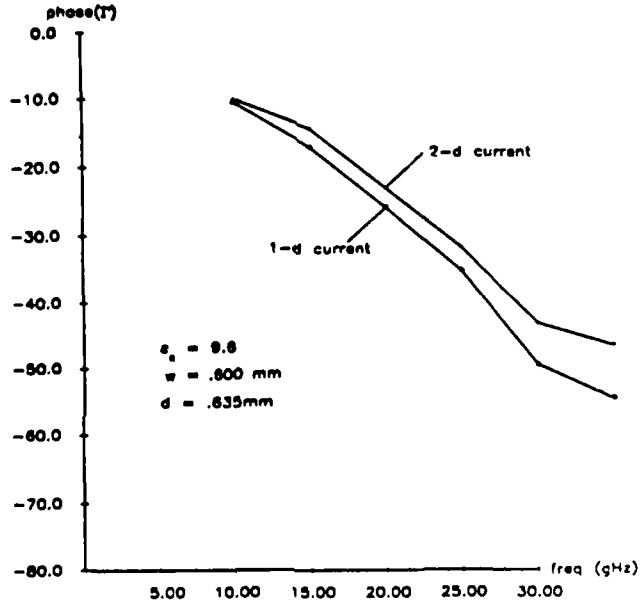

Figure 4.16: Phase of Reflection Coefficient of Microstrip Open-End Discontinuity $\frac{w}{d} \approx .945$

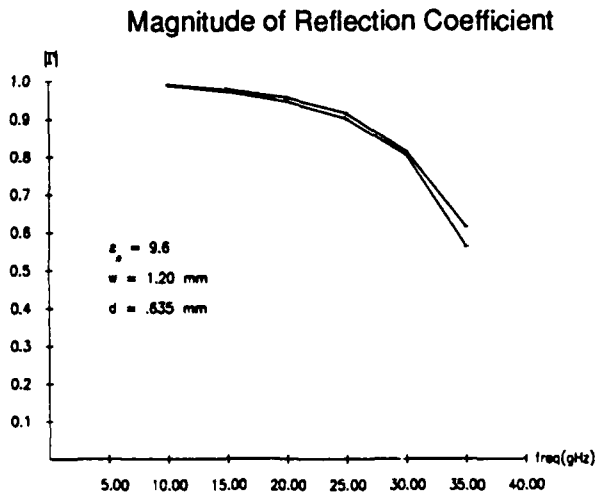

Figure 4.17: Magnitude of Reflection Coefficient of Microstrip Open-End Discontinuity $\frac{w}{d} \approx 1.90$

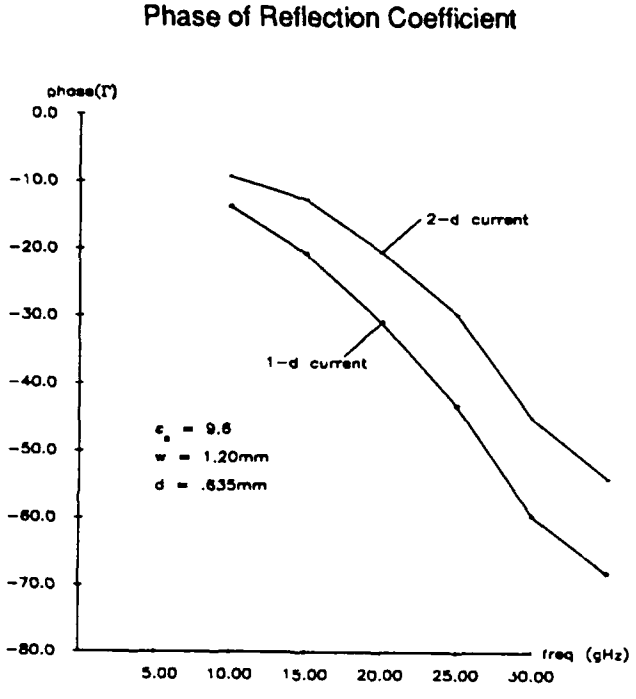

Figure 4.18: Phase of Reflection Coefficient of Microstrip Open-End Discontinuity $\frac{w}{d} \approx 1.90$

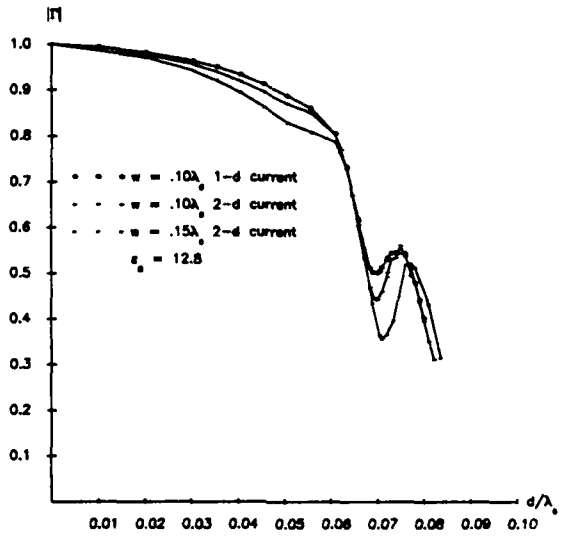

Figure 4.19: Magnitude Reflection Coefficient Coefficient of Microstrip Open-end Discontinuity

shown in Figure 4.19. In the same figure, the magnitude of the reflection coefficient is shown calculated including only longitudinal current on the strip as was done in [15]. This data agrees well with that presented in [15]. It can be seen that for narrow lines such as this one, the inclusion of the transverse current makes little difference in the magnitude of the reflection coefficient for small values of $\frac{d}{\lambda_0}$. However, near the cutoff of the first TE surface wave, it is seen that the magnitude of the reflection coefficient displays a more pronounced trough and peak. This seems reasonable because the inclusion of the energy stored in the transverse current could increase the frequency sensitivity of the reflection coefficient.

Also in Figure 4.19, the magnitude of the reflection coefficient for an open-circuited microstrip line of width $.15\lambda_0$ on a substrate with a relative dielectric constant of 12.8 is shown. It can be seen that the wider line has a more pronounced resonance at the cuton of the first TE surface wave mode.

4.4 Conclusions

Microstrip open-circuit terminations have been analyzed using a deterministic spectral domain method. The radiation loss from the open-end discontinuity can be significant when the substrate is electrically thick. It has been shown that the the transverse current in the microstrip has little effect on the reflection coefficient as long as the line is narrow and the substrate is electrically thin. However, the effects of the transverse current are more pronounced for wider lines and thicker substrates. The effect is most noticeable near the cutoff frequencies of the TE_1 surface-wave mode.

Chapter 5

THE SHORT-CIRCUIT SLOTLINE DISCONTINUITY

5.1 Introduction

The slotline short-circuit discontinuity is the simplest slotline discontinuity. The geometry of the slot line short-circuit is shown in Figure 5.1. Like the open-circuit discontinuity in microstrip, the short-circuit slotline discontinuity is non-ideal because of energy storage near the discontinuity and energy loss from radiation into surface and space waves. The slotline short-circuit discontinuity exhibits a minimum reactance immitance function. Therefore, an appropriate equivalent circuit for a short-circuit slotline discontinuity is the series combination of a resistance and an inductance both of which are in general frequency dependent as shown in Figure 5.2.

In this chapter, slotline short-circuit discontinuities in open environments are analyzed using an extension of the method presented in Chapters 2,3, and 4. This study includes the effects of both longitudinal and transverse electric slot fields and incorporates the proper edge conditions for each component of the field at the edges of the slot and the short-circuited end of the slot.

Although the microstrip open-circuit and the slotline short-circuit are similar in that both radiate power into space waves and surface waves, the

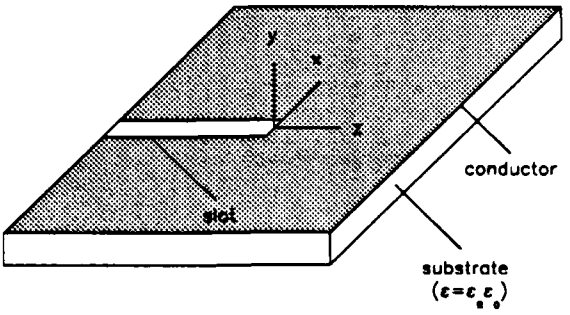

Figure 5.1: The Slotline Short-Circuit Discontinuity

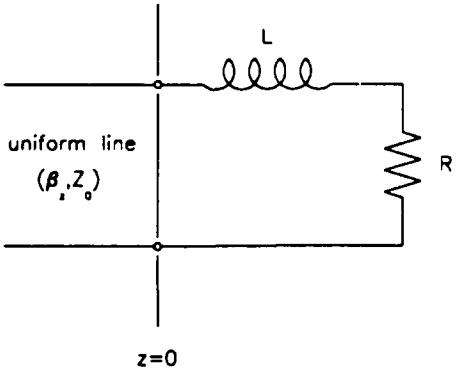

Figure 5.2: Equivalent Circuit of Slotline Short-Circuit Discontinuity

excitation mechanisms are different and therefore, the radiation characteristics are different. In this chapter we compare the non-ideal aspects of open-circuit microstrip and short-circuit slotline discontinuities.

5.2 Method

In principle, the method of analysis described in Chapters 2 and 3 may be used to model slotline discontinuities. However, because the current exists over semi-infinite planes, the representation of the unknown current with basis functions would be difficult and inefficient. Therefore, an alternative approach is used. Consider the spectral domain equations defining the Green's function.

$$\tilde{E}_z(\alpha,\beta) = \tilde{Z}_{zz}(\alpha,\beta)\tilde{J}_z(\alpha,\beta) + \tilde{Z}_{zx}(\alpha,\beta)\tilde{J}_x(\alpha,\beta) \tag{5.1}$$

$$\tilde{E}_x(\alpha,\beta) = \tilde{Z}_{xz}(\alpha,\beta)\tilde{J}_z(\alpha,\beta) + \tilde{Z}_{xx}(\alpha,\beta)\tilde{J}_x(\alpha,\beta) \tag{5.2}$$

This expression can be inverted to give

$$\tilde{J}_x(\alpha,\beta) = \tilde{Y}_{xx}(\alpha,\beta)\tilde{E}_x(\alpha,\beta) + \tilde{Y}_{xz}(\alpha,\beta)\tilde{E}_z(\alpha,\beta) \tag{5.3}$$

$$\tilde{J}_z(\alpha,\beta) = \tilde{Y}_{zx}(\alpha,\beta)\tilde{E}_x(\alpha,\beta) + \tilde{Y}_{zz}(\alpha,\beta)\tilde{E}_z(\alpha,\beta). \tag{5.4}$$

Because the slotline has no ground plane, the Green's function is slightly different from that used for microstrip line. The Green's function is derived in Appendix 2 and is given by

$$\tilde{Y}_{xx} = -N_x^2\tilde{Y}^e - N_z^2\tilde{Y}^h, \tag{5.5}$$

$$\tilde{Y}_{xz} = -N_zN_x(\tilde{Y}^e - \tilde{Y}^h), \tag{5.6}$$

$$\tilde{Y}_{zx} = -N_zN_x(\tilde{Y}^e - \tilde{Y}^h) \text{ and,} \tag{5.7}$$

$$\tilde{Y}_{zz} = -N_z^2\tilde{Y}^e - N_x^2\tilde{Y}^h \tag{5.8}$$

where

$$\tilde{Y}^e = \tilde{Y}_{TM2}\left(\frac{\tilde{Y}_{TM2}+\tilde{Y}_{TM1}\coth(\gamma_2 d)}{\tilde{Y}_{TM1}+\tilde{Y}_{TM2}\coth(\gamma_2 d)}\right), \text{ and} \tag{5.9}$$

$$\tilde{Y}^h = \tilde{Y}_{TE2}\left(\frac{\tilde{Y}_{TE2}+\tilde{Y}_{TE1}\coth(\gamma_2 d)}{\tilde{Y}_{TE1}+\tilde{Y}_{TE2}\coth(\gamma_2 d)}\right). \tag{5.10}$$

Like the Green's function used in the analysis of microstrip, this Green's function has poles corresponding to surface waves in the dielectric. These surface waves correspond to those in a grounded dielectric slab just as those generated by microstrip discontinuities. Therefore, the pole locations are the same as those for the grounded slab. However, the residues at the poles are different because the surface wave excitation mechanism is different. The residue calculation is the same as that given in Chapter 2 except $Z_{zzTM}\ldots Z_{xxTM}$ are replaced by

$$\tilde{Y}_{xxTM} = -N_x^2\tilde{Y}^e_{TM}, \tag{5.11}$$

$$\tilde{Y}_{xzTM} = -N_xN_z\tilde{Y}^e_{TM} \tag{5.12}$$

$$\tilde{Y}_{zxTM} = -N_xN_z\tilde{Y}^e_{TM} \text{ and,} \tag{5.13}$$

$$\tilde{Y}_{xxTM} = -N_z^2\tilde{Y}^e_{TM}, \tag{5.14}$$

where

$$\tilde{Y}^e_{TM} = \tilde{Y}_{TM2}\left(\frac{\tilde{Y}_{TM2}+\tilde{Y}_{TM1}\coth(\gamma_2 d)}{\frac{\partial\tilde{Y}^e_1}{\partial\rho}+\frac{\partial\tilde{Y}^e_2}{\partial\rho}}\right),$$

$$\frac{\partial\tilde{Y}^e_1}{\partial\rho} = \left(\frac{-\rho}{\gamma_1^2}\right)\tilde{Y}^e_1(\rho), \text{ and}$$

$$\frac{\partial\tilde{Y}^e_2}{\partial\rho} = \left(\frac{\rho}{\gamma_1^2}\right)\tilde{Y}^h_1(\rho).$$

For TE modes the residue is given by

$$\tilde{Y}_{xxTE} = -N_z^2 \tilde{Y}_{TE}^h, \tag{5.15}$$

$$\tilde{Y}_{xzTE} = +N_x N_z \tilde{Y}_{TE}^h \tag{5.16}$$

$$\tilde{Y}_{zxTE} = +N_x N_z \tilde{Y}_{TE}^h \text{ and,} \tag{5.17}$$

$$\tilde{Y}_{zzTE} = -N_x^2 \tilde{Y}_{TE}^h, \tag{5.18}$$

where

$$\tilde{Y}_{TE}^h = \tilde{Y}_{TE2}\left(\frac{\tilde{Y}_{TE2} + \tilde{Y}_{TE1}\coth(\gamma_2 d)}{\frac{\partial \tilde{Y}_1^h}{\partial \rho} + \frac{\partial \tilde{Y}_2^h}{\partial \rho}}\right),$$

$$\frac{\partial \tilde{Y}_1^h}{\partial \rho} = \left(\frac{-\rho}{\gamma_1^2}\right)\left(\tilde{Y}_2^e(\rho) + \tilde{Y}_{TM2} d\gamma_2(\coth^2(\gamma_1 d) - 1)\right), \text{ and}$$

$$\frac{\partial \tilde{Y}_2^h}{\partial \rho} = \left(\frac{\rho}{\gamma_2^2}\right)\left(\tilde{Y}_2^h(\rho) + \tilde{Y}_{TE2} d\gamma_2(\coth^2(\gamma_2 d) - 1)\right).$$

With this formulation of the Green's function, we can expand the slot electric field in terms of known expansion functions in the same way the strip current was expanded for microstrip. We can make use of the same expansion and testing functions as used in the analysis of microstrip except that the functions used to model the transverse dependance of the current are reversed.

$$E_{xm}(x) = \frac{\cos(\frac{2(m-1)\pi x}{w})}{\sqrt{1-(\frac{2x}{w})^2}} \tag{5.19}$$

$$E_{zm}(x) = \frac{\sin(\frac{2m\pi x}{w})}{\sqrt{1-(\frac{2x}{w})^2}} \tag{5.20}$$

The functions E_{zm} and E_{xm} include the proper edge condition for the longitudinal and transverse field at the edges of the slot. The spectral domain eigenvalue approach described in Chapter 2 is used to compute the propagation constant

and the transverse and longitudinal electric slot field components for the fundamental mode on an infinitely long open slotline. For the fundamental mode, the propagation constant, β_z is always greater than any the value ρ of any surface-wave pole. Therefore, the fundamental mode on slotline is always slow compared to any surface-wave mode and thus does not radiate into surface-wave modes. Once the fields for the fundamental mode on uniform slotline are determined, the slotline is divided into two regions, a uniform region far from the shorted end and a perturbed region near the shorted end as in [15]. In the uniform region the slot electric field is assumed to consist of only the fundamental mode. The slot electric field in the uniform region is represented by the source function and a reflected wave with an unknown amplitude, Γ.

$$E_x^{uniform}(x,z) = \sum_{l=1}^{L} a_l E_{xl}(x)(\exp(-j\beta_z z) - \Gamma \exp(+j\beta_z z))$$

$$E_z^{uniform}(x,z) = \sum_{l=1}^{L} b_l E_{zl}(x)(\exp(-j\beta_z z) + \Gamma \exp(+j\beta_z z))$$

The constants $a_1 \ldots a_L$, $b_1 \ldots b_L$ and β, the propagation constant are determined using the spectral domain eigenvalue formulation. The longitudinal dependance of the slot electric field in the perturbed region near the shorted end is represented with piecewise linear (rooftop) subsectional basis functions which are defined in Chapter 3. The piecewise linear functions allow a reasonable approximation to the edge condition for the both the transverse and the longitudinal components of the electric field at the shorted end. The transverse dependance of the slot electric field in the perturbed region is represented with Maxwellian basis functions with variable coefficients. The development of the linear system is then the same as that for the open-end microstrip discontinuity which was developed in Chapter 4.

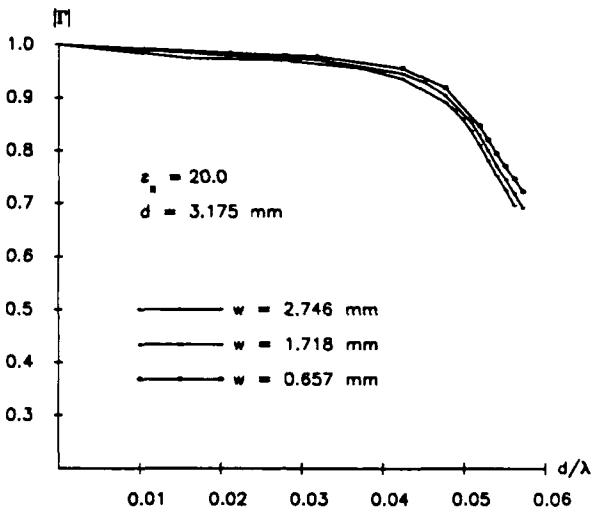

Figure 5.3: Magnitude of Reflection Coefficient of Slotline Short-circuit Discontinuity

5.3 Numerical Results

In Figures 5.3 and 5.4, the magnitude and phase of the reflection coefficient versus frequency is plotted for a shorted slotline on a substrate with a relative dielectric constant of 20.0 and thickness of 3.175 mm for various slot widths. In Figures 5.5 and 5.6, the normalized resistance and inductance of the equivalent circuit are plotted. It can be seen that, as with the microstrip open circuit discontinuity, the radiation loss becomes very large near the cutoff frequency of the second surface wave mode. In Figure 5.7, the magnitude of the reflection coefficient for a short-circuited slotline and an open-circuited microstrip line are plotted for comparison. The substrate thickness and dielectric constant are the same for the microstrip and the slotline. Also, the slot width is

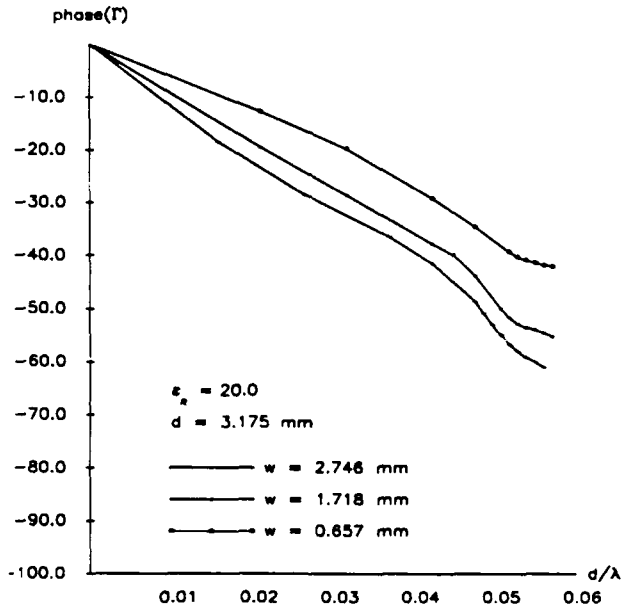

Figure 5.4: Phase of the Reflection Coefficient Slotline Short-circuit Discontinuity

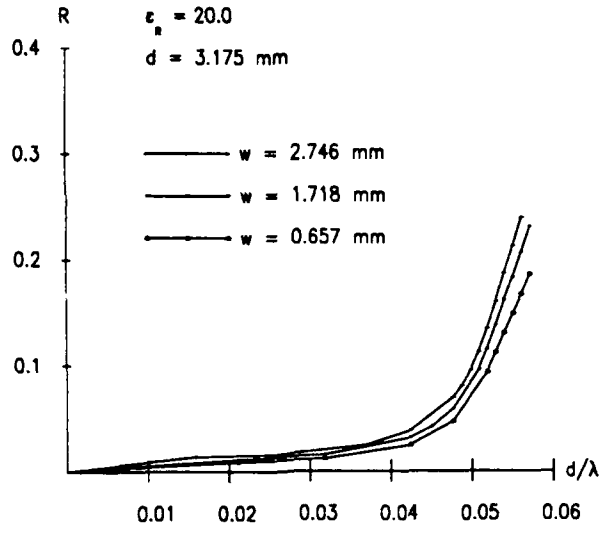

Figure 5.5: Equivalent Resistance of Slotline Short-circuit Discontinuity

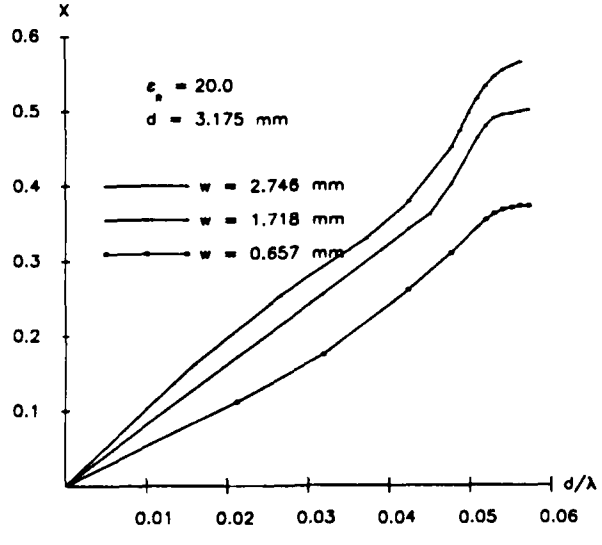

Figure 5.6: Equivalent Inductance of Slotline Short-circuit Discontinuity

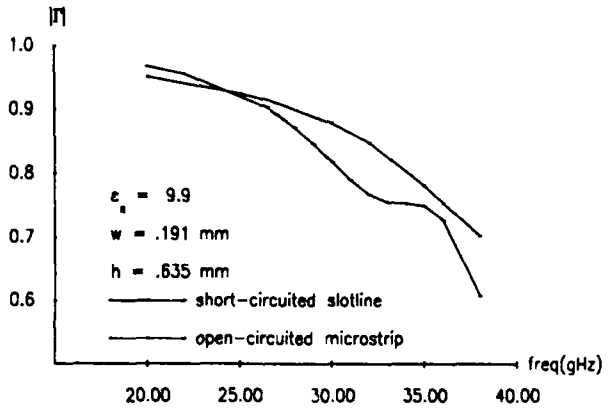

Figure 5.7: Comparison of Slotline Short-circuit and Microstrip Open-end Discontinuities

the same as the microstrip width. The microstrip open-circuit exhibits greater loss because the open-circuited microstrip discontinuity excites the TM_0 surface wave mode more strongly than the slotline short-circuit discontinuity. This is because the fields of the fundamental mode of microstrip match those of the TM_0 surface wave more closely than those of the fundamental mode of slotline.

Chapter 6

THE MICROSTRIP GAP DISCONTINUITY

6.1 Introduction

Microstrip gap discontinuities are commonly used to achieve capacitive coupling in microstrip circuits and antennas. In open structures, microstrip gap discontinuities can radiate into space waves and surface waves resulting in losses and spurious coupling. In this chapter we will analyze gap discontinuities and gap-coupled resonators. This analysis includes the effects of a two-component, two-dimensional current flow on the conductor and mode conversion. Through the use of the exact spectral domain Green's function it includes the effects of space-wave and surface-wave radiation. Like [4], this method can be applied to asymmetric discontinuities. However, it is more efficient due to the travelling wave source formulation, requiring only two matrix fills and inversions to obtain the two-port scattering matrix. In the case of symmetric structures, only one matrix fill and inversion is required with this method, whereas [19] requires two. Unlike the discontinuities analyzed in Chapters 4 and 5, the gap and gap-coupled resonator are two-port devices and therefore, in addition to the reflection coefficient a transmission coefficient must also be determined.

In Figure 6.1 a microstrip gap discontinuity, gap-coupled resonator, and coupled resonator bandpass filter are shown. It was desired to deter-

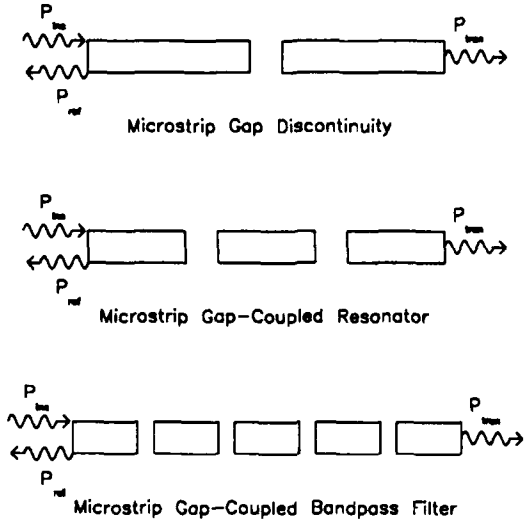

Figure 6.1: Microstrip Gap Discontinuity, Gap-coupled Resonator, and Gap-coupled Bandpass Filter

mine whether gap discontinuities interact significantly on open microstrip when spaced slightly less than one-half wavelength apart as they would be in such a filter. It is shown that the gap discontinuities do interact at high frequencies reducing the Q and the rejection of gap-coupled resonators.

6.2 Application of the Method to Microstrip Gap Discontinuities

As in the analysis of microstrip open-end discontinuities, the spectral domain eigenvalue fomulation is used to compute the propagation constant and the longitudinal and transverse currents for the fundamental mode on an infinitely long open microstrip. In the general case in which the microstrip lines on either side of the gap are of different widths, this analysis must be performed for each side. Far from the discontinuity, the current on the strip is assumed to consist only of the fundamental mode. The current in the uniform region on the source side of the discontinuity is represented by an incident and a reflected wave with an unknown amplitude, Γ.

$$J_z^{uniform}(x,z) = \sum_{l=1}^{L} a_l J_{zl}(x)(\exp(-j\beta_z z) - \Gamma \exp(+j\beta_z z))$$

$$J_x^{uniform}(x,z) = \sum_{l=1}^{L} b_l J_{xl}(x)(\exp(-j\beta_z z) + \Gamma \exp(+j\beta_z z))$$

The current in the uniform region on the load side of the discontinuity is represented by a transmitted wave with an unknown amplitude, T.

$$J_z^{uniform}(x,z) = \sum_{l=1}^{L} a_l J_{zl}(x)(\mathrm{T} \exp(-j\beta_z z))$$

$$J_x^{uniform}(x,z) = \sum_{l=1}^{L} b_l J_{xl}(x)(\mathrm{T} \exp(-j\beta_z z))$$

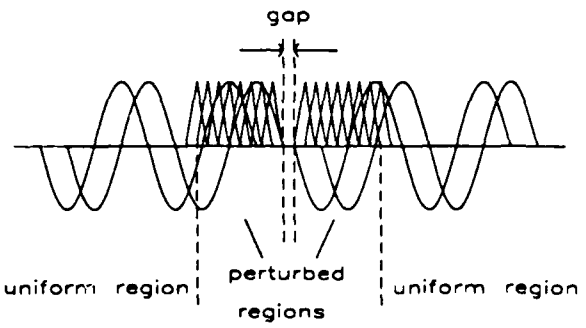

Figure 6.2: Arrangement of Basis Functions for Analysis of Gap Discontinuity

The functions J_{zl} and J_{xl} are the Maxwellian basis functions defined in Chapters 3 and 5. The constants $a_1 \ldots a_L$, $b_1 \ldots b_L$ and β_z, the propagation constant are determined in the spectral domain analysis for uniform line. The longitudinal dependance of the current in the perturbed region near the discontinuity is augmented with piecewise linear subsectional basis functions. A typical arrangement is shown in Figure 6.2 The transverse dependance of the current in the perturbed region is represented with Maxwellian basis functions with variable coefficients thus taking into account mode conversion. Note that the basis functions are really those of two microstrip open-end discontinuities. Therefore, by using the same testing scheme as was used in the analysis of the open-end discontinuity we can generate a system of linear equations with the

following form

$$\begin{bmatrix} [K^{left}] & [K^{cross}] \\ [K^{cross}] & [K^{right}] \end{bmatrix} = \begin{bmatrix} [S^{left}] \\ [S^{right}] \end{bmatrix}$$

Where K^{left} is the coefficient matrix of the linear system developed for the open-end discontinuity in Chapter 4, K^{right} is a similar matrix for the right-hand open-end discontinuity, K^{cross} is a matrix developed from testing the right hand side with the left and vice-versa, and S^{left} and S^{right} are vectors obtained by testing the source functions with the testing functions for the left and right open-end discontinuities. These equations are solved to obtain Γ, T, and the current on the conductors.

6.3 Extension to Microstrip Gap-Coupled Resonators

The method may be extended to gap-coupled resonators with the inclusion of more subsectional basis functions as shown in Figure 6.3

6.4 Results

In Figure 6.6 and 6.7, the magnitudes of the transmission coefficients of two gap-coupled half-wave resonators are shown calculated in the following two ways. First the scattering matrix for an isolated gap is calculated using the spectral domain method. Then the scattering matrix of the resonator is calculated using the scattering matrix of the isolated gap along with those of a section of uniform microstrip line.

$$\begin{bmatrix} [T_{11}^{res}] & [T_{12}^{res}] \\ [T_{21}^{res}] & [T_{22}^{res}] \end{bmatrix} = \begin{bmatrix} [T_{11}^{gap}] & [T_{12}^{gap}] \\ [T_{21}^{gap}] & [T_{22}^{gap}] \end{bmatrix} \begin{bmatrix} e^{-j\beta_z L} & 0 \\ 0 & e^{j\beta_z L} \end{bmatrix} \begin{bmatrix} [T_{11}^{gap}] & [T_{12}^{gap}] \\ [T_{21}^{gap}] & [T_{22}^{gap}] \end{bmatrix}$$

Second, the spectral domain method is used to model the entire res-

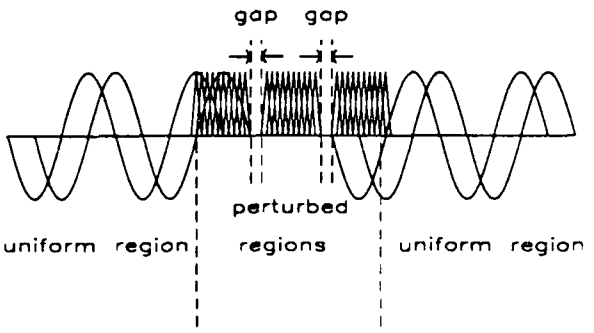

Figure 6.3: Arrangement of Basis Functions for Analysis of Gap-Coupled Resonator

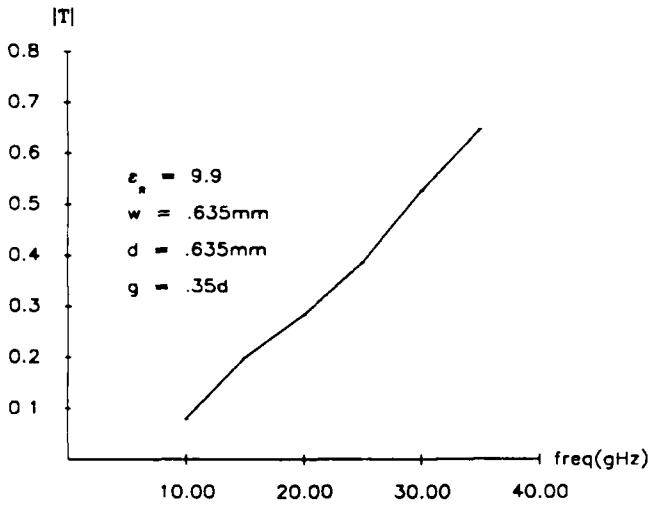

Figure 6.4: Magnitude of Transmission Coefficient of Gap Discontinuity

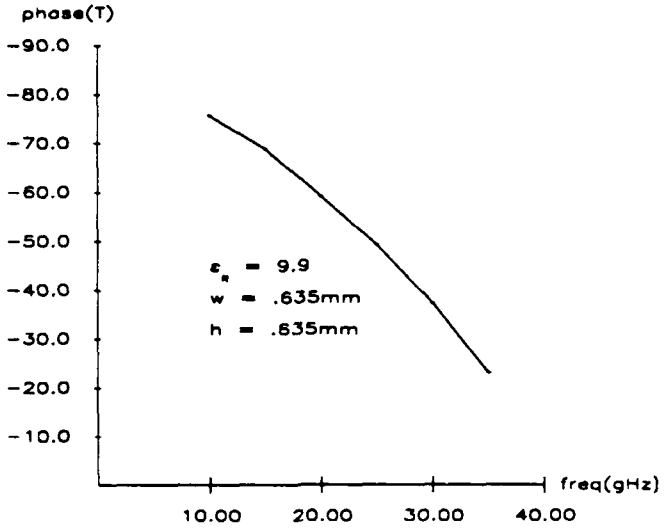

Figure 6.5: Phase of Transmission Coefficient of Gap Discontinuity

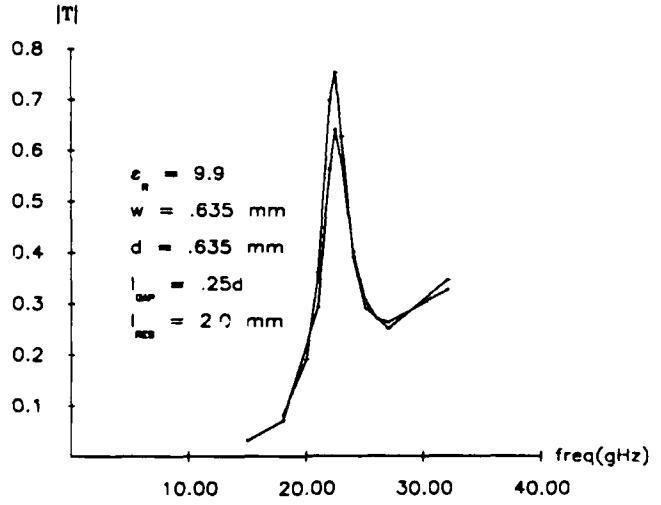

Figure 6.6: Magnitude of Transmission Coefficient of Gap-coupled Resonator

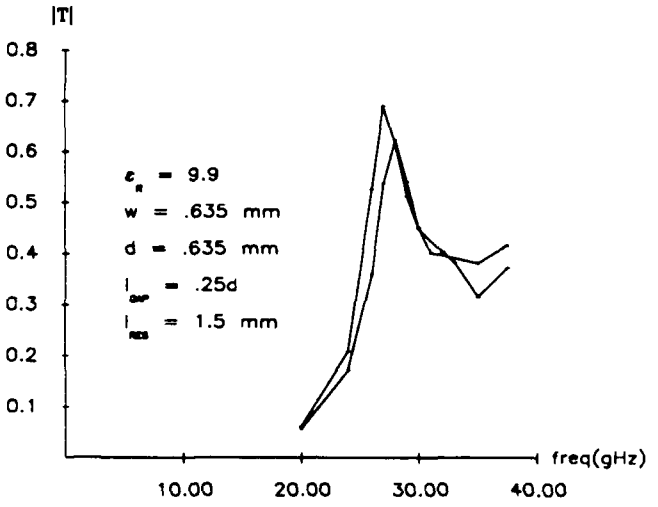

Figure 6.7: Magnitude of transmission coefficient of gap-coupled resonator

onator including coupling between the gaps as shown in Figure 6.1. It can be seen that the coupling between the two gaps has little effect when the resonance frequency of the resonator is low. However, for shorter resonators the coupling between the gaps shifts the resonance frequency, lowers the Q, and lowers the rejection above resonance.

We conclude that the spectral domain method can be effectively applied to the modeling of gap-coupled resonators. Furthermore, such analysis is justified as coupling between the two gaps of a gap-coupled resonator can have a significant effect on the resonant frequency, Q and rejection of the resonator.

Chapter 7

CONCLUSIONS

7.1 Summary

A method for the analysis of planar circuits on open substrates has been presented. Through the use of the exact spectral domain Green's function, the method includes the effects of space wave and surface wave radiation. The method has been shown to be applicable to 1-port and 2-port structures. In particular, the method has been applied to microstrip open-end discontinuities and slot-line short circuit discontinuities. The method has been applied to gap discontinuities and gap-coupled resonators.

7.2 Suggestions for Further Applications

7.2.1 Extension to N-port Networks

The deterministic spectral domain method presented here is very general and should be useful for analyzing multiport planar networks on open substrates. As was pointed out in Chapter 6, the travelling wave formulation is more efficient for analyzing two-port networks than other methods such as [19]. Furthermore, these other methods are difficult to extend to N-port networks. To extend this method to an N-port network we simply excite one port with a known incident wave and then formulate N unknown outward travelling waves as shown in Figure 7.1 for a 4-port. Therefore, in order to determine the

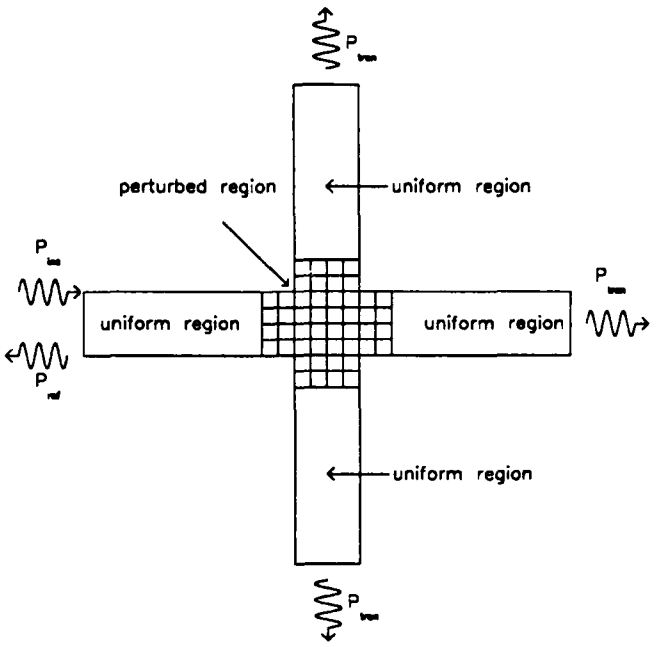

Figure 7.1: Application to N-port Network

entire $N \times N$ scattering matrix of a general N port, N calculations must be performed. Of course, symmetry in the network would reduce the number of necessary calculations.

7.2.2 Extension to Multilayer Structures

By making use of the immitance approach for the Green's function derivation, this method is easily extended to multilayer substrate/superstrate structures. It would be useful to study how surface-wave and space-wave excitation can be controlled through the use of multi-layered substrates and/or superstrates. It should also be noted that this method may be easily adapted through a simple modification of the Green's function to structures which are covered but laterally open.

7.3 Suggestions for Improvement

7.3.1 Asymptotic Evaluation of the Inner Products

The most time consuming part of the method is the evaluation of the asymptotic portion of the inner products. It is straightforward to determine an asymptotic form of the Green's function for large ρ because the Green's function is separable in ρ and θ. However, since the basis functions used here are separable in α and β, an asymptotic form for large ρ is not immediately evident. An asymptotic form for large ρ would be most useful because the space domain calculation of the asymptotic portions of the matrix components is not compatible with the scheme given in Chapter 3 for precomputing and storing the Green's function. Also the space domain integration requires high numerical precision due the subtraction of the source and image contributions. This problem is greater for electrically thin substrates. Using more rapidly converging basis functions does not appear to be a better approach, because the basis functions must be chosen to model the physical current (or field) which will necessarily exhibit edge conditions. These edge conditions in the space domain translate into high spatial frequency components in the spectral domain.

In view of the above difficulties with evaluating the asymptotic portion of the integrands, it seems promising to solve the mixed potential integral equation (MPIE) in the spectral domain instead of the electric field integral equation. This is because the Green's functions used in the MPIE converge faster than those for EFIE. This is easy to see by examining the case of a homogeneous medium. The electric field Green's function has a $\frac{1}{R^3}$ singularity

at the source point. It is this source singularity that gives the spectral domain electric field Green's function its asymptotic tail. On the other hand the Green's functions used in the MPIE have $\frac{1}{R}$ type singularities at the source point. Therefore, they have more rapidly converging spectral domain counterparts. Although the MPIE requires the determination of both charge and current, the added computation may be offset by the savings gained by faster convergance. One disadvantage to this method is that, as far we have found, no straightforward method such as the immittance approach exists for determining the necessary Green's functions.

7.3.2 Generalization of Basis Functions

Although in all of the work presented here, entire domain basis functions were used to represent the transverse dependence of the current or field quantities, it would be useful to also make use of subsectional basis functions for both the transverse and longitudinal dependance. For uniform line, entire domain functions such as the Maxwellian functions are most efficient for modelling the transverse dependance, just as entire domain functions are most efficient to describe the longitudinal dependence of travelling wave functions. However, it appears that in the regions near discontinuties, subsectional basis functions are more efficient for the representation of the current or field. For example, in order to analyze a step-width discontinuity, it would be most efficient to use subsectional basis functions to represent the transverse dependance of the current near the discontinuity. Also, it would be useful to develop more general subsectional basis functions for the modelling of complicated discontinuities such as tapers and smooth bends. The use of rectangular basis

functions to approximate a smooth curve may lead to error due to the large current density along the edge. A triangular based function would allow a more continuous approximation of smooth curves.

7.3.3 Computational Algorithm

By far the largest speedups have been obtained through modifications to the computational algorithm. It appears that great improvements could still be made in this area. The bulk of the computational effort occurs in evaluating the Green's function. As was pointed out in Chapter 3, a large savings was realized by precomputing and storing the Green's function so that the entire matrix could be integrated at once. This savings may be increased by precomputing the Green's function for all β, storing the values in a database, and then using an interpolation scheme to determine intermediate points. It appears that computational methods such as the one presented here are quite amenable to vector processing because of the large amount of non-interelated computation. Therefore, despite the fact that the method requires large amounts of computation, it could be utilized with small vector processors for engineering purposes.

Appendix A

DERIVATION OF THE GREEN'S FUNCTION FOR THE GROUNDED SLAB

In this appendix we give some of the details of the immitance derivation of the spectral domain Green's function. The immittance formalism is due to [13] and is included here for completeness. We begin by noting that from the Fourier transform relationship

$$E(x,y,z) = \frac{1}{2\pi}\int_{-\infty}^{+\infty}\int_{-\infty}^{+\infty}\tilde{E}(\alpha,y,\beta)\exp(-j(\alpha x+\beta z))d\alpha d\beta \qquad (A.1)$$

the space domain field and current quantities are superpositions of the inhomogeneous spectral waves propagating in the direction θ from the z-axis where $\theta = \tan^{-1}\left(\frac{\beta}{\sqrt{\alpha^2+\beta^2}}\right)$. If we define the coordinate transformation

$$u = z\sin(\theta) - x\cos(\theta) \qquad (A.2)$$

$$v = z\cos(\theta) + x\sin(\theta) \qquad (A.3)$$

we can decompose the spectral fields into TM-to-y (E_y, E_v, and H_u) and TE-to-y (H_y, H_v, and E_u). The TM-to-y fields are created by J_v and the TE-to-y fields are created by J_u. We define transmission line characteristic admittances $\tilde{Y}_{TM1}$ and $\tilde{Y}_{TM2}$ as the wave admittances seen by a transverse-magnetic-to-y wave travelling in media 1 and 2 of Figure 2.1

$$\tilde{Y}_{TM1} = \frac{-\tilde{H}_u^+}{\tilde{E}_v^+} = \frac{+\tilde{H}_u^-}{\tilde{E}_v^-} \qquad (A.4)$$

$$\tilde{Y}_{TM2} = \frac{-\tilde{H}_u^+}{\tilde{E}_v^+} = \frac{+\tilde{H}_u^-}{\tilde{E}_v^-} \tag{A.5}$$

where the superscript "+" implies waves travelling in the positive y direction and "-" implies waves travelling in the negative y direction. Likewise, we define transmission line characteristic admittances $\tilde{Y}_{TM1}$ and $\tilde{Y}_{TM2}$ as the wave admittances seen by a transverse-magnetic-to-y wave travelling in media 1 and 2 of Figure 2.1

$$\tilde{Y}_{TE1} = \frac{+\tilde{H}_v^+}{\tilde{E}_u^+} = \frac{-\tilde{H}_v^-}{\tilde{E}_u^-} \tag{A.6}$$

$$\tilde{Y}_{TE2} = \frac{+\tilde{H}_v^+}{\tilde{E}_u^+} = \frac{-\tilde{H}_v^-}{\tilde{E}_u^-} \tag{A.7}$$

The y-propagation constants may be obtained from the dispersion relations for each region and are given by

$$\gamma_1 = \sqrt{\alpha^2 + \beta^2 - k_0^2}, \tag{A.8}$$

$$\gamma_2 = \sqrt{\alpha^2 + \beta^2 - \epsilon_R k_0^2}. \tag{A.9}$$

The wave impedances may be obtained from Maxwell's equations and are given by

$$\tilde{Y}_{TM1} = \frac{j\omega\epsilon_0}{\gamma_1}, \tag{A.10}$$

$$\tilde{Y}_{TM2} = \frac{j\omega\epsilon_0\epsilon_R}{\gamma_2}, \tag{A.11}$$

$$\tilde{Y}_{TE1} = \frac{\gamma_1}{j\omega\mu}, \tag{A.12}$$

$$\tilde{Y}_{TE2} = \frac{\gamma_2}{j\omega\mu}. \tag{A.13}$$

We may now draw the equivalent circuits in for the TE and TM modes as in Figure A.1. We define the driving point impedances $\tilde{Y}_1^e$ and $\tilde{Y}_2^e$ as the

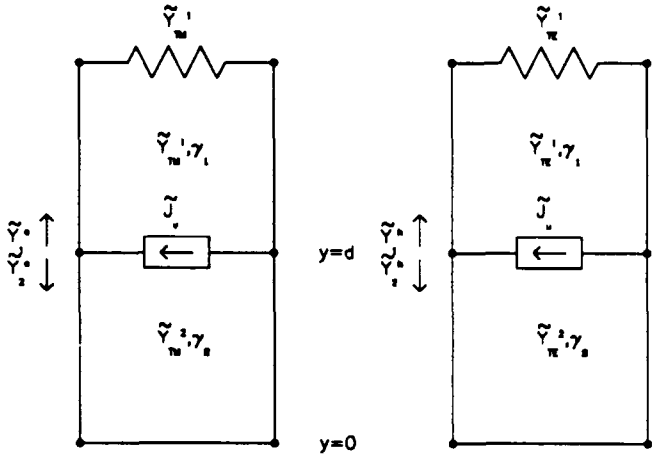

Figure A.1: Equivalent Networks for TE and TM Modes

admittances looking upward and downward at $y = d$ respectively.

$$\tilde{Y}_1^e = \frac{-\tilde{H}_{u1}}{\tilde{E}_{v1}} \tag{A.14}$$

$$\tilde{Y}_2^e = \frac{+\tilde{H}_{u2}}{\tilde{E}_{v2}} \tag{A.15}$$

$$\tilde{Y}_1^h = \frac{+\tilde{H}_{v1}}{\tilde{E}_{u1}} \tag{A.16}$$

$$\tilde{Y}_2^h = \frac{-\tilde{H}_{v2}}{\tilde{E}_{u2}} \tag{A.17}$$

At the interface, $y = d$, the magnetic field is discontinuous because of the electric current at the interface.

$$\tilde{H}_{u1} - \tilde{H}_{u2} = \tilde{J}_v \tag{A.18}$$

$$\tilde{H}_{v2} - \tilde{H}_{v1} = \tilde{J}_u \tag{A.19}$$

At the interface, $y = d$, the electric field is continuous.

$$\tilde{E}_{v1} = \tilde{E}_{v2} = \tilde{E}_v \tag{A.20}$$

$$\tilde{E}_{u1} = \tilde{E}_{u2} = \tilde{E}_u \tag{A.21}$$

Therefore we can write

$$\begin{aligned} \tilde{E}_v &= -\frac{\tilde{J}_v}{\tilde{Y}_1^e + \tilde{Y}_2^e} \\ &= -\tilde{J}_v \tilde{Z}^e \end{aligned} \tag{A.22}$$

$$\begin{aligned} \tilde{E}_u &= -\frac{\tilde{J}_u}{\tilde{Y}_1^h + \tilde{Y}_2^h} \\ &= -\tilde{J}_u \tilde{Z}^h \end{aligned} \tag{A.23}$$

where

$$\tilde{Y}_1^e = \tilde{Y}_{TM1} \tag{A.24}$$

$$\tilde{Y}_2^e = \tilde{Y}_{TM2} \coth(\gamma_2 d) \tag{A.25}$$

$$\tilde{Y}_1^h = \tilde{Y}_{TE1} \tag{A.26}$$

$$\tilde{Y}_2^h = \tilde{Y}_{TE2} \coth(\gamma_2 d). \tag{A.27}$$

The transformation back into the x, z coordinates is

$$\begin{aligned} \tilde{E}_z = &-\left(N_z^2 \tilde{Z}^e + N_x^2 \tilde{Z}^h\right) \tilde{J}_z \\ &-N_z N_x \left(\tilde{Z}^e - \tilde{Z}^h\right) \tilde{J}_x \end{aligned} \tag{A.28}$$

$$\begin{aligned} \tilde{E}_x = &-N_z N_x \left(\tilde{Z}^e - \tilde{Z}^h\right) \tilde{J}_z \\ &-\left(N_x^2 \tilde{Z}^e + N_z^2 \tilde{Z}^h\right) \tilde{J}_x \end{aligned} \tag{A.29}$$

where

$$N_x = \frac{\alpha}{\sqrt{\alpha^2 + \beta^2}} \tag{A.30}$$

$$N_z = \frac{\beta}{\sqrt{\alpha^2 + \beta^2}} \tag{A.31}$$

Therefore, spectral domain Green's function is given by

$$\tilde{Z}_{zz} = -(N_z^2 \tilde{Z}^e + N_x^2 \tilde{Z}^h) \tag{A.32}$$

$$\tilde{Z}_{zx} = -N_z N_x (\tilde{Z}^e - \tilde{Z}^h) \tag{A.33}$$

$$\tilde{Z}_{xz} = -N_z N_x (\tilde{Z}^e - \tilde{Z}^h) \tag{A.34}$$

$$\tilde{Z}_{xx} = -(N_x^2 \tilde{Z}^h + N_z^2 \tilde{Z}^e) \tag{A.35}$$

Appendix B

DERIVATION OF THE GREEN'S FUNCTION FOR THE UNGROUNDED SLAB

The derivation of the Green's function appropriate for the analysis of slotline is a simple modification of that for the Green's function in Appendix 1. Since the medium below the slab is the same as that above, we draw the equivalent circuits in for the TE and TM modes as in Figure B.1.

Therefore, the driving point impedances at $y = d$ are

$$\tilde{Y}_1^e = \tilde{Y}_{TM1} \tag{B.1}$$

$$\tilde{Y}_1^h = \tilde{Y}_{TE1} \tag{B.2}$$

$$\tilde{Y}_2^e = \tilde{Y}_{TM2}\left(\frac{\tilde{Y}_{TM2} + \tilde{Y}_{TM1}\coth(\gamma_2 d)}{\tilde{Y}_{TM1} + \tilde{Y}_{TM2}\coth(\gamma_2 d)}\right) \tag{B.3}$$

$$\tilde{Y}_2^h = \tilde{Y}_{TE2}\left(\frac{\tilde{Y}_{TE2} + \tilde{Y}_{TE1}\coth(\gamma_2 d)}{\tilde{Y}_{TE1} + \tilde{Y}_{TE2}\coth(\gamma_2 d)}\right) \tag{B.4}$$

$$\tilde{Z}^e = \frac{1}{\tilde{Y}_1^e + \tilde{Y}_2^e} \tag{B.5}$$

$$\tilde{Z}^h = \frac{1}{\tilde{Y}_1^h + \tilde{Y}_2^h} \tag{B.6}$$

As pointed out in chapter 4, the inverted Green's function is then given by

$$\tilde{Y}_{xx} = -N_x^2\frac{1}{\tilde{Z}^e} - N_z^2\frac{1}{\tilde{Z}^h} \tag{B.7}$$

$$\tilde{Y}_{xz} = -N_xN_z\left(\frac{1}{\tilde{Z}^e} - \frac{1}{\tilde{Z}^h}\right) \tag{B.8}$$

$$\tilde{Y}_{zx} = -N_xN_z\left(\frac{1}{\tilde{Z}^e} - \frac{1}{\tilde{Z}^h}\right) \tag{B.9}$$

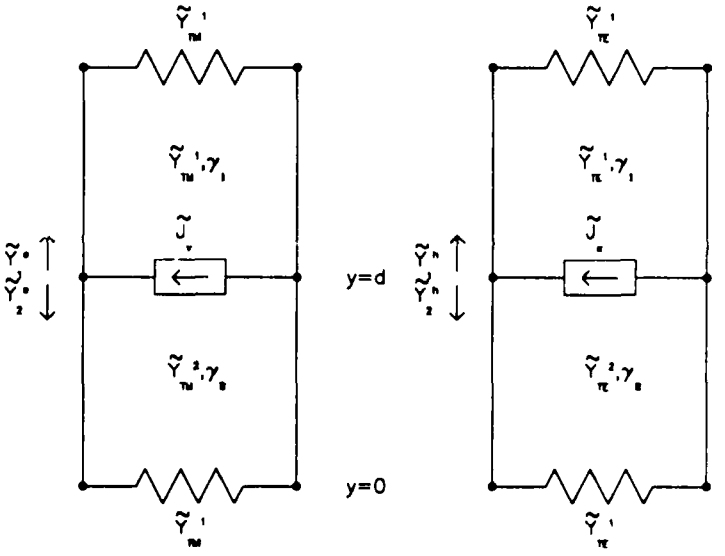

Figure B.1: Equivalent Networks for TE and TM Modes

$$\tilde{Y}_{zz} = -N_z^2 \frac{1}{\tilde{Z}^e} - N_x^2 \frac{1}{\tilde{Z}^h} \tag{B.10}$$

As with the Green's functions $\tilde{Z}_{zz} \ldots \tilde{Z}_{xx}$ for the grounded dielectric slab, $\tilde{Y}_{xx} \ldots \tilde{Y}_{zz}$ have a branch point at $\rho = k_0$. Unlike $\tilde{Z}_{zz} \ldots \tilde{Z}_{xx}$, $\tilde{Y}_{xx} \ldots \tilde{Y}_{zz}$ are not well behaved at the branch point. This can be seen by defining

$$\begin{aligned} \tilde{Y}^e &= \frac{1}{\tilde{Z}^e} \\ &= \tilde{Y}_1^e + \tilde{Y}_2^e \qquad \text{(B.11)} \\ \tilde{Y}^h &= \frac{1}{\tilde{Z}^h} \\ &= \tilde{Y}_1^h + \tilde{Y}_2^h. \qquad \text{(B.12)} \end{aligned}$$

Now the Green's function is rewritten as

$$\tilde{Y}_{xx} = -N_x^2 \tilde{Y}^e - N_z^2 \tilde{Y}^h \tag{B.13}$$

$$\tilde{Y}_{xz} = -N_x N_z (\tilde{Y}^e - \tilde{Y}^h) \tag{B.14}$$

$$\tilde{Y}_{zx} = -N_x N_z (\tilde{Y}^e - \tilde{Y}^h) \tag{B.15}$$

$$\tilde{Y}_{zz} = -N_z^2 \tilde{Y}^e - N_x^2 \tilde{Y}^h. \tag{B.16}$$

It can be seen that, because $\tilde{Y}_{TM1}$ is singular at $\rho = k_0$, $\tilde{Y}^e$ is singular at $\rho = k_0$. It should be stressed, however, that this point constitutes a branch point and does not contribute to the integral.

As with the Green's functions $\tilde{Z}_{zz} \ldots \tilde{Z}_{xx}$ for the grounded dielectric slab, $\tilde{Y}_{xx} \ldots \tilde{Y}_{zz}$ do not have a branch point at $\rho = k_0$.

BIBLIOGRAPHY

[1] I. J. Bahl and P. Bhartia, *Microstrip Antennas*, Artech House, Dedham Massachusetts, 1980.

[2] D. M. Pozar, "Considerations for Millimeter Wave Printed Antennas," *IEEE Transactions on Antennas and Propagation*, vol. AP-31, no. 5, Spetember 1983, pp 740-747.

[3] R. E. Collin, *Field Theory of Guided Waves*, McGraw-Hill, New York, 1961.

[4] D. S. James and S. H. Lee, "Microstrip End Effect," *Electronics Letters*, vol. 8., pp. 46-47, Jan. 1982.

[5] P.Silvester and P. Benedek, "Equivalent Capacitances of Microstrip Open Circuits," *IEEE Transactions on Microwave Theory and Techniques*, vol. MTT-20, pp. 511-516, Aug. 1972.

[6] T. Itoh, R. Mittra and D. R. Ward, "A Method for Computing Edge Capacitance of Finite and Semi-Infinite Microstrip Lines," *IEEE Transactions on Microwave Theory and Techniques*, pp 847-849, Dec. 1972.

[7] A. F. Thompson and A. Gupinath, "Calculation of Microstrip Discontinuity Inductances," *IEEE Transactions on Microwave Theory and Techniques*, vol. MTT-23, pp. 648-655, Aug. 1975.

[8] C. Gupta and A. Gopinath, "Equivalent Circuit Capacitance of Microstrip Step Change in Width," *IEEE Transactions on Microwave Theory and Techniques*, vol. MTT-25, pp. 819-822, Oct. 1977.

[9] P. Stouten, "Equivalent Capacitances of T Junctions," *Electronics Letters*, vol. 9, pp. 552-553, November 1973.

[10] I. Wolff, A. G. Kompa and R. Mehran, "Calculation Method for Microstrip Discontinuities and T-Junctions," *Electronics Letters*, vol. 8, p. 177, April 1972.

[11] P. Silvester and P. Benedek, "Microstrip Discontinuity Capacitances for Right-Angle Bends, T Junctions,and Crossings" *IEEE Transactions on Microwave Theory and Techniques*, vol. MTT-21, pp. 341-346, May 1973.

[12] M. Maeda, "An Analysis of Gap In Microstrip Transmission Lines," *IEEE Transactions on Microwave Theory and Techniques*, vol. MTT-20, pp. 390-396, June 1972.

[13] T. Itoh, *Numerical Techniques for Microwave and Millimeter-wave Passive Structures*, John Wiley & Sons, New York, 1989.

[14] S. Nam and T. Itoh, "Calculation of Complex Resonant Frequency of an Open Microstrip Resonator Using the Spectral Domain Method," *Journal of Electromagnetic Waves and Applications*, Vol. 2, no. 7, 1988, pp 635-651.

[15] R. W. Jackson and D. M. Pozar, "Full-Wave Analysis of Micrstrip Open-End and Gap Discontinuities," *IEEE Transactions on Microwave Theory*

and Techniques, vol. MTT-33, no. 10, October 1985, pp. 1036-1041.

[16] P. B. Katehi and N. G. Alexopoulos, "Frequency-dependent Characteristics of Microstrip Discontinuities in Millimeter-Wave Integrated Circuits," *IEEE Transactions on Microwave Theory and Techniques*, vol. MTT-33,no. 10, October 1985, pp. 1029-1035.

[17] J. Boukamp and R. H. Jansen, "The High Frequency Behaviour of Microstrip Open Ends in Microwave Integrated Circuits Including Energy Leakage," *Proc. of the 14th European Microwave Conferance*, Sept 10-13, 1984, Liege, Belgium, pp. 142-147.

[18] H. Yang, N. G. Alexoupolos, and D. R. Jackson, "Microstrip Open-End and Gap Discontinuities in a Substrate-Superstrate Structure," *IEEE Transactions on Microwave Theory Techniques*, vol. MTT-37, No. 10, October 1989, pp. 1542-1546.

[19] M. Drissi, F. Hanna, P. Lepeltier, and J. Citerne, "Analyse de discontinuites rayonnantes sur ligne microruban au moyen dequations integrales," *Annales des Telecommunications*, Tome 43, No 56, 1988, pp. 246-250.

[20] M. Drissi, F. Hanna, and J. Citerne, "Theoretical and Experimental Investigation of Open Microstrip Gap Discontinuities," *The Proceedings of the 18th European Microwave Conference*, September 12-16, 1988, Stockholm, Sweden.

[21] R. W. Jackson, "Mode Conversion at Discontinuities in Finite-Width Conductor-Backed Coplanar Waveguide," *IEEE Transactions on Mi-*

crowave Theory and Techniques, vol. MTT-37, no. 10, October 1989, pp. 1582-1589.

[22] H. Yang, N. G. Alexopoulos, "A Dynamic Model for Microstrip-Slotline Transition and Related Structures," *IEEE Transactions on Microwave Theory and Techniques*, vol. MTT-36, no. 2, February 1988, pp. 286-293.

[23] M. Abramowitz and I. A. Stegun, "Handbook of Mathematical Functions With Formulas, Graphs, and Mathematical Tables," National Bureau of Standards, Washington, D. C., 1964.

[24] G. Arfken, *Mathematical Methods for Physicists*, pp. 811-814, Academic Press, Inc., New York, 1985.

[25] R. F. Harrington, *Time-Harmonic Electromagnetic Fields*, McGraw-Hill, New York, 1961.

[26] T. Itoh and R. Mittra, "Spectral Domain Approach for Calculating the Dispersion Characteristics of Microstrip Lines," *IEEE Transactions on Microwave Theory and Techniques*, vol. MTT-7, July 1973, pp 496-499.

[27] R. Mittra and T. Itoh, "A New Technique for the Analysis of the Dispersion Characteristics of Microstrip Lines," *IEEE Transactions on Microwave Theory ond Techniques*, vol. MTT-19, no. 1, January 1971, pp. 47-56.

[28] T. Itoh, "Spectral Domain Immitance Approach for Dispersion Characteristics of Generalized Printed Lines," *IEEE Transactions on Microwave Theory and Techniques*, vol. MTT-28, no. 7, July 1980, pp 733-736.

[29] J. Knorr and A. Tufekcioglu, "Spectral Domain Calculation of Microstrip Characteristic Impedance," *IEEE Transactions on Microwave Theory and Techniques*, vol. MTT-23, no. 9, September 1975, pp. 725-728.

[30] J. R. James and A. Henderson, "High frequency behavior of microstrip open-circuit terminations," *Proceeding of the Institution of Electrical Engineers, Part H, Microwaves, Optics and Acoustics*, vol. 3, no. 4, pp. 205-218, Sept. 1979.

[31] P. B. Katehi and N. G. Alexopoulos, "On the effect of substrate thickness and permittivity on printed circuit dipole properties," *IEEE Transactions on Antennas and Propagation*, vol. AP-31, Jan 1983.

[32] N. K. Uzunoglu, N. G. Alexopoulos, "Radiation Properties of Microstrip Dipoles," *IEEE Transactions on Antennas and Propogation*, vol. AP-27, no. 6, November 1979, pp 853-858.

[33] D. M. Pozar, "Input Impedance and Coupling of Rectangular Microstrip Antennas," *IEEE Transactions on Antennas and Propagation*, vol. AP-30, no. 6, November 1982, pp. 1191-1196.

[34] D. M. Pozar, "Finite Phased Arrays of Rectangular Microstrip Patches," *IEEE Transactions on Antennas and Propagation*, vol. AP-34, no. 5, May 1986, pp 658-665.

[35] D. M. Pozar, "Analysis of Finite Phased Arrays of Printed Dipoles," *IEEE Transactions on Antennas and Propagation*, vol. AP-33, no. 10, October 1985, pp 1045-1053.

[36] D. M. Pozar, "Improved Computational Efficiency for the Moment Method Solution of Printed Dipoles and Patches," *Electromagnetics*, vol 3, 1983, pp. 299-309.

[37] R. H. Jansen, "The Spectral-Domain Approach for Microwave Integrated Circuits," *IEEE Transaction on Microwave Theory and Techniques*, vol. MTT-33, no. 10, October 1985, pp 1043-1056.

[38] T. Itoh, "Analysis of Microstrip Resonators," *IEEE Transactions on Microwave Theory and Techniques*, vol. MTT-22, no. 11, November, 1974, pp. 946-952.

[39] T. Itoh and W. Menzal, "A Full-wave Analysis Method for Open Microstrip Structures," *IEEE Transactions on Antennas and Propagation*, Vol. AP-29, pp. 63-68, 1981

[40] A. K. Sharma and B. Bhat, "Spectral Domain Analysis of Interacting Microstrip Resonant Stucture," *IEEE Transactions on Microwave Theory and Techniques*, Vol MTT-31, August 1983, pp 681-685.

[41] M. Kirsching, R. H. Jansen and , N. H. L. Koster, "Accurate Model for Open End Effect of Micrstrip Lines," *Electronics Letters*, Vol 17, No. 3, 5th February, 1981, pp. 123-124.

[42] S. Cohn, "Slot Line on Dielectric Substrate," *IEEE Transactions on Microwave Theory and Techniques*, vol. MTT-17, No. 10, October 1969, pp. 768-778.

[43] G. Gronau, I. Wolff, "A Simple Broad-Band Device De-embedding Method Using an Automatic Network Analyzer with Time Domain Option," *IEEE Transactions on Microwave Theory and Techniques*, vol. MTT-37, No. 3, March 1989, pp. 479-483.

[44] J. Knorr and Juan Saenz, "End Effect in a Shorted Slot," *IEEE Transactions on Microwave Theory and Techniques*, vol. MTT, No. 9, September 1973. pp. 579-580.

[45] T. Itoh and R. Mittra, "Dispersion Characteristics of Slotlines," *Electronics Letters*, Vol. 7,No 13, 1st July, 1971, pp. 364-365.

[46] R. W. Jackson,""Considerations for the Use of Coplanar Waveguide For Millimeter-Wave Integrated Circuits," *IEEE Transactions on Microwave Theory and Techniques*, vol. MTT-34. no. 12, December 1986, pp.1450-1456.

[47] J. R. Mosig and F. E. Gardiol, "Analytical and numerical techniques in the Green's function treatment of microstrip antennas and scatterers," *IEE Proceedings: Part H*, No. 2, March 1983, pp 175-182.

[48] J. R. Mosig, F. E. Gardiol, "General Integral Equation Formulation for microstrip antennas and scatterers," *IEE Proceedings: Part H*, No. 7, December 1985, pp 424-432.

[49] G. Gronau and Ingo Wolff, "A Simple Broad-Band Device De-embedding Method Using an Automatic Network Analyzer with a Time-Domain Option," *IEEE Transactions on Microwave Theory and Techniques*, vol. MTT-37, No. 3, pp. 479-483, 1989.